Spring 2017

Effect of Design Parameters on Thermal Performance of a Vane Type Disc Brake Rotor

Yogesh Satish Dalal
Western Michigan University, dalalyogesh17@gmail.com

EFFECT OF DESIGN PARAMETERS ON THERMAL PERFORMANCE OF A VANE TYPE DISC BRAKE ROTOR

by

Yogesh Satish Dalal

A thesis submitted to the Graduate College
in partial fulfillment of the requirements
for the degree of Master of Science
Mechanical Engineering
Western Michigan University
April 2017

Thesis Committee:

Dr. Jennifer Hudson, Ph.D., Chair
Dr. Christopher Cho, Ph.D.
Dr. Willium Liou, Ph.D.

EFFECT OF DESIGN PARAMETERS ON THERMAL PERFORMANCE OF A VANE TYPE DISC BRAKE ROTOR

Yogesh Satish Dalal, M.S.

Western Michigan University, 2017

The ever-increasing need of effective transportation puts automobile manufacturers in a situation of continuous improvement and innovate the safety systems. The brake system of an automobile has always been considered as one of the most critical active safety systems. Thermal characteristics of the brake are an important aspect to consider for brake disc durability and performance. The convective cooling of a brake disc is an important factor since design changes in the brake rotor can significantly improve cooling characteristics. The focus of this research is to study and optimize the disc brake rotor for a given heat dissipation rate and predict the effect of various design parameters on the thermal performance of brake rotor. Computational Fluid Dynamics (CFD) simulations are used to validate the Limpert's empirical formulae for convective heat transfer coefficient, which further used and integrated with suitable inequality and equality constraints to form optimization problem. Sensitivity study is performed using a MATLAB algorithm to determine the effects of these design parameters. The results of this thesis may be used as a supporting framework for future research in the field of thermal performance of vane-type brake discs.

ACKNOWLEDGMENTS

I would like to thank Western Michigan University for providing me such a wonderful opportunity to pursue my master's in Mechanical Engineering. Also, I would like to thank ZF-TRW team, my manager Jeff Britner and Rich Swarich for providing me necessary facilities and help for the completion of the thesis.

I would like to express my deepest and sincerest gratitude to my supervisor Dr. Jennifer Hudson, without her unwavering support and encouragement this work would have not been possible. I thank her for her guidance even before starting of this thesis. I believe that her guidance will forever be a source of encouragement.

I also want to thank my thesis committee members Dr. Willium Liou and Dr. Christopher Cho for their valuable advice and encouragement. Special thanks to Dr. Liou who took efforts to make me understand what thesis is stands for.

I would like to thank my best friends, Ameya, Bhushan, Sameer and Ateet for their strong support and motivation. I also owe my greatest thanks to my parents. I thank them for being a rock-solid support over the years. I thank my cousins Pallavi, Akshay and Shailesh who have always cared for me since the very beginning. Words are not enough for me at this very moment to thank.

I feel the luckiest human being alive to have all of you around, and this is truly dedicated to all of you.

Yogesh Satish Dalal

TABLE OF CONTENTS

Table of Contents - Continued

Table of Contents - Continued

Table of Contents - Continued

LIST OF TABLES

LIST OF FIGURES

List of Figures - Continued

List of Figures - Continued

List of Figures - Continued

NOMENCLEATURE

ICEM	-	Integrated Computer Engineering and Manufacturing
CCM	-	Carbon Ceramic Material
OEM	-	Original Equipment Manufacturer
CFD	-	Computational Fluid Dynamic
CFX	-	Computational Fluid Xerography
CAD	-	Computer Aided Drawing
CAE	-	Computer Aided Engineering
SAE	-	Society of Automotive Engineering
GM	-	General Motors
ΔH	-	Wear displacement
K	-	Specific wear rate coefficient
P	-	Contact pressure
V1	-	Slide rate
t1	-	Running time
a, b, c	-	Constants
h	-	Convective heat transfer coefficient
Re	-	Reynolds number, dimensionless
Pr	-	Prandalt number, dimensionless
l	-	Length of cooling vane
dh	-	Hydraulic diameter

ka	-	Thermal conductivity of air
V_{avg}	-	Average vent speed
V_{in}	-	Inlet velocity
V_{out}	-	Outlet velocity
D	-	Outer disc diameter
R	-	Outer disc radius
d	-	Inner disc diameter
r	-	Inner disc radius
A_{in}	-	Inlet area
A_{out}	-	Outlet area
RPM	-	Revolution per minute
Z	-	Total number of vanes
D_0	-	Middle diameter of rotor
t	-	Vane thickness
B_y	-	Cooling rate
b_o	-	Loss of heat by mode of conduction
b_c	-	Loss of heat by mode of convection
K1	-	Constant
V	-	Velocity
m1	-	Constant depends on the type of air flow
Q_{cond}	-	Amount of heat transfer due to mode of conduction
A	-	Area expose

Λ	-	Thermal conductivity of the material
dt/dx	-	Ratio of change in temperature to distance cover
Q_{conv}	-	Heat transfer due to convection
Q_{rad}	-	Heat transfer due to radiation
Σ	-	Stephen Boltzmann constant (5.67 * 10-8)
E	-	Emissivity ($0 \leq \varepsilon \leq 1$)
T_{obj}	-	Temperature of the object
T_{env}	-	Temperature of the surrounding
ρ	-	Density
U	-	Velocity vector
P	-	Pressure
T	-	Temperature
E1	-	Kinetic energy generated
m	-	Mass of a rotor
Cp	-	Specific heat capacity of rotor
ω	-	Angular velocity
Q	-	Total amount of heat generated
Bv	-	Cooling rate
v2	-	Speed of car
m1	-	Constant depending on air flow
h_{avg}	-	Average convective heat transfer coefficient
Q_{cov}	-	Rate of heat transfer by mode of convection

Q_{rad}	-	Rate of heat transfer by mode of radiation
GCI	-	Grid Convergence Index
rr	-	Refinement ratio
P1	-	Order of the discretization scheme
E	-	Estimated fractional error
Fs	-	Factor of safety coefficient
e	-	Internal energy
τ_{zx}	-	Viscous stress
f1	-	Value of respective property on cores grid
f2	-	Value of respective property on medium grid
f3	-	Value of respective property on fine grid
h1	-	Vane height
N	-	Number of vanes
t	-	Thickness of vane
ξ	-	Correction factor
W	-	Total weight of rotor
Rc	-	Radius of curvature of curved vane

1. BACKGROUND

The National Motor Vehicle Crash Caution Survey (NMVCCS) collected data from 2005 to 2008 and published its report in February 2015. Over a period of two and half years, NMVCCS investigated 2,189,000 national wide to figure out most critical reasons for crash. In most of the cases (94%) critical reason was driver's lack of attention or lack of judgement. Component failure was recorded second significant factor (2%). As shown in (Figure 1), it is equivalent to 44,000 crashes. Out of 2% of crashes, an estimated 22% of the component failures were brake related, which amounts to 10,000 accidents caused by brake component failures [1]

Critical Reason	Estimated (Based on 2% of the NMVCCS crashes)	
	Number	Percentage* ± 95% conf. limits
Tires /wheels-related	15,000	35% ± 11.4%
Brakes-related	10,000	22% ± 15.4%
Steering/suspension/transmission/ engine-related	2,000	3% ± 3.3%
Other/unknown vehicle-related problems	17,000	40% ± 24.0%
Total	44,000	100%

*Percentages are based on unrounded estimated frequencies
(Data Source: NMVCCS 2005–2007)

Figure 1: National motor vehicle statistical data for accident cause *[1]*

Considering the data presented, development in active safety systems is needed to minimize the accidents caused due to component failure.

a. Brake System Description

The main purpose of a disc brake system is to decelerate the vehicle; this takes place by converting the kinetic energy of the vehicle into thermal energy. During braking, a large amount of heat is created because of friction between the brake disc and brake pads. The brake rotor absorbs the total generated heat cause by braking action. The absorbed heat must be effectively dissipated to achieve satisfactory performance of the braking system. Excessive heat can damage the brake component and cause complete brake failure. Hence it is necessary to select proper brake rotor parameters from a thermal stability point of view. [2]

i. Disc brakes

Frederick William Blanchester invented the disc brake system in 1902, commercial use of these brakes started in the early 1950s [3]. The brake system consists of a rotor, brake pads, piston, hydraulic unit, caliper, and clamping unit. shown in (Figure 2), the rotor is mounted on the wheel and it rotates with the same speed as wheel. Brake pads are attached on either side of the brake rotor which is clamped in a caliper. Translation motion of a piston inside a cylinder pushes the brake pad onto the rotor. The complete brake system is operated on hydraulic fluid. [4]

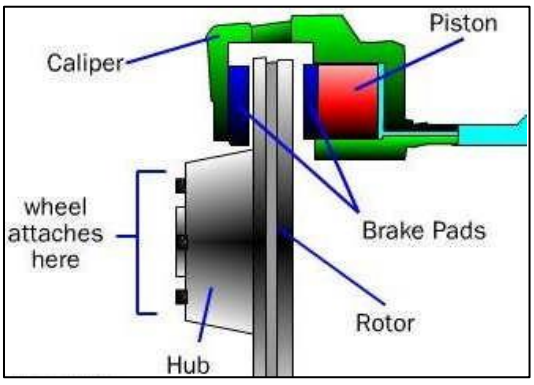

Figure 2: Schematic of the disc brake system *[4]*

The braking action causes friction between the brake disc and brake pads which produce heat energy; this heat energy gets stored in the brake disc rotor. The rotating brake rotor extracts the heat by modes of conduction, convection, and radiation. Two main types of brake rotors are,

- Solid disc brake rotor
- Ventilated disc brake rotor

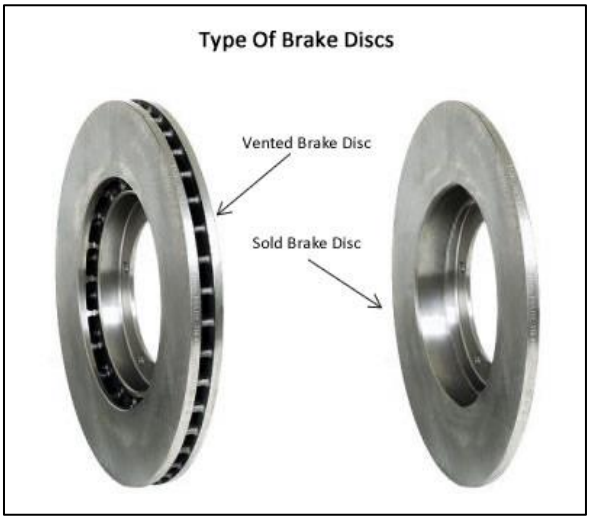

Figure 3: Brake rotor types *[5]*

The advantage of a ventilated rotor over a solid rotor is that ventilated rotors help in better heat dissipation due to air flow between the vanes and also due to an increase in the total area available for heat transfer. Shown in (Figure 3), disc brakes are exposed to air and hence heat is dissipated directly from the surface to the atmosphere, which improves the thermal performance. Due to these advantage, the disc brake system is extensively used. [6]

b. Current Commercial Brake Rotors

Disc brakes are very popular with consumers and automakers. They are likely to remain popular in the future as well. The following three manufacturers capture more than 80% of the business in disc brake system. They are currently working on performance enhancement.

i. Brembo

Brembo SpA is the world leader and acknowledged innovator of disc brake technology. As shown in (Figure 4), Brembo supplies high-performance brake systems for cars, commercial vehicles, and motorbikes worldwide. Brembo has registered an impressive 370 families of patents thus far. Currently, Brembo is working on enhancing the structural and thermal characteristics of vane rotor. They are working on material characteristics of Carbon Ceramic Material (CCM) and design integration of curved and straight vanes for producing high performance vented rotor. [7]

Figure 4: Brembo vane rotor (al) for Ford Mustang *[8]*

ii. Willwood

Willwood Engineering designs and manufactures high-performance disc brake systems. Since the company's inception in 1977 by Bill Wood, Willwood developed a substantial matrix of brake components and engineering techniques. Willwood produces over 120 different disk brake rotors in various styles and diameters for street, racing and other high-performance applications in standard slotted and drilled and slotted styles shown in (Figure 5). Rotors are made of high-grade steel, iron, and carbon ceramic composites. [9]

Figure 5: Wilwood curved vane rotor *[9]*

iii. ZF-TRW

ZF- TRW produces about 12 million brake disc every year for Original equipment manufacturer (OEM) and independent aftermarket worldwide. As a leader in Foundation Brake design, development, and supply, ZF TRW offers a wide range of applications for passenger cars and trucks, including disc and drum brake solutions typical disc brake shown in (Figure 6) To address ever-increasing CO_2 emission reduction and fuel economy requirements, ZF TRW has developed improved residual drag features and is offering lightweight components to meet fuel efficiency requirements. [10]

Figure 6: Verities of vane rotor produced by ZF –TRW *[10]*

iv. Industrial trends for thermal stability

A foremost criterion for rotor manufacturers is to satisfy customers' requirements. To achieve the customer's desired performance in terms of thermal stability of the rotor, rotor manufacturers have the following options.

Change in geometry

A change in geometry affects the total exposed area of the rotor, material content, and flow pattern of air. Geometric changes are responsible for thermal stability and structural stability. This thesis concentrates on design changes and their effect on the thermal stability of the rotor.

Change in the material

Brake rotors are usually made of Aluminum, Cast iron, Duralumin, Bronze, or Steel. Material properties such as thermal conductivity, specific heat capacity, and tensile strength are different for each material. Some of the critical material requirements for disc brake rotors are

- High strength at elevated temperatures
- High stiffness (modulus of elasticity)
- Low density
- High thermal conductivity

Depending upon requirements and considering the cost of production, the brake rotor material is selected. Composites material or carbon-ceramic material (CCM) are generally used for manufacturing brake rotors of high-performance cars.

Anodization / coating

Anodization on brake rotor is used to prevent corrosion. Also, coating or anodization increases the heat transfer of brake rotor by mode of radiation at very high temperature.

Emissivity can be increase by coating on brake rotor and hence brake rotor of a high-performance car is coated with a material having high emissivity value.

Brake duct design

Brake rotors are designed to dissipate heat effectively, but air flow inside and around the brake rotor is turbulent in nature. Because of aggressive braking, heat is built up around the brake rotor and the rotor alone is not capable of extracting all the generated heat in a short amount of time. As shown in (Figure 7) brake ducts works by channeling air from the front surface of the car to the brake rotor. Atmospheric air taken in by the brake duct is much cooler than the air around the brake disc. Air flow through the duct continuously moves hot air away, which allows the brake to cool at a faster rate, lowering the operating temperature of the brake assembly.

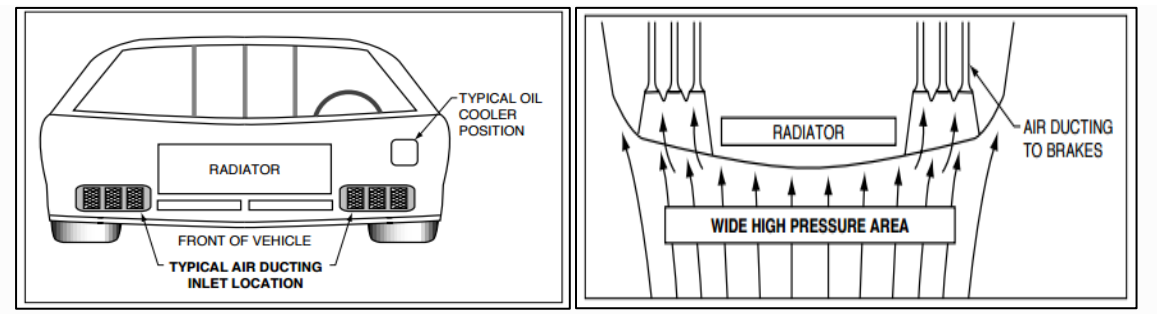

Figure 7: Air ducts for brake system *[11]*

Brake ducts have the following advantages:

- Increases the life of brake pads and rotor
- Higher cooling performance
- Cost effective and consistent performance [11]

c. Brake Rotor Thermal Failure Types

To understand the thermal characteristics of the brake rotor, it is important to understand the different thermal failure modes associated with it.

Thermal judder

- Hot judder

Thermal deformation of the rotor causes hot judder. When the brake rotor with varying thickness on its periphery is subjected to braking, surface variations cause uneven heat distribution. Because of temperature variations on the brake rotor, uneven thermal expansion may occur. A typical example of hot judder is shown in (Figure 8). [12]

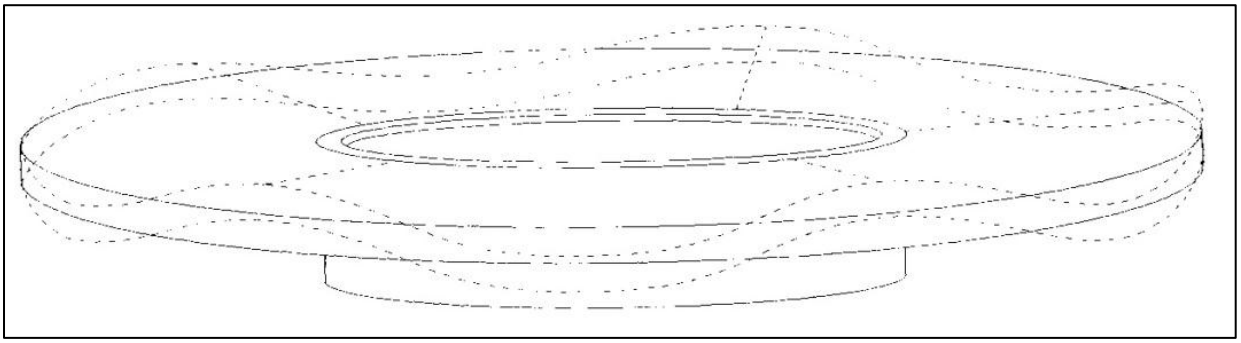

Figure 8: Corrugated effect due to thermal judder *[13]*

Cracking

Cracking is the next phase of hot judder. Due to uneven heat distribution, thermal and structural stresses are not uniform on the rotor, which may result in development and propagation of a crack. [14]

Thermo-mechanical distortion

Thermo-mechanical distortions are caused by overheating of the disc brake rotor. Poor rotor design or material use can cause overheating which may result in poor heat dissipation. As the temperature of the rotor increases, the metal becomes softer and gets easily reshaped when forces are acting on it. [14]

Brake fade

Brake fade can be caused due to high temperature. During brake fade, braking force is reduced because of loss of contact between rotor and brake pad. At very high-temperatures, the coefficient of friction between the brake pad and the rotor is reduced, which results in reduced braking effectiveness and ultimately failure. Generally, it is very rare that brake fade happens. [13]

Excessive component wear

The amount of the wear of brake pads is directly proportional to contact pressure, but exponentially related to temperature. High temperatures in the braking system can cause thermal deformation of the rotors, leading to uneven braking. therefore, more rapid wear may occur at elevated temperatures. [2]

$$\Delta H = K * P^{a} * V1^{b} * t1^{c} \quad (1)$$

2. PROJECT MOTIVATION

Most of the disc brake failures occur due to the problems associated with heat distribution, heat absorption, and overheating of the rotor. Therefore, it is paramount to enhance the heat dissipation of the disc brake rotor for its effective functionality.

a. Objectives

The purpose of this study is to validate the convective heat transfer coefficient derived by Limpert's empirical formulae using CFD approach; and to optimize the vane type brake rotor for a given rate of heat dissipation. A Computational Fluid Dynamic (CFD) approach is used to calculate the convective heat transfer coefficient. Further the empirical formulae were integrated into vane brake rotor's optimization algorithm with suitable constraint's and bounds. Using the designed algorithm, significant factors and their effect on rotor's performance is discussed. The various design parameters include:

i. Number of vanes

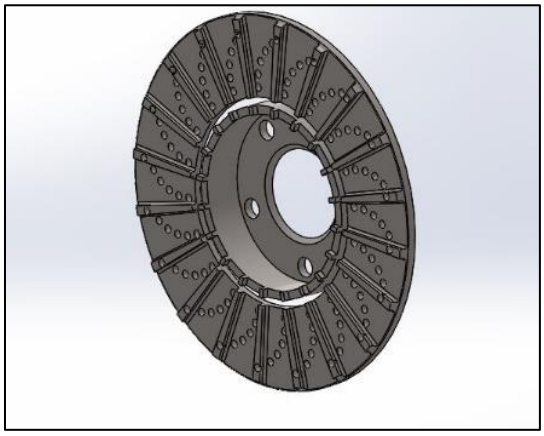

Figure 9: Straight vane rotor sectional view

Shown in (Figure 9), vanes are the extruded surface over the disc and the area between two successive vanes is called the air passage. Total number of vanes can be increasing or decrease depending upon the requirement. There are different types of vane available such as straight vane, curved vanes, pillar post etc.

ii. Vane thickness

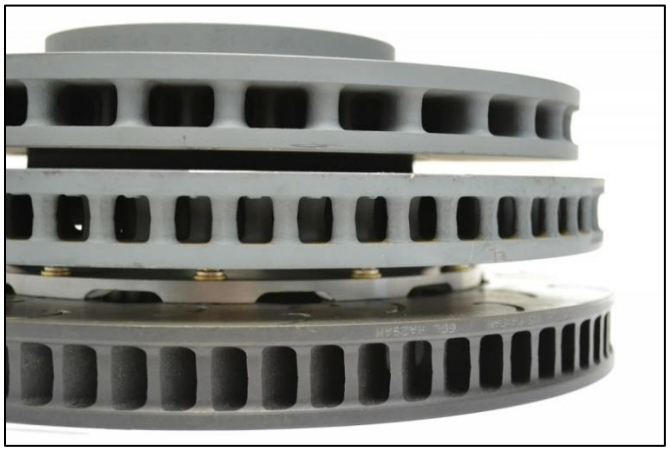

Figure 10: Variation in vane thickness

Shown in (Figure 10), area between two successive vanes from where air can pass is called as air passage. It can be changed by increasing vane thickness or the total number of vanes on a rotor. Shown in fig. if vane thickness is increased, width of air passage get reduced and vice versa.

iii. Type of vanes

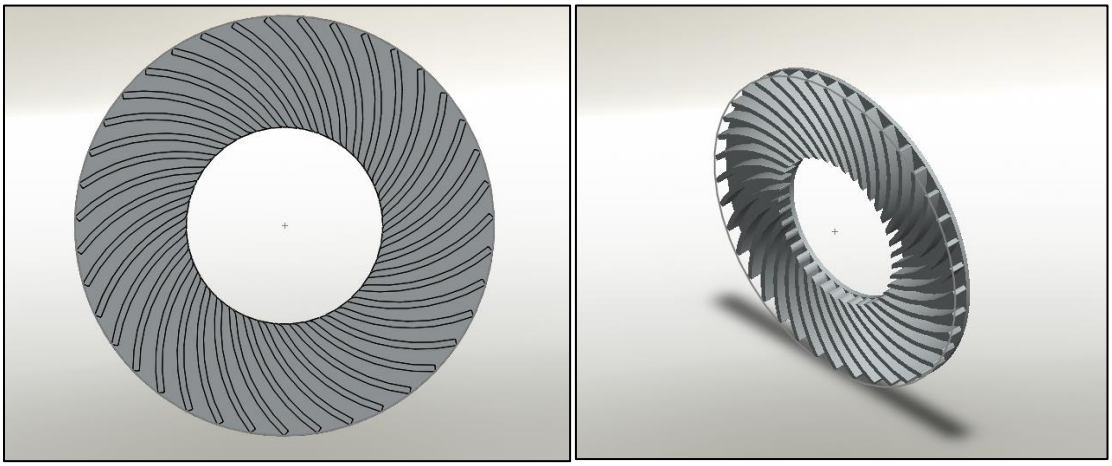

Figure 11: Cross-sectional view of 39 curved vane rotors

(Figure 11) shows front and isometric views of typical curved vane rotor design. Curve vanes are defined as extruded surface over brake which is curvilinear in nature. Because of curvature, surface area of curved vane is rather than straight vane. Surface area increases if the curvature increases. Curve vane can be a straight vane if radius of curvature is INF.

iv. Total surface area

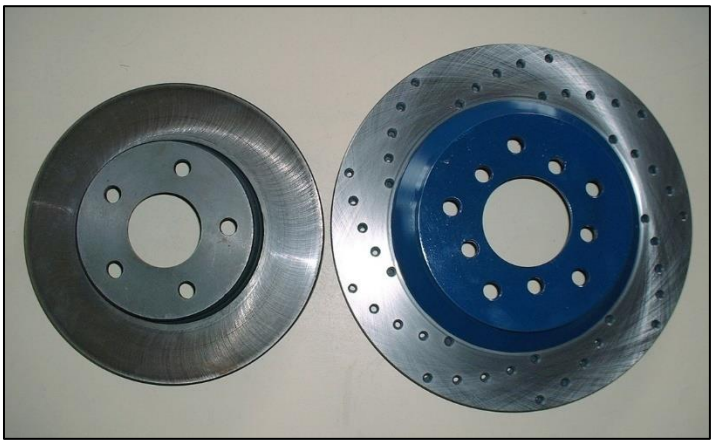

Figure 12: Rotor with different OD and ID

Shown in (Figure 12), two rotors with different outer diameter (OD) and inner diameter (ID). Surface area across the periphery can be increased or decreased by changing OD and ID of a rotor. As well as increasing the OD increased the length of cooling vane which contributes in heat dissipation.

3. LITERATURE REVIEW

a. Experimental and Numerical Work

The various advantages of a disc brake over a drum brake are universally acknowledged and hence most current commercial vehicles have disc brakes [15]. Limpert, who was one of the pioneer researchers in the domain of numerical study of vane brake rotors, studied characteristics of the solid brake rotor and disc rotor cooling. Per his study out of the three modes of heat dissipation from brake discs, convective heat dissipation attains high importance due to the exposure of the brake to the surrounding air. Forced convective cooling is dominant over the other heat transfer modes, as the vehicle is in motion. Newcomb and Day performed experiments and suggested that radiation contributes to less than 5% of the total heat transfer at normal braking conditions. [16]

It was shown that at higher temperatures the contribution of radiation is as much as 1/3 the total heat transfer. It was also suggested that the total convective heat transfer coefficient was approximately 1/3 from vanes and 2/3 from the surfaces, but at higher speeds of around 2000 rpm, internal cooling increased up to 60% of total cooling. For estimation of the convective heat transfer coefficient inside the vane, the following relation can be used, [17]

$$h = \left(0.023 * \left[1 + \left(\frac{dh}{l} \right)^{0.67} \right] * Re^{0.8} * Pr^{0.33} * \left(\frac{ka}{dh} \right) \right) \quad 2.$$

D.Parish and D.G.MacManus [18] carried out aerodynamic investigation of ventilated disc brakes; according to their research, heat dissipation of a ventilated brake rotor depends strongly on the aerodynamic behavior of the flow through the rotor passages. All three mechanisms of heat dissipation contribute to the disk cooling, but convection has a large

impact for most ventilated rotor configurations. Conduction is frequently kept to a minimum in the design process to protect other components and radiation only plays a significant role at high temperatures. The aerothermodynamics of a ventilated brake rotor are complex and highly dependent on the geometry of both the brake rotor and its surrounding environment.

A.D. McPhee [19] used the experimental and analytical method to understand convection through vanes of the brake rotor. The experimental approach involved two aspects, assessment of heat transfer and fluid motion. A transient experiment was conducted to quantify the internal (vane) convection and external (rotor surface) convection terms for three nominal speeds. Analysis on rotor rotational speeds was carried out. Three different RPM were used for the study, 342, 684, and 1025 (rpm). Convective heat transfer coefficients were found out to be 27.0, 52.7, 78.3 (W/m^2K) respectively, indicating a linear relationship. At the slowest speed, the internal convection represented 45.5% of the total heat transfer, increasing to 55.4% at 1025 (rpm). Convection is one of the most dominant factors among the 3 modes of heat transfer. Limpert [17] also provided an expression for average vent speed at exit of rotor as,

$$V_{avg} = \left[\frac{Vin + Vout}{2}\right] \qquad 3.$$

After Limpert, Sisson [20] did experimental work and proposed an expression for the average vent speed at the exit of the rotor, where he used a radial bladed rotor for his experimental analysis. According to Sisson's study, air speed is a function of rotors' outside diameter, inside diameter and rotational speed. The test data was used to derive the empirical equation as follows,

$$V_{avg} = \left[\frac{\pi * D * RPM}{60} * [(-0.0201 + 0.2769\,d - 0.0188 * d\text{^}2)]^{0.5}\right] \qquad 4.$$

Later Hudson [21] compared the average velocity derived by Limpert and Sisson and pointed out that the value of average velocity given by Limpert is approximately one third as compared to average velocity derived by Sisson.

With the collaboration of Chrysler Corporation, Hudson [21] performed experimental studies on the design modifications for the improvement of mass flow rate through the rotor passage. For his study, he chose Chrysler LH-series front brake rotor. Radial blades were considered for the analysis. The goal was to improve vane air flow to increase brake rotor cooling. Hudson [21] compared the exit velocity values for datum rotor, a rotor with inlet horn with the empirical values obtained from Limpert [15] and Sisson [20] at two different rotational speeds of 600 and 800 rpm. The increase in the average vent velocity due to this inlet horn was observed to be 32%

Daudi [22] has performed CFD simulations to compare a 42-radial bladed rotor with a 72-curved fin rotor with an inlet angle of 450 and outlet angle of 1050. He observed an increase in the mass flow rate by approximately 34.8% at 800 rpm in the curved vane rotor. He also conducted the analysis on five different rotor speeds. The air inlet and outlet angles were chosen based on air flow inlet and exit angles obtained from CFD analyses. Daudi also gave a 50% inboard and 50% outboard entry and noted an increase of 5% in mass flow rate through vane brake rotor.

Zhang [23] in collaboration with General Motors conducted CFD simulations; he considered three stages

- Rotor configuration design
- Selection of number of vanes
- Flow passage design

He used the above-mentioned models to study the effect of number of vanes on the mass flow rate through the rotor passages. He designed the passage in such a way that the cross-section is square instead of a rectangle. This is because, for a given area, a square cross section has the least perimeter and thereby reducing the frictional losses. Using a CFD approach for determining flow passage design, he successfully achieved an increase of 42% cooling flow rate compared with the conventional rotor.

For determining optimal number of vanes, he used,

$$Z = [(\pi \, Do) \, / \, (w + t)] \qquad 5.$$

Zhang concluded that long-short alternative type vane rotor configuration had a technical advantage over the conventional simple straight vane rotor, because it accounts the variation of vane passage area.

T.P.Newcomb et al [16] carried out an experimental investigation of cooling rate of drum and disc brake rotor where thermocouple was mounted midway on the disc to measure temperature. Cooling rate was expressed based on experimental observation as,

$$B_v = b_0 + b_C \qquad 6.$$

But the rate of heat transfer by the mode of convection depends on the speed of vehicle and type of air flow. So, the equation becomes,

$$B_v = b_0 + K1 * V_2^{m1} \qquad 7.$$

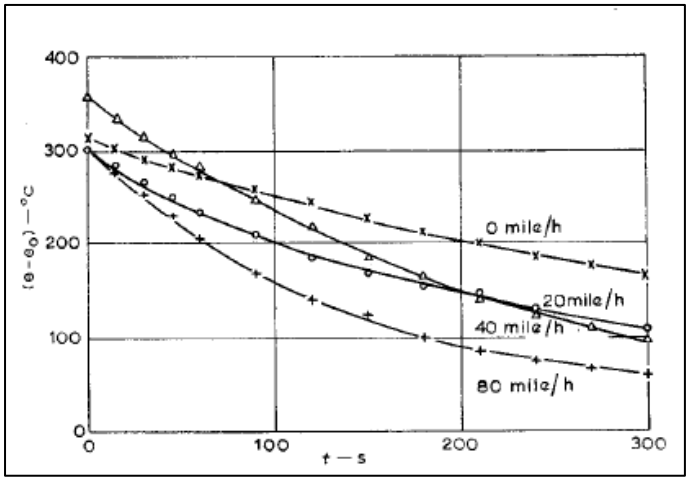

Figure 13: Variation of (T-To) with time for various vehicle speeds *[16]*

As shown in (Figure 13) variation of temperature with respect to time for different vehicle speed. At same instant of time, temperature drops at faster rate for higher vehicle speed.

b. Computational Fluid Dynamics (CFD) Approach Compared with Experimental Results

G.Barigazzi and A.Perdichizzi et al [24] conducted series of experiments on the aero-thermal performance of vane rotor and concluded that, for the analysis of a newly designed component, detailed experimental investigations are not always convenient; especially at the beginning of a design process, when several geometries need to be tested. From this point of view, CFD simulation can be very useful when thoroughly validated against experimental data.

G.Barigazzi and A.Perdichizzi et al [25] performed an experimental study on aero-thermal characteristics of automotive Carbon Ceramic Material (CCM) vented brake disc rotor. They found that in the optimization process, CFD is an essential tool to predict the disc heat transfer. Further, they carried out an investigation, which shows a better understanding of the thermal energy transfer taking place inside the disc channels. The computational and experimental air temperature profile showed similar structure for all tested conditions. A similar behavior was also observed while testing multiple vane brake rotor of different material.

G.Barigazzi and M.Donati et al [24] performed a combined experimental and CFD investigation of brake disc aero-thermal performance. The aim of this study was to assess the available CFD codes and to determine how confidently one should use a CFD approach in the automotive brake rotor design process. Many experimental studies were also conducted to measure the air flow and temperature field inside the discs in the application of braking. It has been demonstrated that CFD simulation results were in good agreement with experimental studies.

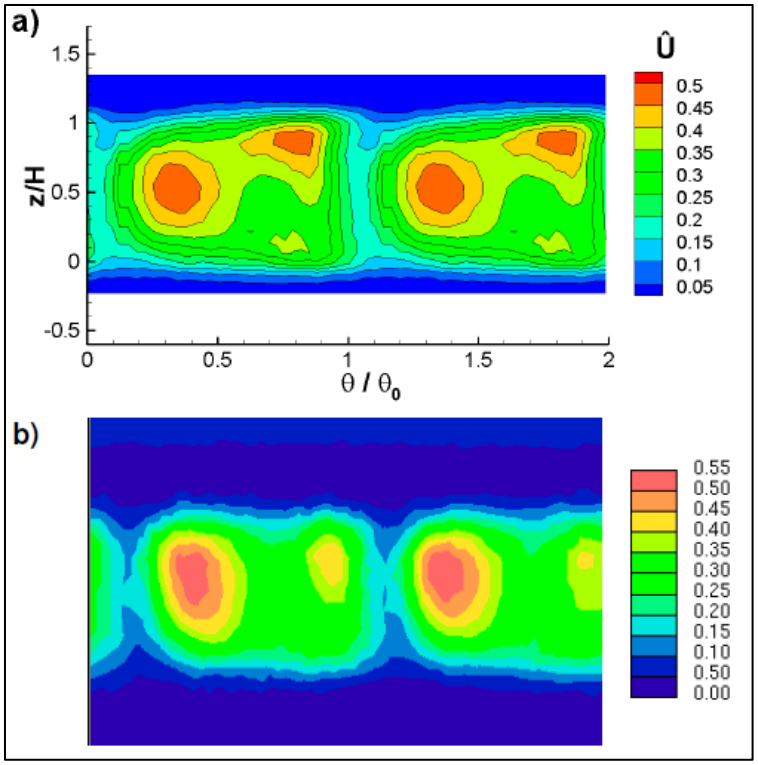

Figure 14: Velocity (U) distribution in non-braking condition a) experimental b) CFD *[24]*

(Figure 14) shows the comparison between experimental and numerical result, in term of normalized radial velocity distribution. Looking at velocity distribution of experimental and numerical result, it can be concluded that results are in good agreement. CFD captures all the complex flow phenomena taking place inside of multiple pin disc configurations.

G.Barigazzi and A.Perdichizzi et al [24] concluded that the comparison between numerical and experimental data demonstrated the capability of CFD to correctly simulate the internal disc flow field resulting in a very good prediction of vented mass flow rate. Some differences in the air temperature mean level were observed, even if the structure of the temperature field was well reproduced. Nevertheless, CFD simulation proved to be a useful tool in the design process, as it provided the correct trend for all the relevant parameters, including the heat transfer coefficient.

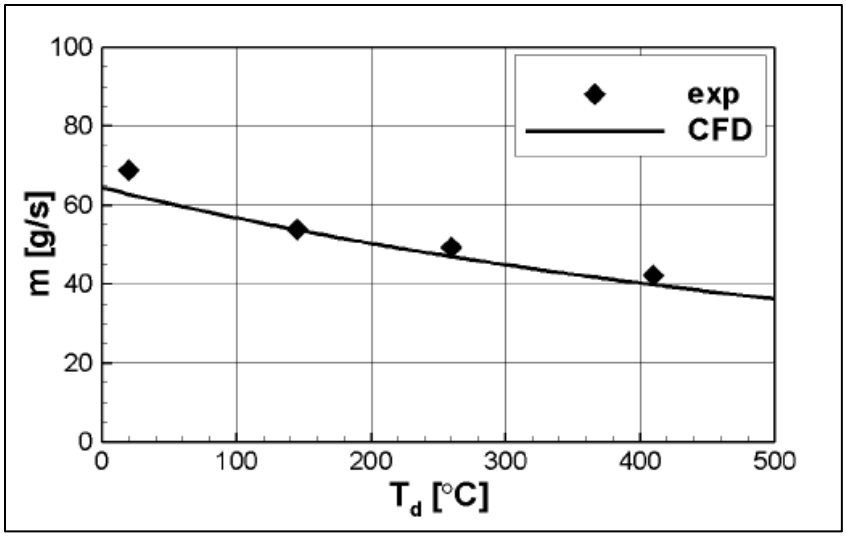

Figure 15: Mass flow rate comparison experimental and CFD *[25]*

(Figure 15) represents the comparison between numerical and experimental mass flow rate versus the disc temperature. An agreement between the experimental and numerical result can be observed.

With cooperation of General Motors, F. Shen, D. Mukutmonal, J.Whaite, K. Thorington [26] executed experimental and computational analysis of brake cooling to determine the reliability of the computational solution. For the experiment, a cast iron rotor was selected and the thermal properties of rotor were defined to carry out computational analysis. The three-dimensional mesh was created all over the computational domain which consists of more than 9,000,000 cells. The experimental and computational results were in good agreement which indicates, thermos-fluid process associated with cooling of brake rotor can be accurately modeled in the computational domain.

R. Krusemann from Mercedes-Benz AG and G. Schmidtfro Adapco [27] carried out the same investigation; they worked on aero-thermal analysis and optimization of disc brake cooling via Computational fluid dynamics (CFD). The achieved results from computational method were found to be reasonable and they concluded that the further optimization can be done on a result obtained from CFD method.

4. THEORETICAL BEHAVIOR

a. Mode of Heat Transfers

The heat transfers from the brake disc to the ambient takes place in three different modes; conduction, convection, and radiation shown in (Figure 16)

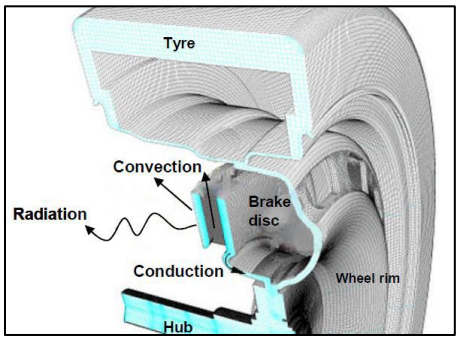

Figure 16: Heat transfer modes for brake rotor

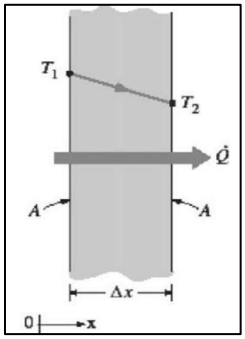

Figure 17: Conduction heat transfer

Conduction

During braking, a large amount of heat is generated at the brake pads and disc interface, which is then conducted through the disc. The degree of temperature distribution depends upon material properties and the area affected by heat flux. The largest portion of energy is absorbed in the disc. Thermal conduction or heat conduction is usually described as the energy transfer in a solid, between particles. Thermal conductivity is

used as the material property for conducting heat and is usually represented by λ. A material with a higher thermal conductivity transfers heats at a higher rate. A typical example of conduction is shown in (Figure 17). [28] [29]

$$Q_{cond} = A * \lambda * (dt/dx) \qquad 8.$$

Convection

Convection is the physical behavior of heat transfer by moving fluids that transport heat energy from one place to another (fluid can be air or liquid). For disc brake cooling, convection is the main contributor to the total heat loss out of the three modes of heat transfer. There are two types of convective heat dissipation, namely natural convection and forced convection; in both cases the mechanisms of heat removal are similar. However, the difference between the two phenomena is fluid speed around the surface. Convection driven by external sources (e.g.: a fan blowing air, or brake disc rotation) is called forced convection. For the brake rotor case, natural convection is defined as, if after a braking event, the vehicle remains stationary for a long time. Convective heat dissipation attains high importance due to the exposure of the brake to the surrounding air. [28] [29]

$$Q_{conv} = A * h_{avg} * (dt), \qquad \text{where } h_{avg} = (1/A) * \int h \,.\, dA \qquad 9.$$

Per the definition of convective heat transfer, the rate of heat transfer depends on the convective heat transfer coefficient (h), area, and the temperature difference. The convective heat coefficient mainly depends on the air flow inside and around the brake disc, i.e. the flow velocity which generally increases the heat transfer rate. The turbulence intensity usually increases the heat transfer rate through increasing intensity and the flow structure.

Radiation

Another contributor to the total heat loss of the brake disc is the radiative heat transfer. The Stefan-Boltzmann law explains radiation as given in equation below.

$$Q_{rad} = \varepsilon^* A * \sigma^* (T^4_{obj} - T^4_{env}) \qquad 10.$$

Radiative heat transfer is defined as transfer of heat in the form of electromagnetic waves. Shown in (Figure 18) radiation emitted by a body is a consequence of thermal agitation of its composing molecules. Per the radiative equation, it is proportional to fourth-order function of temperature and hence for brake analysis at very high temperature, radiation plays a vital role. [28] [29]

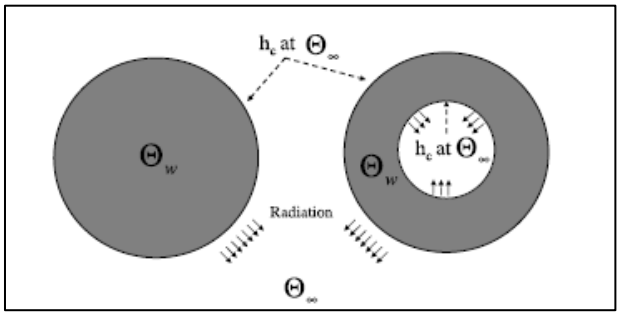

Figure 18: Radiation and convection from solid and hollow bodies *[28]*

b. CFD Overview

CFD is the branch of fluid dynamics providing a simulation of fluid flow and heat transfer by the numerical solution of the governing equations, namely the Navier-Stokes equations. Computational techniques replace the governing partial differential equations with systems of algebraic equations that are much easier to solve using computers. However, the development of reduced forms of these equations is still an active area of research the turbulent closure problem of the Reynolds-averaged Navier-Stokes equations (RANS). Experimental methods have played an important role in validating and exploring the limits of the various approximations to the governing equations.

To convert a physical problem into the CFD domain, flow related phenomena must be described using conservation form of equation. Which involve conservation of mass, momentum, and energy. These fundamental equations are mathematical statements upon which fluid dynamics is based. Conservation equation are in form of derivative term or integral terms. [29]

Mathematical model

The starting point of any numerical method is a mathematical model, i.e., the set of partial differential equations or integral equations and boundary conditions. Depending upon the problem statement, to simplify the conservation form of equations, an appropriate model can be used ex. (incompressible, turbulent, inviscid etc.). In CFD, trying to produce a general-purpose solution method, i.e. one which is applicable to all flows, is not practical and possible so far. The base of mathematical equations are conservation equations defined as follows,

Conservation of mass,

Net mass flow out of given control volume through surface is equal to time rate of decrease of mass inside control volume.

$$\frac{\partial \rho}{\partial t} + \nabla \cdot (\rho V) = 0 \qquad 11.$$

For incompressible flows density has a known constant value, i.e. it is no longer an unknown.

$$\nabla \cdot (V) = 0 \qquad 12.$$

which means that the velocity field of an incompressible flow should be divergence free, which is known as the divergence free constraint in CFD literature.

Conservation of momentum,

Conservation of momentum is based on newton's second aw of motion. In case of moving fluid, net force on moving fluid element equals its mass times the acceleration of the element. This is vector relation, and hence can be split into three scalar relations along x, y, z axes. Further body forces which are directly proportional on volumetric mass of the fluid element and surface forces which are directly proportional on the surface of fluid element are considered in momentum equation.

x-component,

$$\frac{\partial(\rho u)}{\partial t} + \nabla \cdot (\rho u V) = -\frac{\partial p}{\partial x} + \frac{\partial \tau_{xx}}{\partial x} + \frac{\partial \tau_{yx}}{\partial x} + \frac{\partial \tau_{zx}}{\partial x} + \rho f_x \qquad 13.$$

y- component

$$\frac{\partial(\rho v)}{\partial t} + \nabla \cdot (\rho v V) = -\frac{\partial p}{\partial y} + \frac{\partial \tau_{xy}}{\partial x} + \frac{\partial \tau_{yy}}{\partial x} + \frac{\partial \tau_{yz}}{\partial x} + \rho f_y \qquad 14.$$

z-component

$$\frac{\partial(\rho w)}{\partial t} + \nabla \cdot (\rho w V) = -\frac{\partial p}{\partial z} + \frac{\partial \tau_{xz}}{\partial x} + \frac{\partial \tau_{yz}}{\partial x} + \frac{\partial \tau_{zz}}{\partial x} + \rho f_z \qquad 15$$

General form of momentum equations for incompressible flows viscous stress tensor given is zero. Considering this simplification together with viscosity being constant, Eqn can be written as follows

$$\rho\left[\frac{\partial V}{\partial t}+(V.\nabla)V\right]=\ -\nabla p+\mu\nabla^2V+\rho f \qquad 16.$$

Dividing the equation by density we get the following form of the Navier-Stokes equation

$$\frac{\partial V}{\partial t}+(V.\nabla)V=\ -\frac{1}{\rho}\nabla p+\nu\nabla^2V+f \qquad 17.$$

Where ν is kinematic viscosity.

The term $(V.\nabla)V$ is known as the convective term. It is the term which makes the Navier-Stokes equation nonlinear. $\nu\nabla^2V$ is known as the viscous term or the diffusion term. For diffusion dominated flows the convective term can be dropped and the simplified equation is called the Stokes equation, which is linear. Stokes equations can be used to model very low speed flows known as creeping flows or flows with very small length scales (micro or nano flows) where Reynolds number is small. Convection dominated flows, which are typically characterized by high Reynolds numbers, are much more difficult to solve numerically compared to diffusion dominated flows.

In the continuity equation, there is no pressure term and in the momentum equation there are only the derivatives of pressure, but not the pressure itself. This means that the actual value of pressure in an incompressible flow solution is not important, only the changes of pressure in space are important. Additionally, there is no time derivative of pressure, even for incompressible flows.

Conservation of energy,

The physical principle of energy conservation is like first law of thermodynamics. When applied to any flow model of the fluid element moving with the flow, it states that rate of change of energy inside fluid element is equal to summation of net flux of heat into element and rate of work done on element due to body and surface forces.

$$\frac{\partial}{\partial t}\left[\rho\left(e+\frac{V^2}{2}\right)\right]+\nabla\left[\rho\left(e+\frac{V^2}{2}\right)V\right] \qquad 18$$

$$= \rho q+\frac{\partial}{\partial x}\left(k\frac{\partial T}{\partial x}\right)+\frac{\partial}{\partial y}\left(k\frac{\partial T}{\partial y}\right)+\frac{\partial}{\partial z}\left(k\frac{\partial T}{\partial z}\right)-\frac{\partial(up)}{\partial x}-\frac{\partial(vp)}{\partial x}$$

$$-\frac{\partial(wp)}{\partial x}+\frac{\partial(u\tau_{xx})}{\partial x}+\frac{\partial(u\tau_{yx})}{\partial y}+\frac{\partial(u\tau_{zx})}{\partial z}+\frac{\partial(v\tau_{xy})}{\partial x}+\frac{\partial(v\tau_{yy})}{\partial y}$$

$$+\frac{\partial(v\tau_{zy})}{\partial z}+\frac{\partial(w\tau_{xz})}{\partial x}+\frac{\partial(w\tau_{yz})}{\partial y}+\frac{\partial(w\tau_{zz})}{\partial z}+\rho f.V$$

Simplified form of energy equation can be written as,

$$\rho C_p\left[\frac{\partial h}{\partial t}+(\nabla.(hV))\right]=-\frac{D\rho}{Dt}+\nabla.(k\nabla T)+\phi, \qquad 19.$$

$$h=e+\frac{p}{\rho}, \qquad \phi=(\tau.\nabla)V=\tau_{ij}\frac{\partial v_i}{\partial x_j}$$

where h is the specific enthalpy which is related to specific internal energy. T is the absolute temperature and ϕ is the dissipation function representing the work done against viscous forces, which is irreversibly converted into internal energy. To derive this energy equation, heat transfer governed by Fourier's law with being the thermal conductivity of the fluid. Also, radiative heat transfers and internal heat generation due to a possible chemical or nuclear reaction are neglected.

Energy equation can be more simplified, since density is constant for incompressible flow,

$$\rho C_p \left[\frac{\partial T}{\partial t} + (V.\nabla)T\right] = k\nabla^2 T + \phi \qquad 20.$$

Here it is important to note that for incompressible flows equation of state does not exist. In practice this means that the energy equation is decoupled from the other two equations. Therefore, we can first solve continuity and Navier-Stokes equations to find the unknown velocity and pressure distribution without knowing the temperature (We assume that fluid properties are taken to be constant, i.e. not functions of temperature). If fluid properties change with temperature all equations become coupled as in the case of compressible flows. After finding the velocity field, energy equation can be solved by itself to find the temperature distribution. However, for buoyancy driven flows (natural convection) where the density changes due to temperature variations are considered in the body force term of the momentum equation (Boussinesq approximation), all three conservation equations again become coupled. For isothermal (constant temperature) incompressible flows energy equation can be dropped and only the mass and linear momentum equations are solved to obtain the velocity and pressure fields. Numerical solution of incompressible flows is usually considered to be more difficult compared to compressible flows. The main numerical difficulty of solving incompressible flows lies in the role of pressure. For incompressible flows pressure is no longer a thermodynamic quantity and it cannot be related to density or temperature through an equation of state. It just establishes itself instantaneously in a flow field so that the velocity field always remains divergence free. [29]

Discretization model

After selecting the proper mathematical model, next step is to select the suitable discretization model. Discretization model is defined as a method of approximating the differential equations by system of algebraic equations for the variables at some set of discreet locations in space and time. There are 2 major approaches used for discretization Finite difference (FD) and finite volume (FV).

Most of the CFD software are using FV approach as Finite volume methods use piecewise constant approximation for integrals. This yields exact conservation statements and Finite Volume method integrates across the entire area and hence, chance of error is minimized. The key step in FV method is integrating the governing equation over the control volume to yield the discretized equation. The representation of control volume is,

$$\frac{\partial}{\partial t}\int_{v} \rho\phi \, dv + \oint_{A} \rho\phi \, v.dA = \oint_{A} \Gamma_{\phi} \, v\phi.dA + \int_{v} S\phi \, dv \qquad 21.$$

First term on left hand side is unsteady term and second is convection term. On the right-hand side first term is diffusion and other is generation/source. FV have direct interpretation of physical interpretation. Summation of diffusive flux entering and leaving from different faces is equal to amount of flux generated. Discretized equation must be set up at each nodal point to solve the problem. Simplifying the discretized equation will result into system of linear algebraic equation which can be solved further to obtain value of respective property.

Solution method

Discretization on given geometry yields a large system of non-linear algebraic equations. The method of solution depends on problem statement. As equation, which we got from discretization technique are non-linear, it is not possible to solve them directly and hence suitable iterative scheme is used to solve them. These methods use successive linearization of the equation and the resulting linear system can be solved by iterative technique. Some solver is,

- Gauss elimination
- Conjugate gradient method
- Conjugate gradient [30]

Rotational reference frame

A rotating reference frame approach is used in many CFD simulations. The disc brake rotor attached to the wheel rotates at the speed of the wheel. The flow inside the rotor is predominantly swirling and rotating. In problems involving rotating motion, CFX handles such a problem using rotating reference frame approach, shown in (Figure 19) [28] [29]

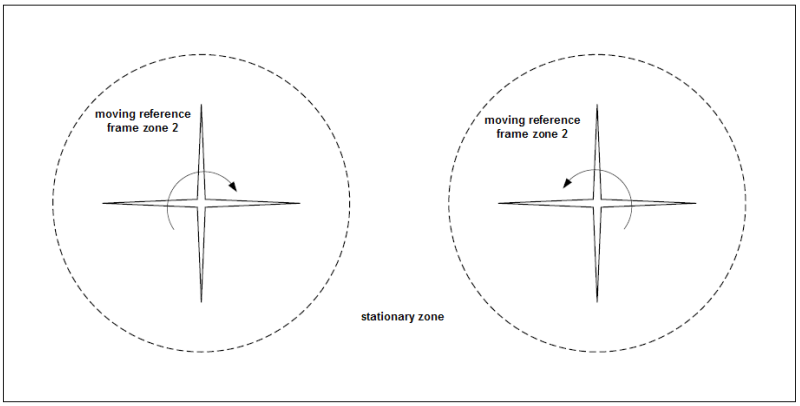

Figure 19: Example of rotating frame *[31]*

Modeling rotating frame gives lower computation time for analysis, lower storage space, easy for post processing analysis. There are many problems where it is advantageous to solve the equations in a moving (or non-inertial) reference frame. Such problems typically involve moving parts (such as rotating blades, impellers, and similar types of moving surfaces), and it is the flow around these moving parts that is of interest. In most cases, the moving parts render the problem unsteady when viewed from the stationary frame. With a moving reference frame, however, the flow around the moving part can (with certain restrictions) is modeled as a steady-state problem. [31]

Periodicity

Periodic boundary conditions are used to simulate a small portion of the rotor out of complete 360^0 deg. In vane brake rotor, geometry and flow pattern repeats itself after certain degree/period about the centerline. The flow exiting one periodic plane is same as the flow entering the other periodic plane. The domain must be cut somewhere from the rest of the world such that geometry and flow pattern must repeat. [31]

c. Turbulent Modeling

"Turbulence is that state of fluid motion which is characterized by apparently random and chaotic three-dimensional vorticity. When turbulence is present, it usually dominates all other flow phenomena and results in increased energy dissipation, mixing, heat transfer, and drag." [32]. Typical representation of turbulent flow shown in (Figure 20) used to derive RANS equation.

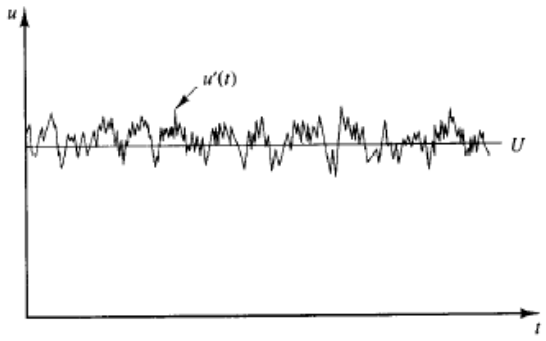

Figure 20: Typical representation of turbulent

Reynold Average Naviar Strokes (RANS)-based models

Analysis of different physical properties in turbulent flow is bit difficult task because of its random and chaotic nature. Hence, effect of turbulent flow on the gross properties of the flow is easy to analyze with good approximation. consequently, there is no need to solve for the instantaneous variables if averaged variables are all that is required. the instantaneous variables are decomposed into mean and fluctuating quantities:

$$U_i = \overline{U}_i + u_i \; ; \; P = \overline{P} + p \; ; \; H = \overline{H} + h \; ; \; C = \overline{C} + c$$

where the mean values are obtained by averaging over a time scale, which is long compared to that of turbulent motion. The Navier–Stokes equations govern the velocity and pressure of a fluid flow. In a turbulent flow, each of these quantities may be decomposed into a mean part and a fluctuating part. Averaging the equations gives

the Reynolds-averaged Navier–Stokes (RANS) equations, which govern the mean flow. The Reynolds stresses are additional six unknowns introduced by the averaging procedure, hence they must be modeled (related to the averaged flow quantities) to close the system of governing equations. Comparing number of unknown and number of equations, in RANS mode

- Three velocity components
- Six Reynolds stresses
- One pressure component

So, total ten unknown quantities and total number of equation are

- Continuity equation
- Three Momentum equation

Hence to solve the problem, less equation available compare to number of unknown. To solve it, we need turbulence modelling.

An algebraic equation is used to compute a turbulent viscosity, often called eddy viscosity. The Reynolds stress tensors then computed using an assumption which relates the Reynolds stress tensor the velocity gradients and the turbulent viscosity. This assumption is called the Boussinesq assumption. Models which are based on a turbulent (eddy) viscosity are called eddy viscosity model.

In eddy viscosity turbulence models the Reynolds stresses are linked to the velocity gradients via the turbulent viscosity: this relation is called the Boussinesq assumption, where the Reynolds stress tensor in the time averaged Navier-Stokes equation is replaced by the turbulent viscosity multiplied by the velocity gradients.

As viscous stresses are defined in NS equation, Reynolds stresses can be defined as

$$\tau_{ij} = -\rho\, u_i' u_j' = \mu_t \left(\frac{\partial U_i}{\partial X_j} + \frac{\partial U_j}{\partial X_i}\right) \qquad 22.$$

This is standard eddy-viscosity model for Reynolds stresses. μ_t is called as eddy viscosity or turbulent viscosity. The turbulent viscosity is not homogeneous, i.e. it varies in space. It is, however, assumed to be isotropic. It is the same in all directions. This assumption is valid for many flows, but not for all. [29].

K-Epsilon Turbulent Model

One of the most prominent turbulence models, the (k-epsilon) model, has been implemented in most general purpose CFD codes and is considered the industry standard model. It has proven to be stable and numerically robust and has a well-established regime of predictive capability. For general purpose simulations, the model offers a good compromise in terms of accuracy and robustness.

The k-ε model focuses on the mechanisms that affect the turbulent kinetic energy k. The instantaneous kinetic energy k(t) of a turbulent flow is the sum of mean kinetic energy K. Turbulent kinetic energy. By deriving the mean flow kinetic energy K and turbulent kinetic energy k, model equation of kinetic energy can be calculated. Following model equation for k is commonly used.

$$\frac{\partial(\rho k)}{\partial t} + \mathrm{div}(\rho k U) = \mathrm{div}\left[\frac{\mu_t}{\rho_k}\mathrm{gard}\ k\right] + 2 * \mu_t E_{ij.} E_{ij.} - \rho\varepsilon \qquad 23.$$

The equation for k contains additional turbulent fluctuation terms, that are unknown. Again, using the Boussinesq assumption, these fluctuation terms can be linked to the mean flow. In physical term, it can be defined as,

Summation of Rate of increase and convective transport is equal to summation of diffusive transport and rate of production minus rate of destruction.

A model equation for ε is derived by multiplying the k equation by (ε/k) and introducing model constants. The following (simplified) model equation for ε is commonly used

$$\frac{\partial(\rho\varepsilon)}{\partial t} + \mathrm{div}(\rho\varepsilon U) = \mathrm{div}\left[\frac{\mu_t}{\sigma_\varepsilon}\mathrm{gard}\,\varepsilon\right] + C_{1\varepsilon}\frac{\varepsilon}{k}2\mu_t E_{ij.}E_{ij.} - C_{2\varepsilon}\rho\frac{\varepsilon^2}{k} \qquad 24.$$

The physical interpretation of equation is, Summation of Rate of increase and convective transport is equal to summation of diffusive transport and rate of production minus rate of destruction.

Standard values of all the model constant are fitted with benchmark experiments (Launder and Sharma, Heat, and mass transfer 1974) Typically values for the model constants C1ε and C2ε of 1.44 and 1.92 are used. After getting values of turbulent kinetic energy and turbulent dissipation rate, Reynolds stresses can be calculated defined in Basqueness formulae. Within CFX, the turbulence model uses the scalable wall function approach to improving robustness and accuracy when the near-wall mesh is very fine. This is two equation model in the RANS-based model class. Rotating brake disc doesn't experience that high-pressure gradients compared to a compressor-turbine case, hence this model is used by most of the researched for Brake cooling analysis. [30]

d. Properties and Error Associated in Numerical Solution

Numerical solution of any fluid flow or heat transfer problem is approximate solution. It is because, error that might be introduce in course of development of solution or during setting up the boundary conditions. Numerical solution includes mainly following errors

- Modelling error
- Discretization error

Modeling error

Modeling errors are those due to uncertainty in the formulation of the model and deliberate simplifications of the model. Converting the model to discrete form is a part of discretization errors. Errors in the modeling of the fluids or solids problem are concerned with the choice of the governing equations which are solved and models for the fluid or solid properties. Further, the issue of providing a well-posed problem can contribute to modeling errors. Even when a physical process is known to a high level of accuracy, a simplified model may be used within the CFD for the convenience of a more efficient computation. These errors are not known a prior; they can only be evaluated by comparing solutions in which the discretization and convergence error are negligible.

Discretization error

Discretization errors are those errors that occur from the representation of the governing flow equations and other physical models as algebraic expressions in a discrete domain. The discrete spatial domain is known as the grid or mesh. Discretization error is also known as numerical error. A consistent numerical method will approach the continuum representation of the equations and zero discretization error as the number of grid points increases and the size of the grid spacing tends to zero. As the mesh is refined, the solution should become less sensitive to the grid spacing and approach the continuum solution. This is grid convergence. The grid convergence study is a useful procedure for determining the level of discretization error existing in a CFD solution. The discretization error is of most concern to a CFD during an application. Discretization errors are of major

concern because they are dependent on the quality of the grid; however, it is often difficult to precisely indicate the relationship between a quality grid and an accurate solution prior to beginning the simulation. The level of discretization error is dependent on grid quality. The grid should be generated with consideration of such things as resolution, density, aspect ratio, stretching, orthogonality, grid singularities, and zonal boundary interfaces.

Properties of numerical solution

The solution methods which are used to solve discretized equation should have certain properties to trust the result obtained from it. In most cases, it is not possible to analyze the complete solution methods so, few component of method can be analyzed. if the component doses not possess the desired properties, neither the method and solution. The most important properties are summarized below.

Stability

The numerical solution is said to be a stable if it does not magnify the error that appears in course of numerical solution process. For an iterative method, a stable method is one the does not diverge. For stability analysis, post processing results can be used. Analysis of residues can be a good point to check if the solution is stable or converging or diverging.

Convergence

Non-linear problem which are strongly influence by boundary condition, the stability and convergence of method are difficult to demonstrate. Therefore, convergence is usually checked using numerical experiments., i.e. repeating the calculations on series of successive refined grids. If the method is stable and if all the approximations used in discretization process are consistent, we usually find that the solution does not converge to gird-independent- solution.

Conservation

Equations that are solved for problem are conservation laws. This means that at steady state and in absence of source, the amount of conserved quantity leaving a close volume in equal to amount of entering the volume. This is an important property of solution method, since it imposes the constrain on solution error. If conservation of mass, momentum and energy is ensured, the error can only improperly distribute these quantities over the solution domain.

Boundedness

Boundedness is defined as physically non-negative quantities. Like density, KE of turbulence. Those quantities must always positive. If the solution is not bounded, it is an indication that the error in solution are large and grid need some refinement. [30]

5. CFD MODELING

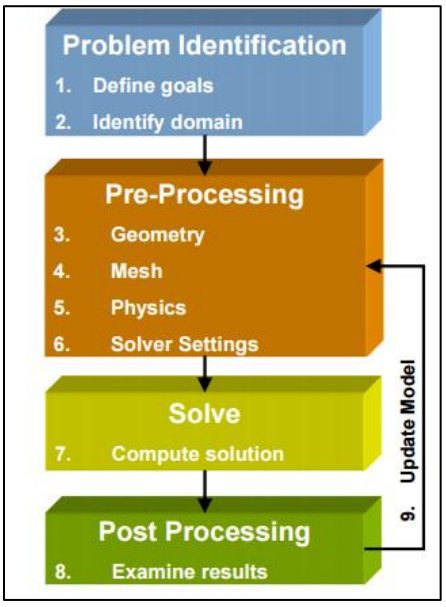

Figure 21: CFD modeling overview

(Figure 21) shows basic workflow of CFD modeling. To carry out, CFD analysis following steps is used.

1. Pre-processing

This is the first step of CFD simulation process which helps in describing the geometry in the best possible manner. Identify the fluid domain of interest. The domain of interest is then further divided into smaller segments known as mesh generation step.

2. Solver setting

Once the problem physics has been identified, fluid material properties, flow physics model, and boundary conditions are set to solve using a computer. Using this software; it is possible to solve the governing equations related to flow physics problem.

3. Post-processing

The next step after getting the results is to analyze the results with different methods like contour plots, vector plot, streamlines, data curve etc. for appropriate graphical representations and report.

a. Geometric Modeling

To start with Pre-Processing, desired geometric model must be available. Following brake rotors were considered for computational analysis.

Table 1: 44 Straight vane rotor specifications

Design parameters	Numerical value
Number of vanes	44
Outer diameter (m)	0.343
Inner diameter (m)	0.233
Vane thickness (m)	0.005

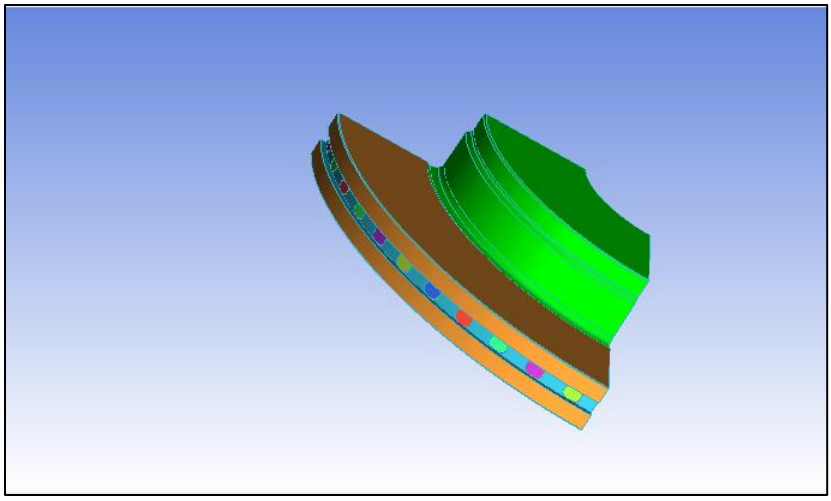

Figure 22: CAD model of 44 straight vanes

(Table 1) shows detailed geometric parameters. As shown in (Figure 22), 44 straight vane brake rotor was used for case comparison and to calculate the initial Heat flux. Taking a certain part and applying periodic boundary condition can save computational time and memory. The brake rotor is periodic in nature and hence an angle of 90^0 degrees was considered for analysis. In the given rotor, 11 number of vanes were analyzed in 90^0 degree. The respective angle between successive vanes is calculated to be 8.18^0 degrees.

b. Meshing

A mesh can be defining as a discretization of geometry into a small subdomain. To analyze fluid flows and heat transfer, flow domains are split into smaller subdomains. The governing equations are then discredited and solved inside each of these subdomains.

Meshing can be a triangular, quadrilateral, tetrahedral, or hexahedral. The subdomains are often called elements or cells, and the collection of all elements or cells is called a mesh or grid where physics calculates the respective parameters on each node point. [33]

e. Types of meshing

1. Tetrahedron

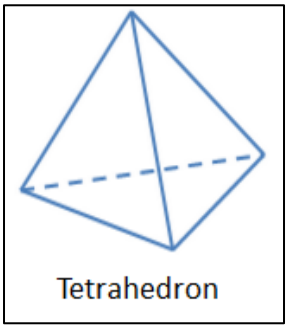

Figure 23: Tetrahedron mesh representation

(Figure 23: Tetrahedron mesh representation) shows typical tetra mesh. The ANSYS ICEM CFD Tetrameter takes full advantage of object-oriented unstructured meshing technology. With no tedious up-front triangular surface meshing required to provide well-balanced initial meshes, ANSYS ICEM CFD Tetra works directly from the CAD surfaces and fills the volume with tetrahedral elements using the Octree approach. A powerful smoothing algorithm provides the element quality. Options are available to automatically refine and coarsen the mesh both on geometry and within the volume. Also included are a Delaunay algorithm and an Advancing Front algorithm to create tetras from an existing surface mesh and to give a smoother transition in the volume element size. The Delaunay

method is robust and fast; the advantage of the Advancing Front method is its ability to generate a smoothly transitioning Tetra mesh with a controlled volume growth ratio. [33]

2. Hexahedron

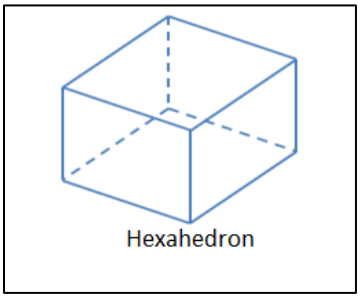

Figure 24: Hexahedron mesh representation

The ANSYS ICEM CFD Hexa mesher is a semi-automated meshing module which allows rapid generation of multi-block structured or unstructured hexahedral volume meshes. (Figure 24) shows typical hexahedral mesh. ICEM CFD hexa represents a new approach to grid generation where the operations most often performed by experts are automated and made available at the touch of a button. Blocks can be built and interactively adjusted to the underlying CAD geometry. This blocking can be used as a template for other similar geometries for full parametric capabilities. Complex topologies, such as internal or external O-grids can also be generated automatically. For the same cell count, hexahedral meshes will give more accurate, especially if the grid lines are aligned with the flow. [33]

3. Prism

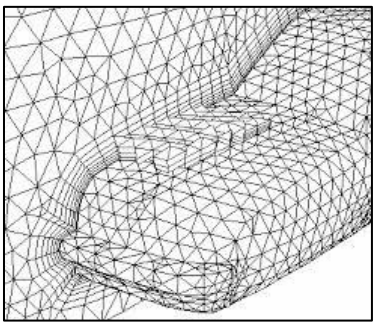

Figure 25: Prism layer mesh representation

ANSYS ICEM CFD Prism generates hybrid tetrahedral or hexahedral grids consisting of layers of prism elements near the boundary surfaces and tetrahedral or hexahedral elements in the interior for better modeling. A typical example of tetra meshing with prism layer is shown in (Figure 25) Compared to pure tetrahedral or hexahedral grids, prism layer at boundary gives the better convergence of the solution and better analysis results. [33]

Meshing details for vane rotor

Mesh skewness:

This determines how much the mesh cell/ elements differ from an ideal mesh cell or element. The maximum value thus obtained is normalized so that 0 corresponds to a bad element and 1 corresponds to a perfect cube. In short it means how closely the element is close to the cube.

Mesh aspect ratio:

It is the ratio of the longest edge length to the shortest edge length. If ratio is not equal to 1 which means, it's not perfectly square and its rectangular. So the increased aspect ratio may not give the best accurate results. Also for a triangle an equilateral triangle has the perfect aspect ratio, but as we stretch, it will give a bad aspect ratio. These values are scaled so that an aspect ratio of 1 is perfectly regular, & an aspect ratio of 0 indicates that the element has zero volume. So as in the figure above, if the triangle is stretched too much it will end-up with zero volume & thereby forming the worst cell/ element. For vane brake rotor, aspect ratio is greater than 0.6

Determinant

Determinant – (Smallest determinant of the Jacobian Matrix / Largest determinant of the Jacobian Matrix) where each determinant is calculated at each node of the element. In general, determinant value > 0.3 is acceptable to most solvers.

c. Grid Sensitivity Analysis

Grid sensitivity analysis involves performing the simulation on two or more successively finer grids. As the grid is refined (grid cells become smaller and the number of cells in the flow domain increase) the spatial and temporal discretization errors should asymptotically approaches zero, excluding computer round-off error. The ratio of number of grid points in each direction of a one level of grid to another is called refinement ratio(r). Richardson's extrapolation (Richardson [1910]) links the exact solution of the partial differential equations to the solution due to the presence of a grid using Taylor series of expansions.

$$f_{exact} = f_1 + \frac{(f_1 - f_2)}{(r^p - 1)} \qquad 24.$$

Where, f_{exact} is the exact solution of the equation, f1 is the fine grid solution and f2 is the coarse grid solution, p is the order of the discretization method and r is the refinement ratio. One should often start with a grid resolution and then conduct a series of grid refinements to assess the effect of grid resolution. This is known as a grid refinement study.

Roache has provided a methodology for the uniform reporting of grid refinement studies. The basic idea is to approximately relate the results from any grid refinement test to the expected results from a grid doubling using a second-order method. The GCI is a measure of the percentage the computed value is away from the value of the asymptotic numerical value. It indicates how much the solution would change with a further refinement of the grid. A small value of GCI indicates that the computation is within the asymptotic range.

The GCI on the fine grid is defined as:

$$GCI_{12} = \frac{F_s|E|}{(r^p - 1)}, \quad E = (f_2 - f_1) / f_1 \qquad 25.$$

$$GCI_{23} = \frac{F_s|E|}{(r^p-1)}\ ,\ E = (f_3 - f_2) / f_2 \qquad 26.$$

where F_s is a factor of safety. The refinement may be spatial or in time. The factor of safety is recommended to be F_s=3.0 for comparisons of two grids and F_s=1.25 for comparisons over three or more grids. The higher factor of safety is recommended for reporting purposes and is quite conservative of the actual errors. The grid is made finer in two stages. First the coarse grid is converted into an intermediate grid and then to a still finer grid. The values are then verified so that they lie in the asymptotic range. Roache [1998] has proposed an expression for verification of asymptotic range using the grid convergence index.

$$\frac{GCI_{23}}{r^p\ GCI_{12}} \cong 1 \qquad 27.$$

Where, GCI_{21} is the fine grid convergence index by coarsening the grid from medium to course grid, GCI_{32} is the grid convergence index by coarsening the grid from fine to medium grid, r is the refinement ration and p is the order of convergence of the discretization method.

Grid independent study

The datum rotor was taken as reference to carry out the grid sensitivity analysis. With 804RPM (approximately 128 Km/h) with cell count of 3000000 and initial case was run. Wall convective heat transfer coefficient whose grid dependency is analyzed.

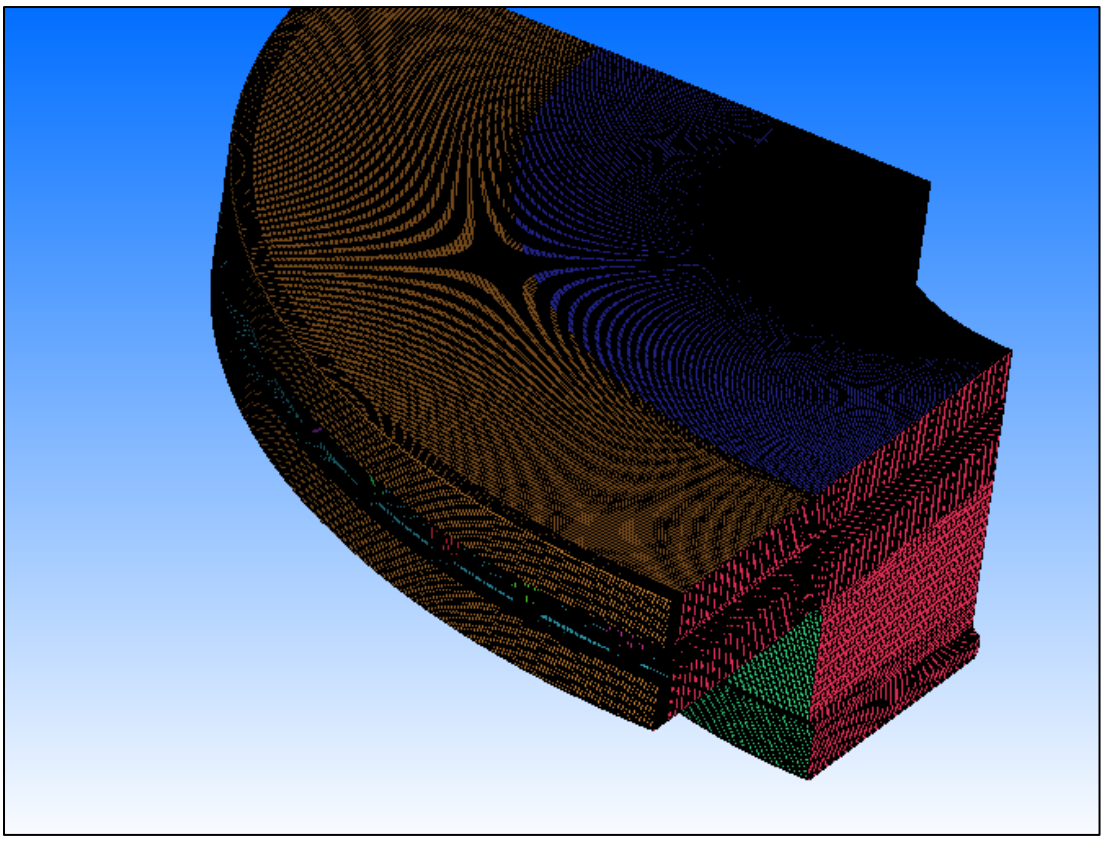

Figure 26: Fine mesh model

The Fine grid model shown in (Figure 26) was made cores by subtracting the number of cells in each direction by a factor of 1.5 to reduce the total number of grid points. This mesh is referred to as a medium grid with 2000000 cells.

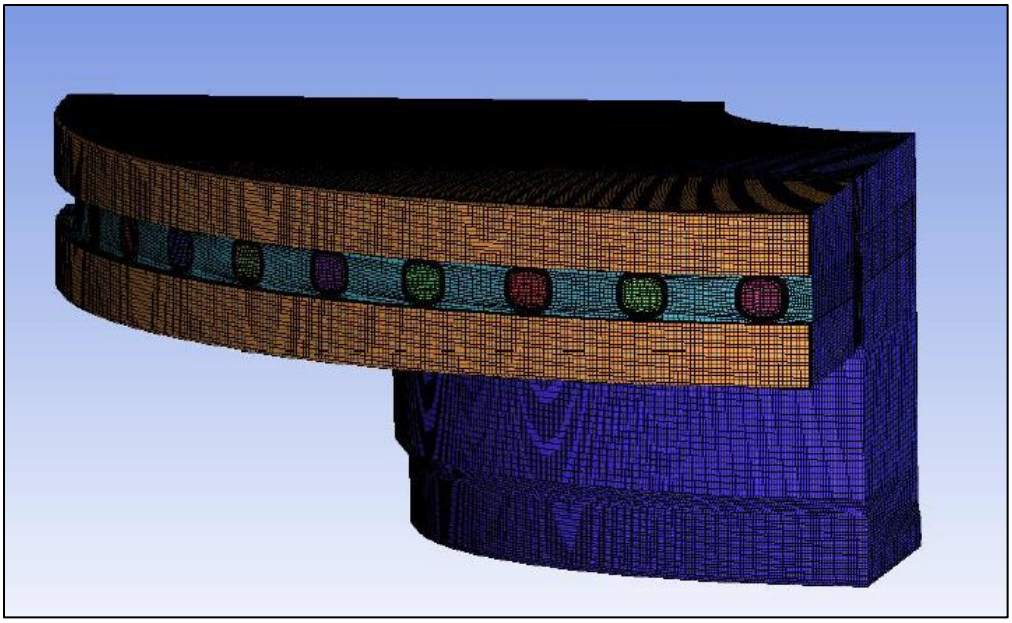

Figure 27: Medium mesh model

The medium mesh model shown in (Figure 27) was further coarsened by reducing the grid points in each direction by a factor of 1.5 thus reducing the total number of grid 1333333. This mesh is referred to as a coarse grid

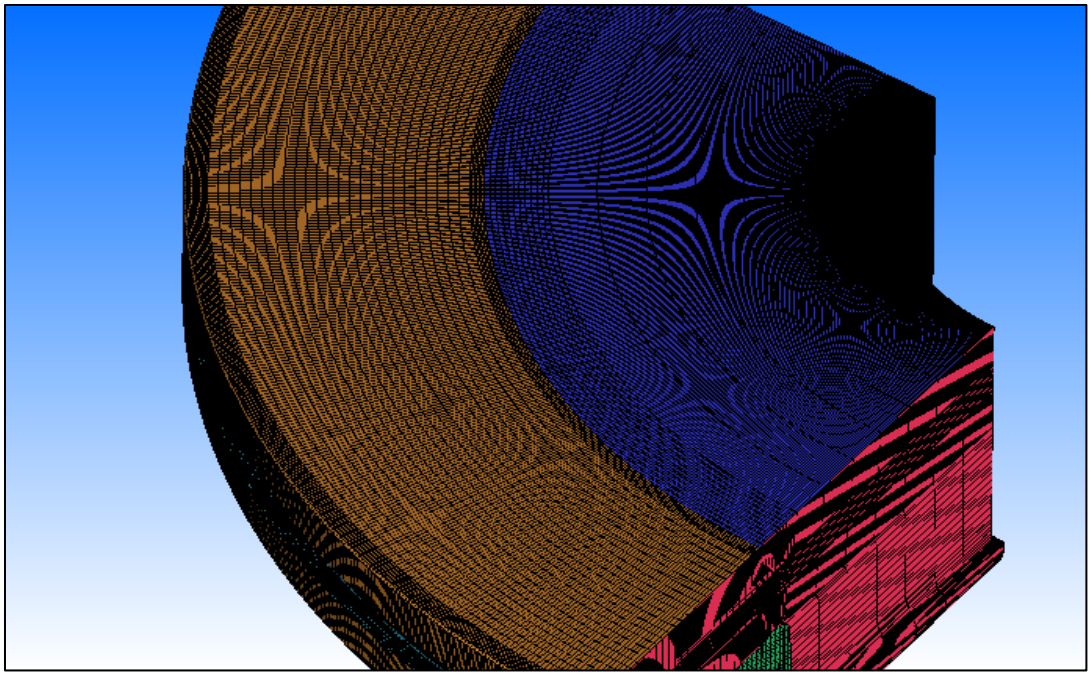

Figure 28: Cores mesh model

Table 2: Effect of mesh size on wall convective heat transfer co-efficient

Grid Size	**Wall convective heat transfer coefficient (W/m^2K) 804RPM**
Fine mesh (f_3)	99.5
Medium mesh (f_2)	97.5
Coras mesh (f_1)	94.0

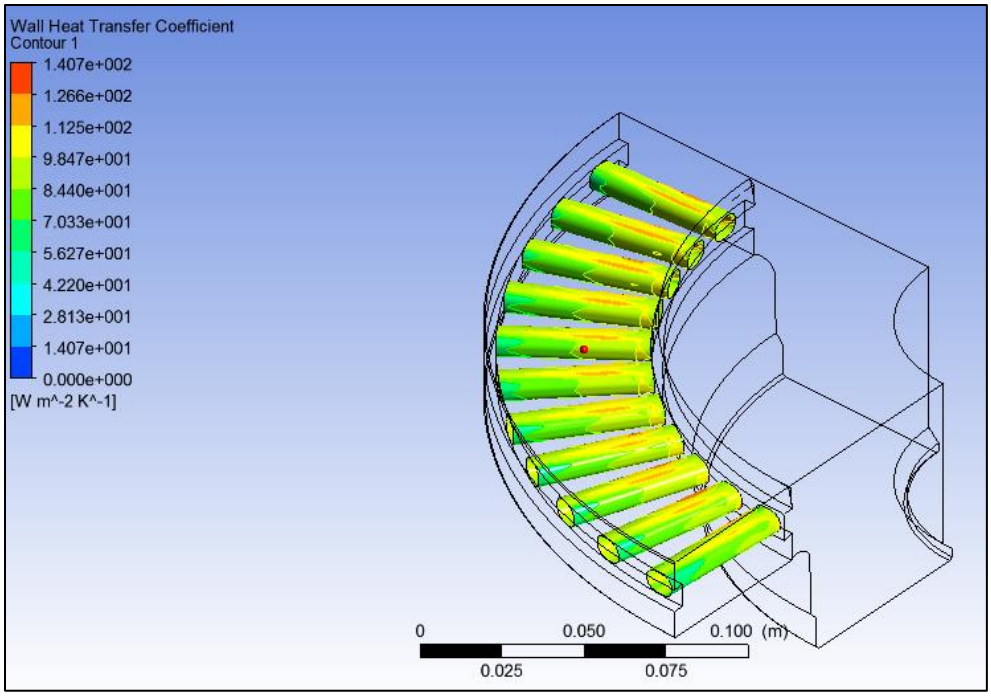

Figure 29: Wall convective heat transfer coefficient for cores mesh

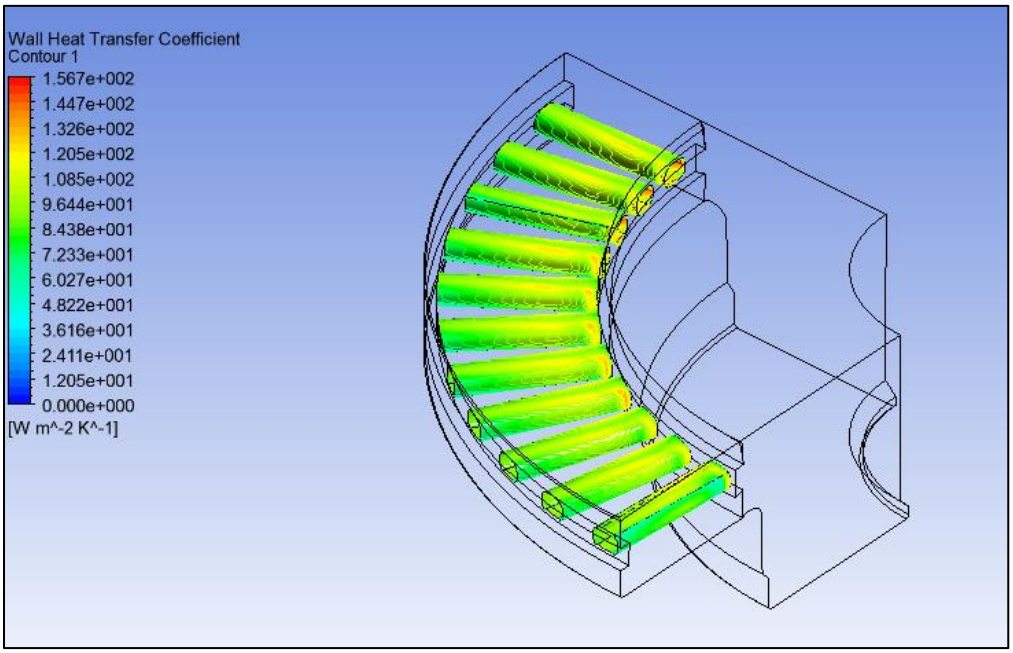

Figure 30: Wall convective heat transfer coefficient for medium mesh

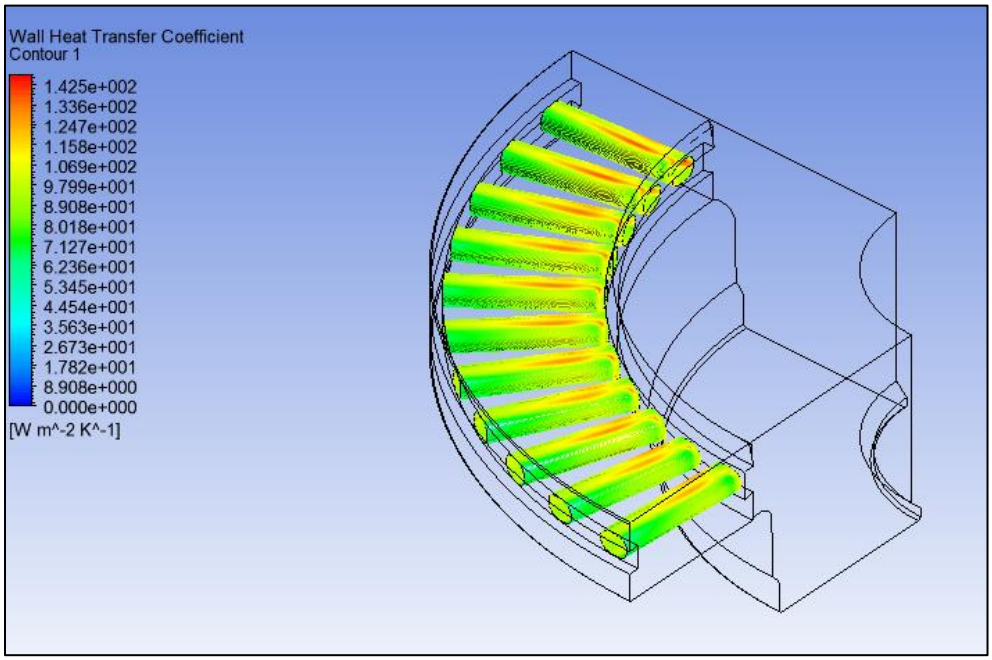

Figure 31: Wall convective heat transfer coefficient for fine mesh

To calculate the order of convergence, following formula is used,

$$p = \frac{\ln\left(\frac{f_3 - f_2}{f_2 - f_1}\right)}{\ln(r)} \qquad 28.$$

$$p = \ln [(98.5- 97.5) / (97.5 - 97)] / \ln(1.5) = 1.7$$

The theoretical order of convergence is p=2.0. The difference is most likely due to grid stretching, grid quality, non-linearity in the solution, turbulence modeling.

We now can apply Richardson extrapolation using the two finest grids to obtain an estimate of the value of the wall convective heat transfer coefficient at zero grid spacing per equation 24,

$$f_{h=0} = 98.5 + (97 – 97.5) / (2^{1.7} - 1)$$

$$= 98.1$$

The GCI is evaluated for convective heat transfer coefficient. The GCI for a medium grid by increasing the number of cells from a course grid is calculated as follows, according to equation 25.

$$GCI_{12} = 1.25 * (97.5- 97) / 97 / (1.5^{1.7} - 1) = 0.006493$$

According to equation no 26,

$$GCI_{23} = 1.25 * (98.5 – 97.5) / 97 / (1.5^{1.7} - 1) = 0.01398$$

For the solution to lay in the asymptotic range the following condition has to be fulfilled. According to equation no 27,

$$\frac{GCI_{Fine}}{r^{p} * GCI_{medium}} \cong 1$$

$$0.6493 / (1.5^{1.7} * 1.398) = 0.96$$

which is approximately one and indicates that the solutions are well within the asymptotic range of convergence.

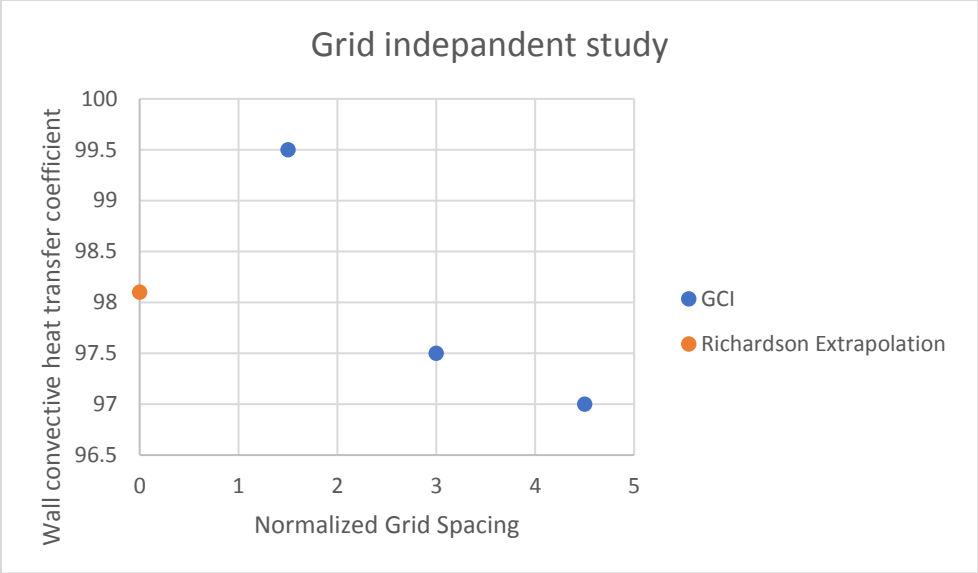

Figure 32: Gird independent study

Higher grid sizes lead to better resolution of the convective heat transfer coefficient leading to a more realistic solution. Wall convective heat transfer coefficient did not change by significant amount from medium mesh to fine mesh shown in (Figure 32) as well as GCI index is approximately 1 and hence at this point, we can conclude that solution is grid independent.

d. Error Analysis

To trust CFD solution, it should satisfy following properties. If the solution satisfied following properties, it can be concluded that the given computational solution is good approximation of exact solution.

Convergence

At convergence, the following should be satisfied:

All discrete conservation equations (momentum, energy, etc.) are obeyed in all cells to a specified tolerance or the solution no longer changes with subsequent iterations. Overall mass, momentum, energy, and scalar balances are achieved. Convergence can be monitored using residual history,

- Generally, a decrease in residuals by three orders of magnitude indicates at least qualitative convergence. At this point, the major flow features should be established.
- Scaled energy residual must decrease to 10^{-6} (for the pressure-based solver).

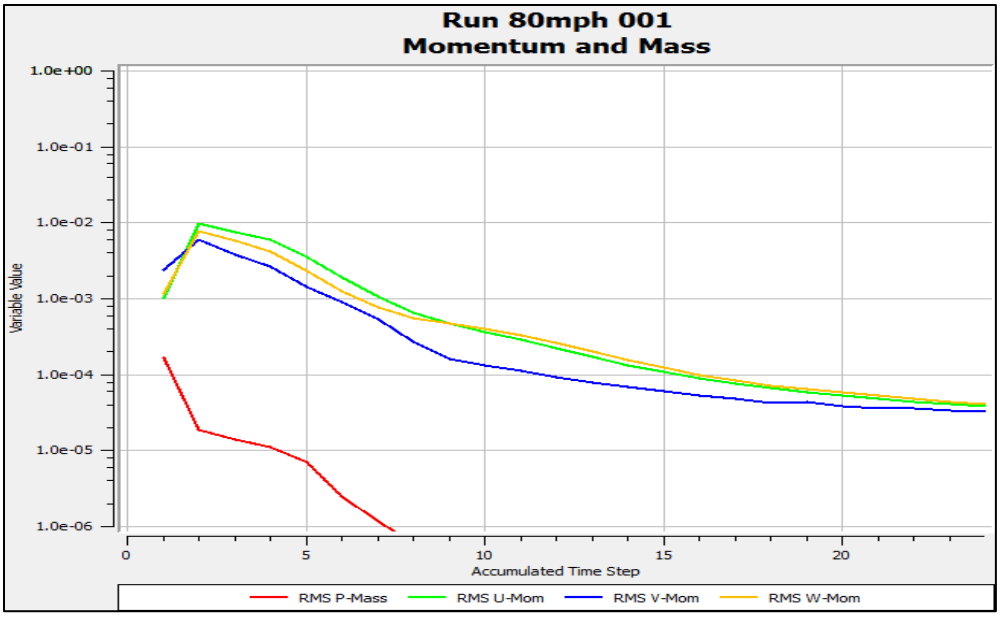

Figure 33: Residual plot for vane brake disk rotor

For stability analysis, residual plots can be used. Which will give good estimation about error is converged or diverged. Looking at residual plots shown in (Figure 33) for vane brake rotor, it can be concluded that solution is stable as residues are converged and error are not magnified in course of numerical solution process.

Conservation

To analyze the conservation, one need to see how much quantity is going into system and how much mass is coming out of the system. At steady state and in absence of source. comparing the mass and momentum entering system and leaving out of the system, we can conclude that conservation of quantities is achieved. In addition to residuals, overall heat and mass transfer can be checked. It is also good practice to check if solution is converged per tolerance criteria and not by maximum number of iterations. For the current simulation, solution stopped according to tolerance criteria.

Table 3: Mass flow inlet and outlet

Mass flow @inlet	Mass flow @outlet
$3.99*10^{-7}$ kg/sec	$-4.02*10^{-7}$ kg/sec

Looking at above table of mass flow inlet and outlet, conservation of mass is achieved.

Boundedness

To analyze the boundedness, physical quantities such as KE, velocity must be positive. for given problem all physical quantities like velocity, turbulent KE are positive and hence we can conclude that solution is boundedness.

e. Case Comparison

In industry, a fast and efficient process is always preferable due to the tough competition. Computer Aided Engineering (CAE) is assumed to be an efficient and result-oriented process. CAE analysis gives good estimation over the structural and thermal behavior of the system. In the case of brake rotor design, it is not feasible to manufacture the different designed rotors and conduct an actual experimental study on them. Instead, CAE analysis can give a rough estimation of the result, which reduces manufacturing cost and time.

As far as this thesis is concerned, the primary property that will be evaluated is wall convective heat transfer coefficient. To trust a model or a simulation, a correlation of some kind needs to be present. This section will, therefore, handle the correlating/comparing part of this study. This part of the study is made for having a trustworthy and well-defined model which can be compared with experimental tests.

i. Experimental procedure and test methodologies for analysis of brake rotor cool down test

The experiment was conducted in GM facility. The test method used for analysis of vane brake rotor cooling is described below.

Test track location and information

The test was conducted on Milford Proving Ground at GM Corporation shown in (Figure 34). For the brake cooling analysis test, the oval track was used. It is a 3.8-mile circuit with four lanes posted with speed limits increasing towards the outermost lane. The speed limit for the outermost lane is 120MPH. The outermost lane has banking, so at a higher speed, no steering input is required.

Rotor specification

Baseline rotor is used for experiment. Rotor specifications are provided in Chapter 6 section c.

Figure 34: Arial view of oval track MPG, GM facility *[7]*

Test methodology/procedure

The rotors were heated to 814K (1000^0F) by performing snubs from 80 mph to 20 mph at the highest possible deceleration without locking the wheels or activating ABS. (snub can be defined as harder brake apply and release). Upon completion of the final snub, the driver accelerated the vehicle to 80 mph and triggered the instrumentation to start recording. The vehicle maintained a steady speed of 80 mph until the rotor temperatures reached a point where the average rotor temperature dropped less than 5^0F within a

minute. Eight temperature sensors were mounted on four brake discs, where each brake rotor consisted of two sensors, one from the inside of rotor and another from outside of the rotor. The average of eight rotor temperatures was used for analysis.

Brake rotor cool down test data

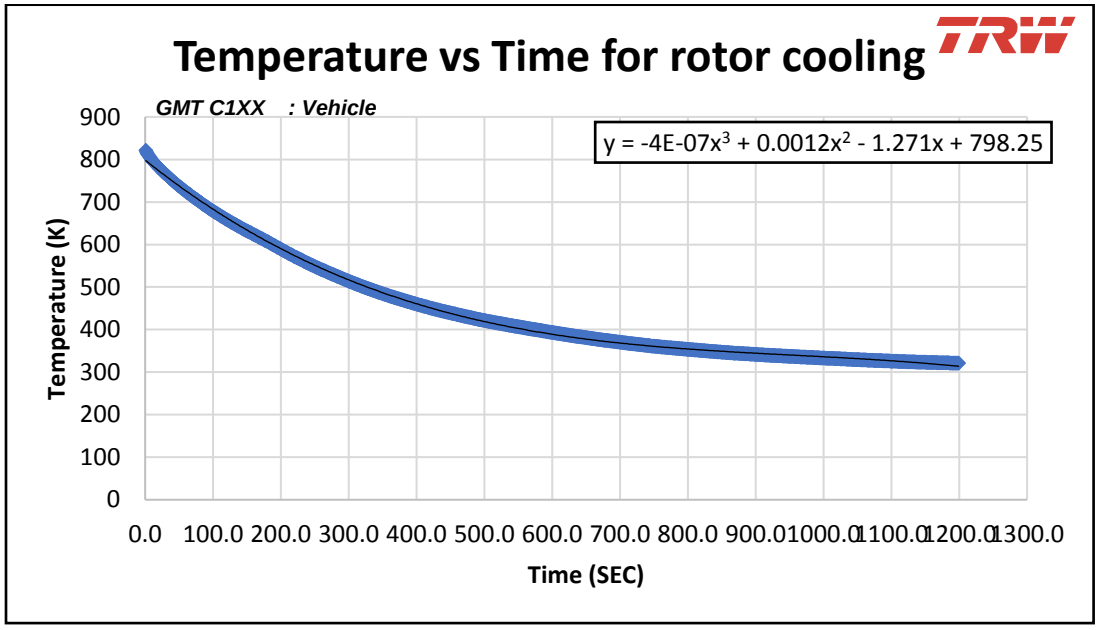

Figure 35: Experimental transient analysis for temperature vs time

(Figure 35) shows the experimental cool down test for the 44-straight vane rotor. The curve follows a cubic polynomial equation of,

$$y = -4 * 10^{-7}x^3 + 0.0012x^2 + 1.271x + 798.25 \qquad 29.$$

The rotor reached the steady state temperature after 20 min at 312 K. It was very difficult to monitor the temperature of each rotor individually at 814K so, an average of eight temperatures was considered and as the average rotor temperature rises above 814K, vehicle was driven at a steady speed for cooling analysis.

ii. CFD model, Transient analysis

To compare the CFD model's efficiency and accuracy, results of CFD model were compared with experimental data given by TRW automotive.

The following assumptions are made for CFD analysis

- Flow is assumed as incompressible, viscous, and turbulent
- External walls of the brake rotor disk are modeled as convective heat transfer.
- The ambient temperature for convection is taken as 300 K.
- Mass momentum and energy equations are solved using Ansys CFX RANS solver
- Inlet and outlet boundary are open to atmosphere.
- Outlet boundaries are defined as pressure outlet.
- Moving reference frame at 804RPM (80mph for 285/55 R20 tire)
- Standard k-epsilon vicious turbulence model

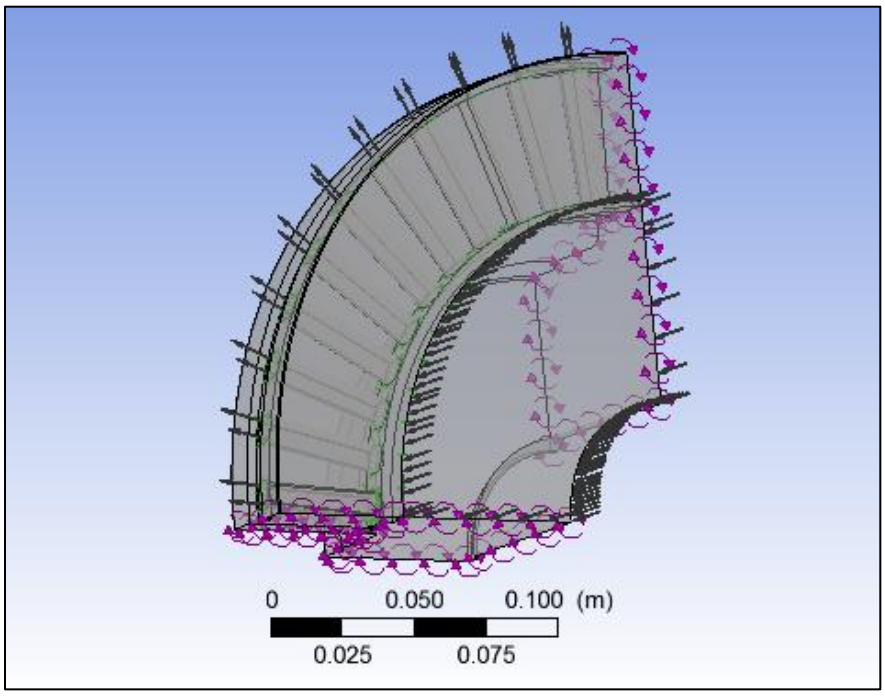

Figure 36: Geometric model prepared for simulation

Shown in (Figure 36), Inlet, outlet, and periodicity were defined to 44 straight vane model.

As described above the test procedure for vehicle brake rotor, TRW measures only temperature drops on rotor's outer surface, as K type modular thermocouple is attached to it. So, to calculate the heat flux data for brake rotor the following procedure was used.

- In steady state analysis, rotors wall was given a boundary condition of a surface temperature at 814K and heat flux is calculated.

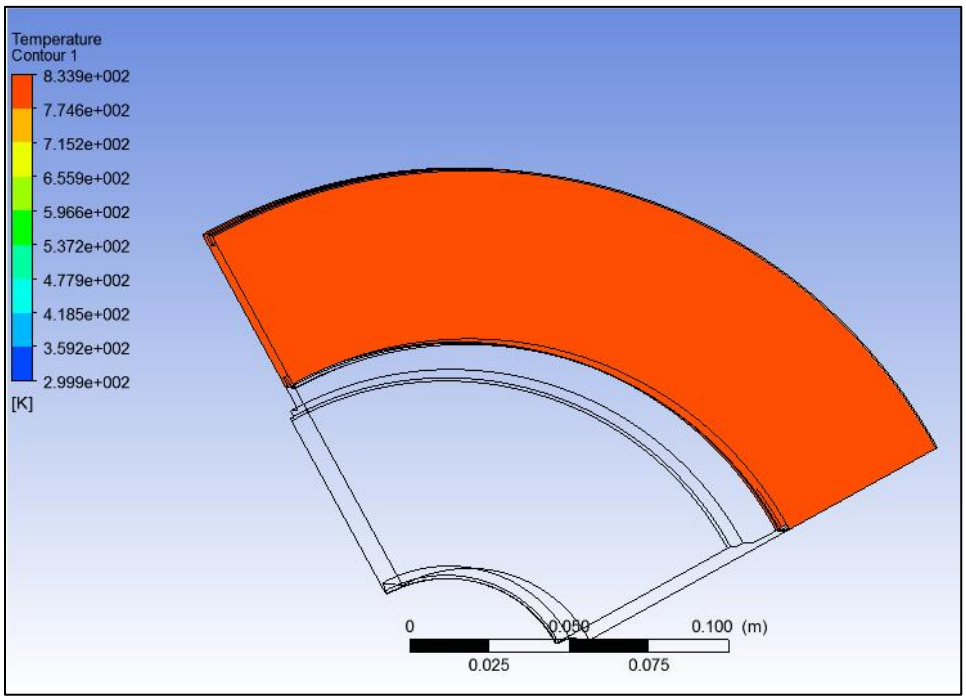

Figure 37: Brake disc wall temperature boundary condition

(Figure 37) shows the temperature profile of brake rotor, where wall temperature was defined as 814K

- Calculated heat flux was used for the second simulation as a boundary condition and temperature of brake wall was calculated.

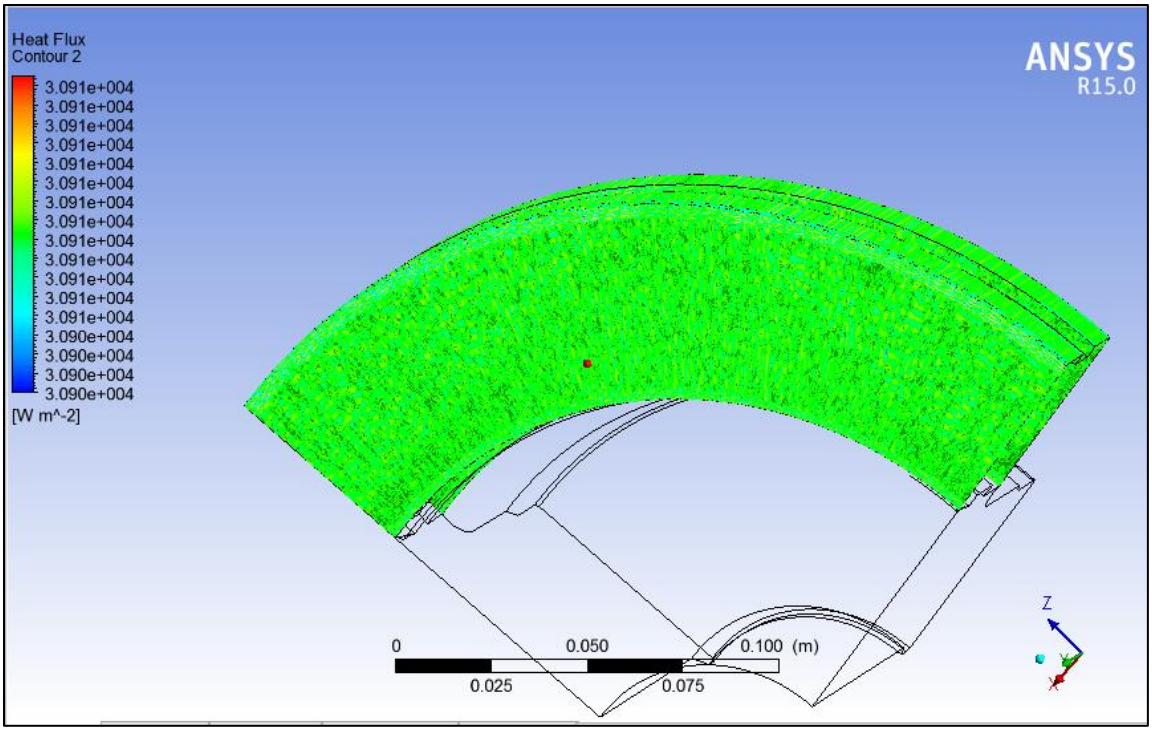

Figure 38: Calculated heat flux from temperature boundary condition

(Figure 38) shows heat flux after imposing temperature boundary condition. Heat flux value was found to be 30906 W/m^2. This value was further imposed on the brake disk walls to carry next simulations.

To compare the CFD model with experimental analysis only single transient analysis was done for 80 MPH. For transient analysis, Heat flux was given as boundary condition and the temperature was recorded. The transient analysis monitored the time and temperature. From the transient analysis, we could compare the amount of time required to reach the steady state.

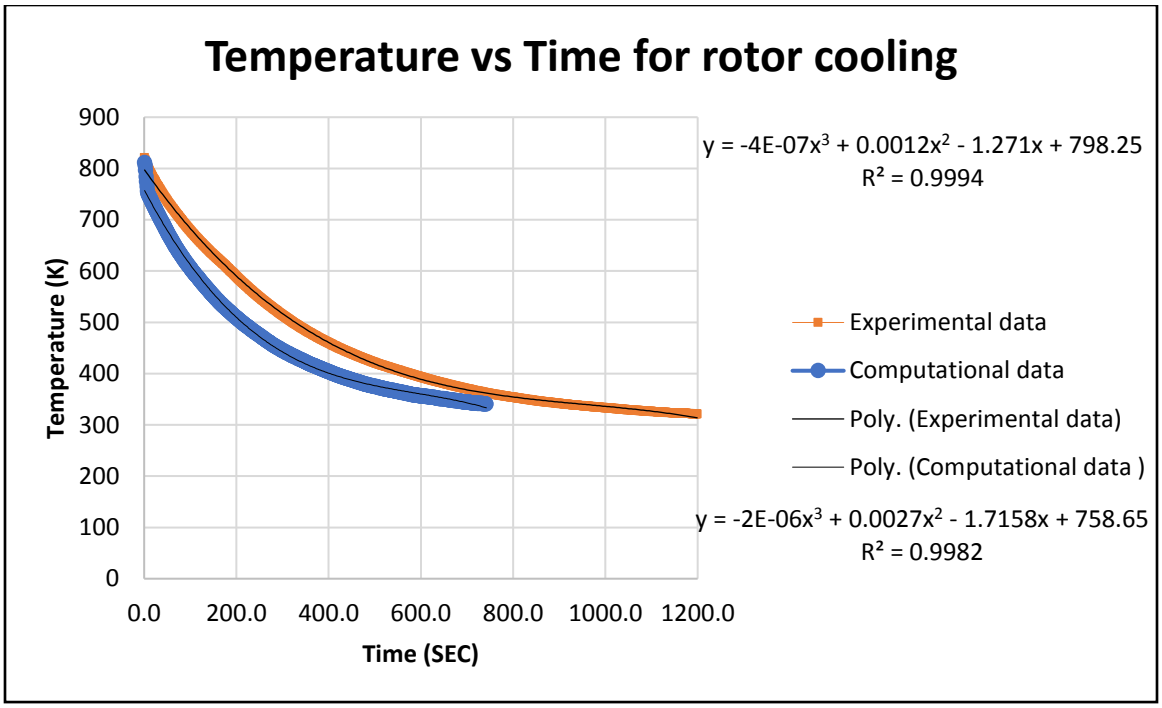

Figure 39: Computational and experimental results

Trendline function was used to calculate the response model for computational and experimental analysis. As seen in (Figure 39), the temperature vs time graph is polynomial with third order. As explained earlier average rotor temperature for the experiment was greater than 814K; wherein computational analysis it was possible to start the simulation at exact 814K. It can be seen from the graph that both cooling curves followed third order polynomial function. For an experimental model, temperature reached steady state in 20 minutes at 312K; whereas for the computational model it took 13.3 minutes to reach steady state at 342K. The time take to reach steady state in the computational model was lower.

Table 4: Experimental and computational results for rotor cooling

	Experimental	Computational
Steady state temperature (K)	321	342

As shown in the (Table 4) comparisons of experimental and computational results for steady state temperature and time taken to reach it.

Now for analysis of inverse condition, after imposing the generated heat flux as boundary condition to brake rotor for steady state analysis, average rotor temperature was noted as 342K

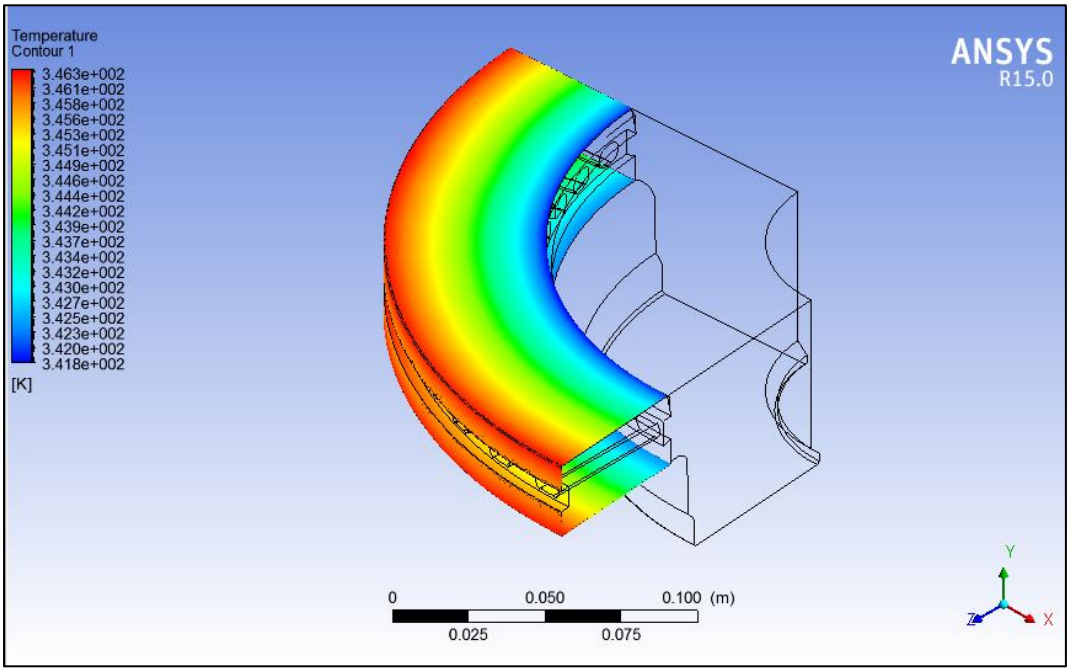

Figure 40: Steady-state temperature of brake wall

Generated heat flux was given as boundary condition and steady state analysis was run on 44 straight vane rotors. As shown in (Figure 40), steady state temperature of brake rotor after imposing heat flux as a boundary condition. From the above analysis, it can be concluded that computational model used for analysis is in good agreement with the experimental results.

f. Limitations for correlation of CFD and experimental data

For experimental model, steady state temperature reached at 317.09 K, where for computational model steady state temperature reached at 342.02 K. In the actual experiment, time taken to reach the steady state was 1200 sec (20min), wherein computational analysis time take to reach steady state was 800 secs (13.33 min). Although, the main purpose of the correlation study was to validate the assumptions, CFD model, and technique which were used for this thesis. CFD analysis was performed with a vane type disc brake rotor and not with the complete vehicle model. Only the convective flow behavior was studied. The brake disc temperature was assumed to be constant over the surface as it also depends on brake load, which makes analysis complex. Steady-state thermal analyses were used in this study for the conclusion

Following might be reasons for deviation of computational and experimental results:

- Coating or anodization on rotor

Anodizing is an electrochemical process that converts the metal surface into a durable, corrosion-resistant, anodic oxide finish. Anodizing increases the emissivity of the rotor where the black coating gives emissivity up to 0.9. Due to company restriction, this value was not available and hence the general value of gray cast iron of 0.5 was chosen for simulation. At 814K radiation might play a major role with greater emissivity which might be a point of concern.

- Location of thermocouple

Two thermocouples were mounted on the rotor, one was on the outer surface and another on inner surface. Generated heat at rotor pad interface conducted through the material. Hence the temperature indicated by the thermocouple may not be accurate.

- Effect of cruise control

The test was conducted on the oval track at Milford Proving Grounds (MPG, GM facility center). Per the standard test procedure, one needs to maintain a constant speed of

80MPH as soon as rotor's desired temperature is achieved. It was difficult to maintain constant speed because of slopes and relying on track. Cruise control was disabled because it communicates with engine and brake to maintain desired speed. If the speed is increasing the corrective braking action can take place which is not desirable in this case as it will increase the rotor temperature.

g. Effect of RPM

RPM of rotor is a good indicator to analyze the computational model. Increasing the RPM which means increasing the speed of the vehicle, which has a positive effect on heat transfer rate. The study is conducted to analyze the dependence of wall heat transfer coefficient on flow pattern. A rotor having 44 vanes with vane thickness of 5 mm is used for the simulation. Five different RPM 201,402,602,804,1004 is selected to study the variation of heat transfer rate.

Table 5: Effect of rotor RPM on velocity, mass flow rate, and heat transfer

Vehicle speed	20mph	40mph	60mph	80mph	100mph
Rotor RPM	201	402	602	804	1004
Average heat transfer coefficient (W/m^2K)	30.64	54.78	76.44	98	117.47
Avg. velocity at outlet (m/s)	1.70	3.58	5.43	7.43	9.09
Heat transfer rate (Kw)	2.12	3.8	5.3	6.8	8.1

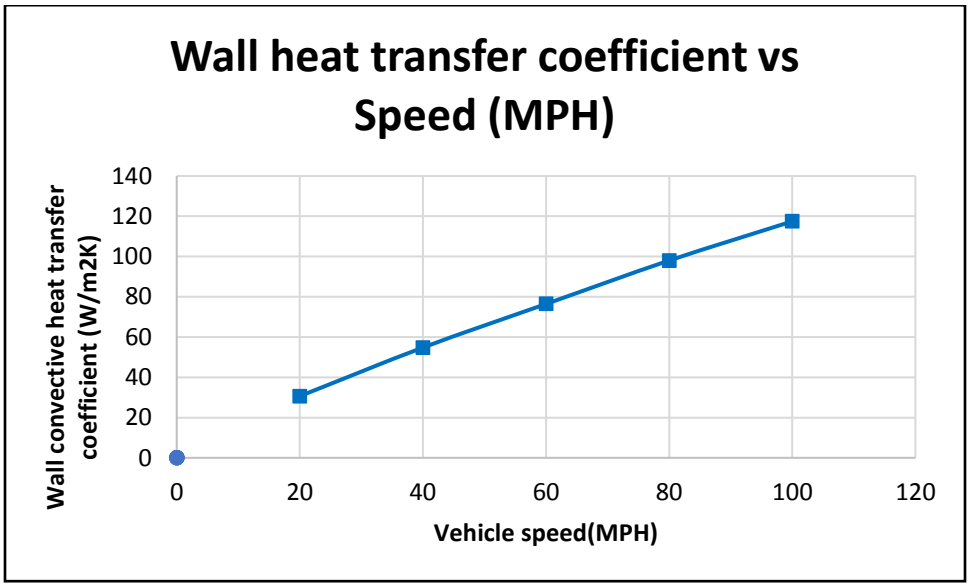

Figure 41:Effect of vehicle speed on wall heat transfer rate

(Table 5) shows effect of RPM on physical parameters. As shown in (Figure 41), Wall heat transfer coefficient increases linearly with increasing vehicle speed mentioned by A.D. McPhee [19], from the above analysis it can be stated that wall heat transfer is a function of vehicle speed, the relationship can be defined as,

$$y = 1.0836x + 10.434 \qquad 30$$

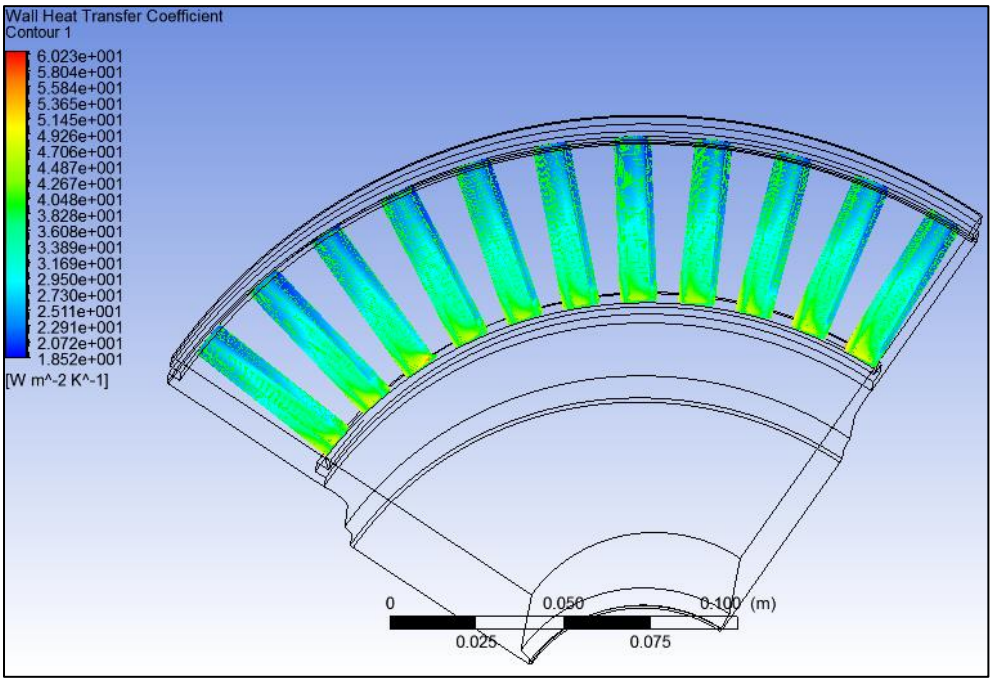

Figure 42: 44 Straight vanes wall convective heat transfer profile (20mph)

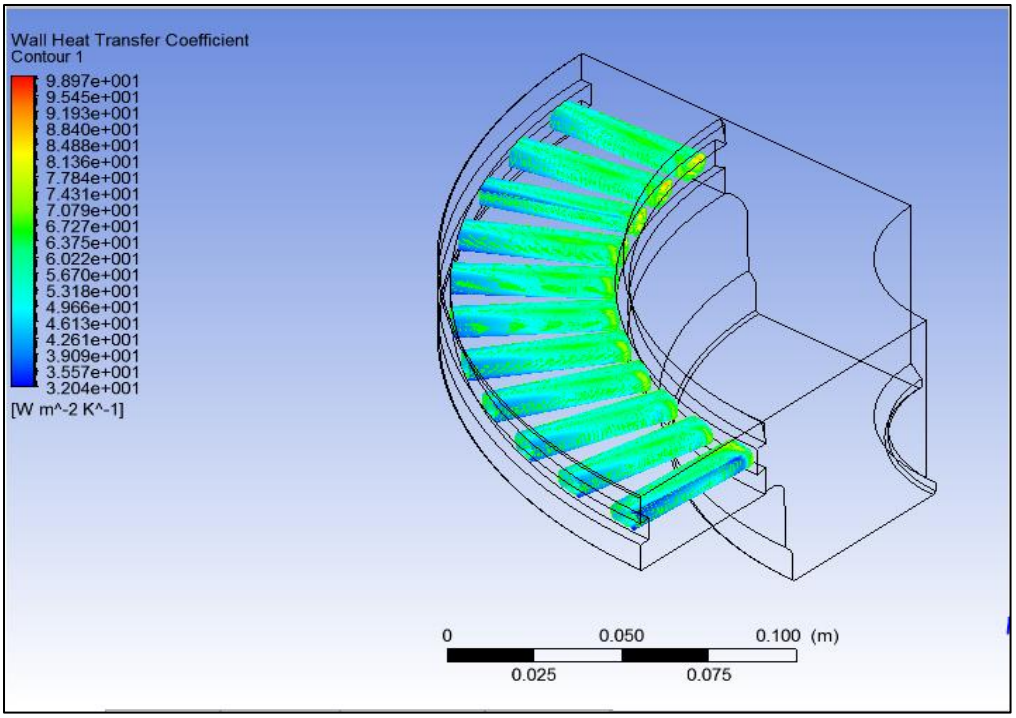

Figure 43: 44 Straight vanes wall convective heat transfer profile (40mph)

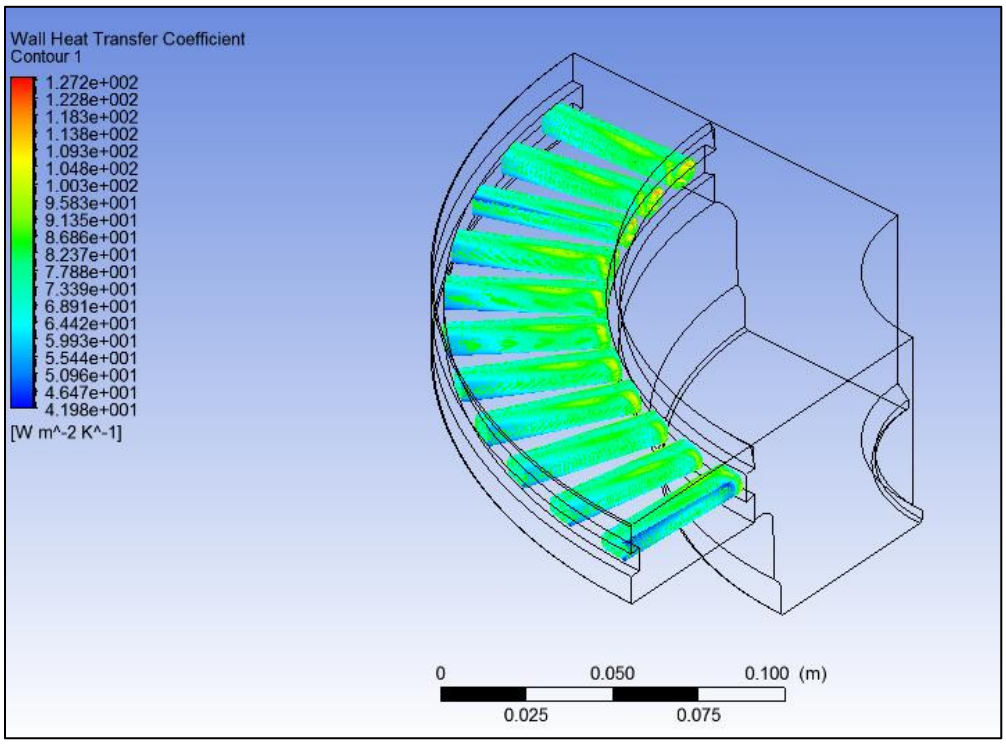

Figure 44: 44 Straight vanes wall convective heat transfer profile (60mph)

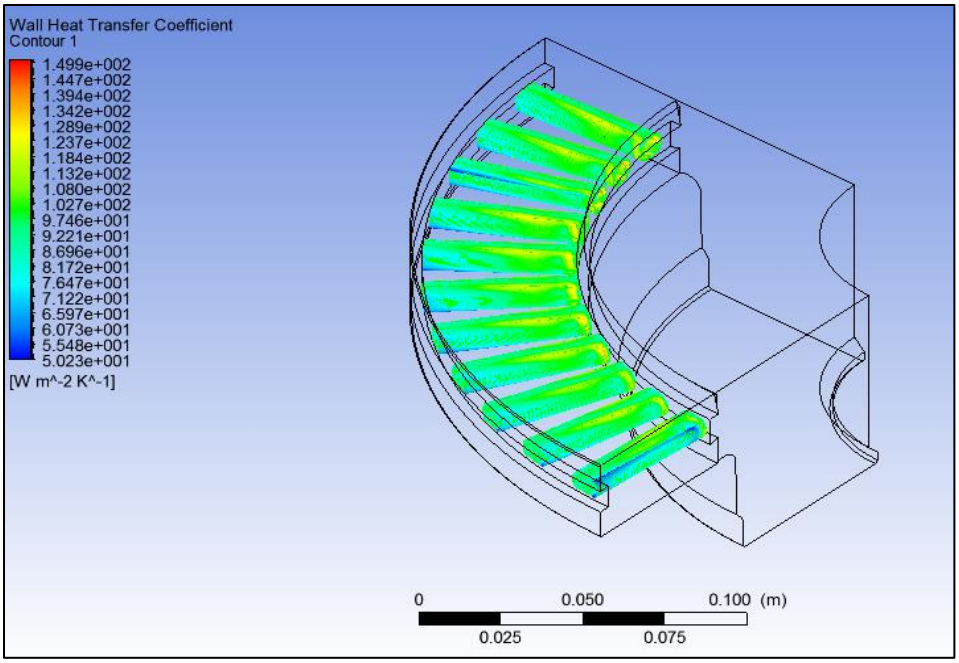

Figure 45: 44 Straight vanes wall convective heat transfer profile (80mph)

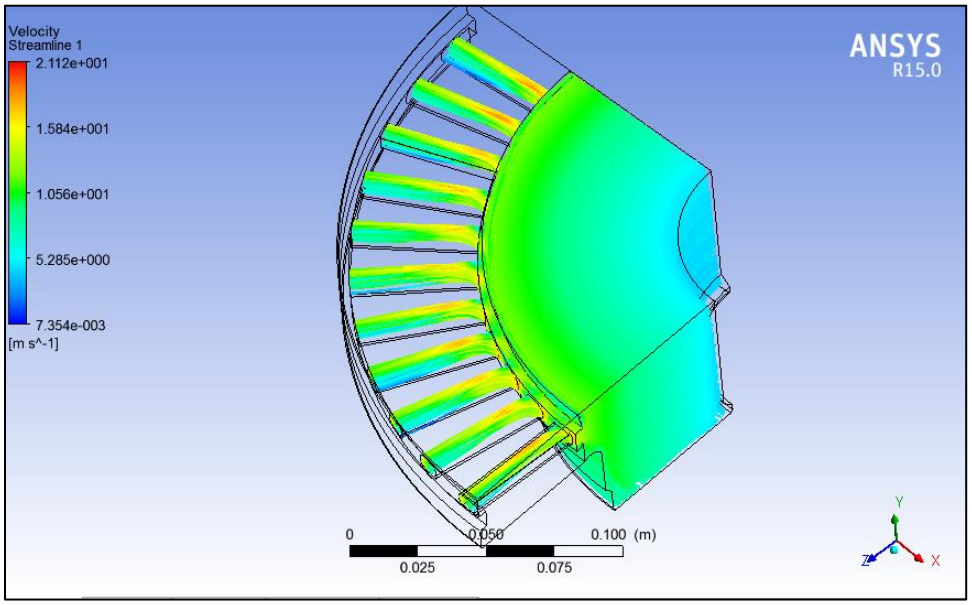

Figure 46: 44 Straight vanes wall convective heat transfer profile (100mph)

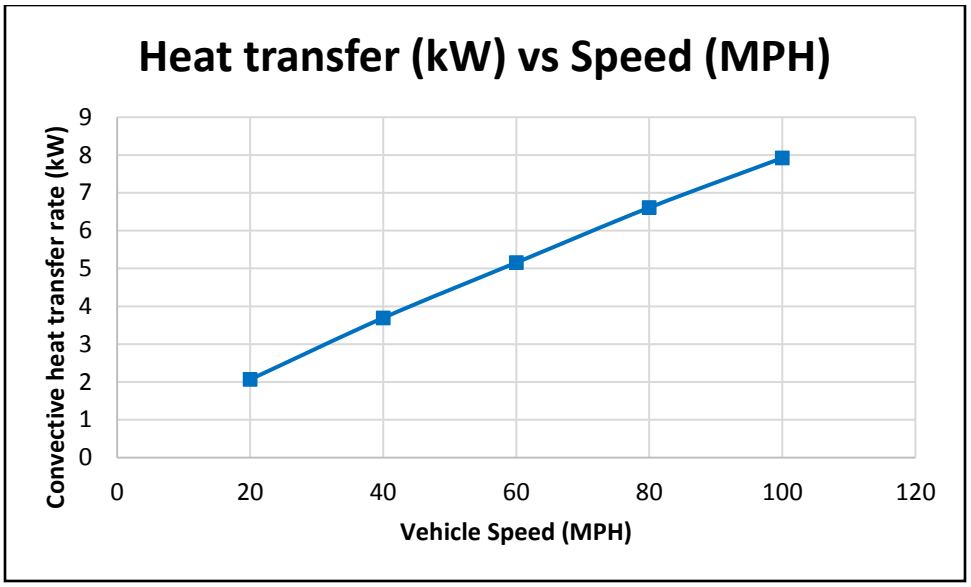

Figure 47: Effect of vehicle speed on convective heat cooling

As shown in (Figure 47), heat transfer rate by mode of convection increases linearly with increasing vehicle speed mentioned from the above analysis it can be stated that wall is transfer is function of vehicle speed and can be defined as,

$$y = 0.0706x + 0.6799 \qquad 31$$

Average flow velocity increases linearly with increasing the rotor RPM. Following (Figure 48, Figure 49), shows velocity streamlines for rotor rotating at 20, 40, 60, 80, 100 MPH respectively.

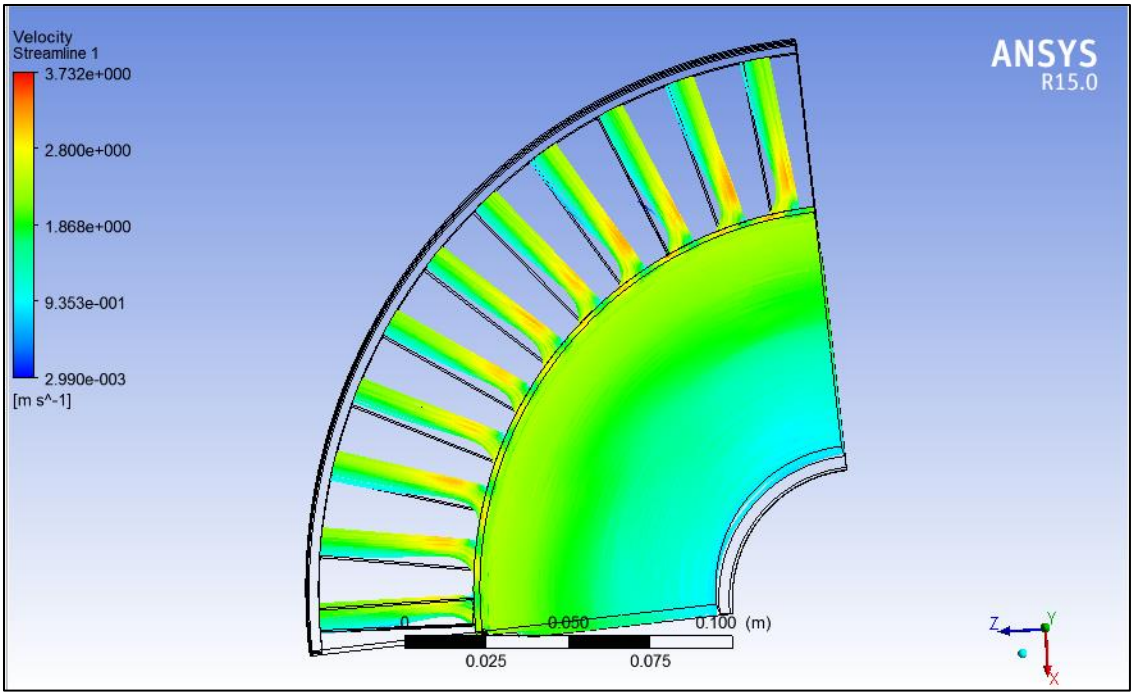

Figure 48: Streamlines for vehicle speed 20 MPH (201 RPM)

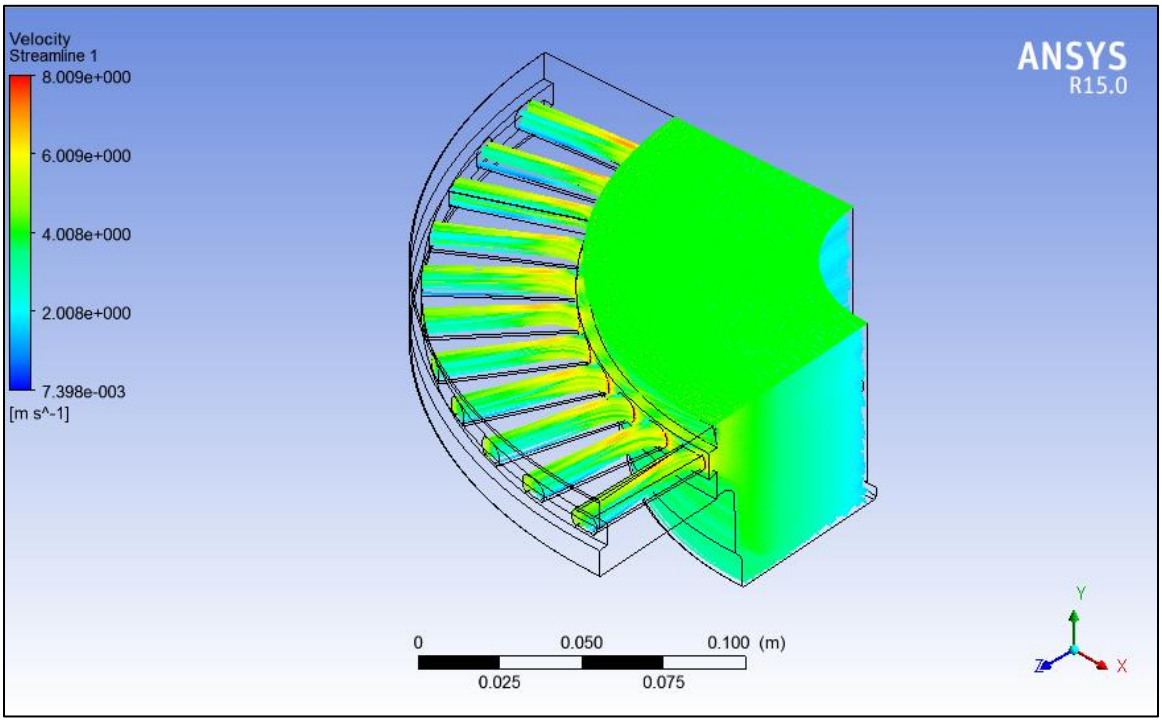

Figure 49: Streamlines for vehicle speed 40 MPH (401 RPM)

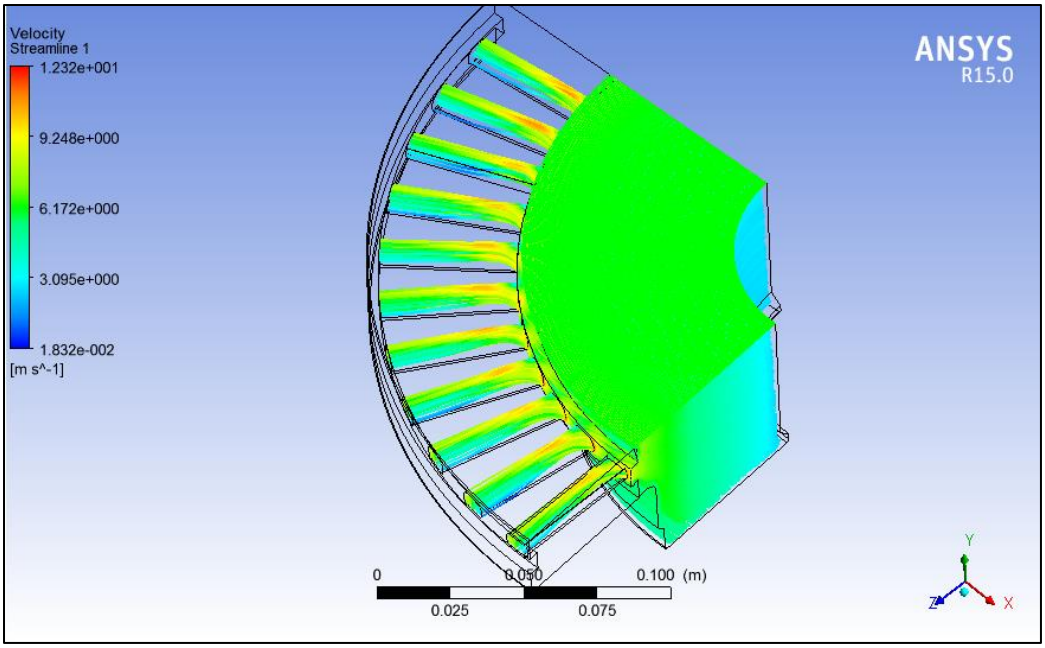

Figure 50: Streamlines for vehicle speed 60 MPH (602 RPM)

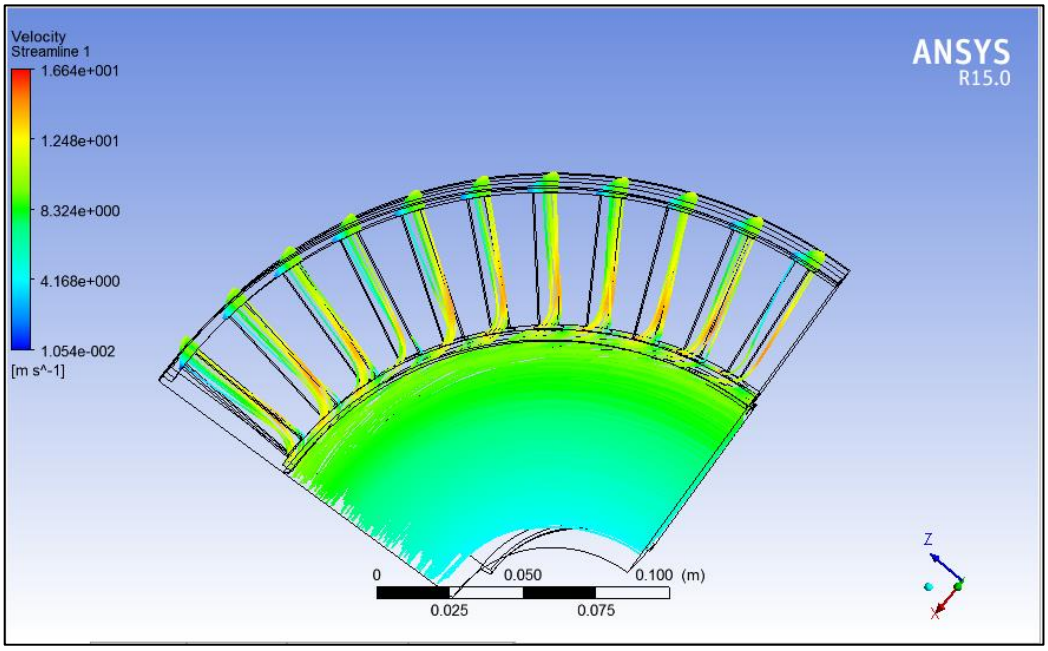

*Figure 51:*Streamlines for vehicle speed 80 MPH (804 RPM)

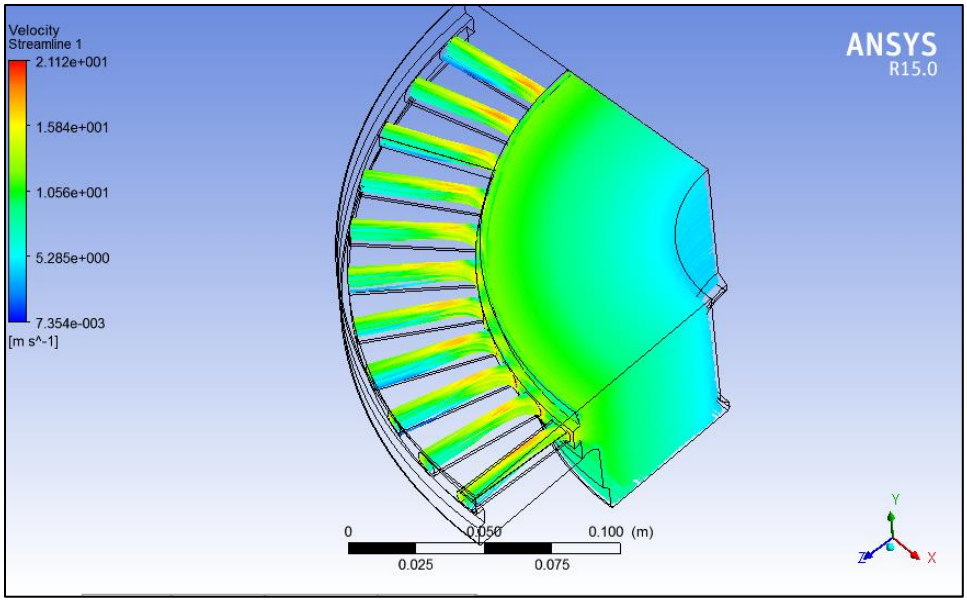

Figure 52: Streamlines for vehicle speed 100 MPH (1004 RPM)

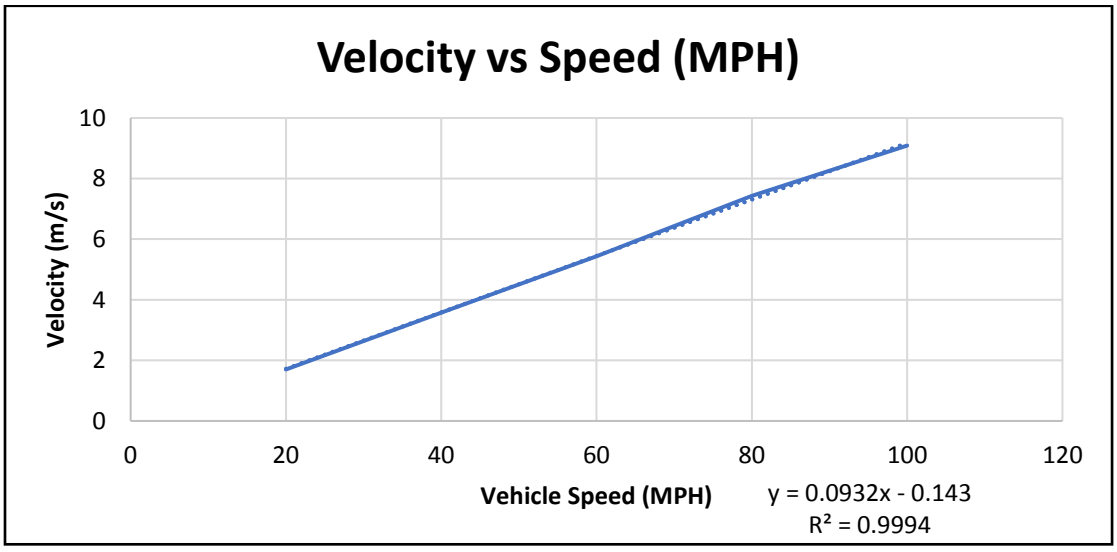

Figure 53: Average air flow velocity vs vehicle speed

As shown (Figure 53), average flow velocity from vent increases linearly with increasing vehicle speed. It can be stated that velocity is function of vehicle speed and can be defined as,

$$y = 0.0923x - 0.143 \qquad 32$$

h. Comparison of Convective Heat Transfer Coefficient from CFD and Mathematical Model

After the CFD analysis on vane type brake rotor, results obtained for convective heat transfer coefficient are compared with empirical formulae. Rudolf Limpert [17] did the experimental study on solid brake rotor and vane brake rotor. He derived the empirical relation to calculate the heat transfer coefficient inside the vanes of the brake rotor. He also derived the equation to calculate the heat transfer coefficient for solid rotors and the drum brake. (refer equation 2)

To calculate the value of convective heat transfer coefficient, surface temperature of disc brake and ambient air was assumed to be 814 K and 300 K respectively. Following parameters which are associated with the flow are,

- Hydraulic diameter, associated with geometry.
- Reynold number, to determine the type of flow.
- Thermal conductivity of the fluid, energy exchange along the vane passage.

Equation (2) is valid for turbulent flow only. To calculate the wall convective heat transfer coefficient, it is necessary to calculate the Reynolds number, which is based on the velocity of air through the rotor passage. Hudson and Ruhl [21] researched air flow characteristics through ventilated brake rotor, where they compared the empirical formulae derived by Limpert and Sisson.

$$\mathrm{Vavg} = \varepsilon * \omega * \mathrm{R}, \qquad \varepsilon = \sqrt{-.020 + .908\mathrm{Di} - 0.202\mathrm{Di\hat{}2}} \tag{33.}$$

Now, to validate the accuracy of given empirical relations, computational results is compared with experimental.

Table 6: Computational and experimental velocity

Rotor type	Average flow velocity $(V_{in}+V_{out})/2$(Math.) (m/s)	Average velocity (CFD) (m/s)
44 Straight vanes	6.67	7.5

The (Table 6) shows the difference in velocity for mathematical model and CFD model, as said by the Limpert 5-10% error with computational and experimental are acceptable. Now using the same velocity, wall convective heat transfer coefficient, Reynolds number is calculating is

Table 7: Computational and experimental wall convective heat transfer coefficient

Rotor type	Vane inner channel surface area (m^2)	Total perimeter (m)	Reynold's number	h Computational (w/m^2K)	h Limpert's model (w/m^2K)	Percentage of error (%)	Total heat transfer (kW)
44 straight vanes	0.128	5.632	92943	97.5	92.7	3.26	6.8

As shown in (Table 7), the percentage of error for Wall convective heat transfer coefficient seems to be reasonable. From this table, it can also be concluded that velocity which we calculate from empirical relation was in good agreement. The objective for this mathematical model is to prove that mathematical answers are in good agreement with computational.

After comparing wall convective heat transfer coefficient, it can be concluded that mathematical model is in good agreement of actual convective heat transfer coefficient and hence for further optimization study mathematical model is used for generating optimization algorithm.

6. VANE BRAKE ROTOR OPTIMIZATION, FORMULATION OF MATHEMATICAL EQUATIONS

The heat transfer rate of a brake rotor depends on following design variables.

1) Number of vanes (N)
2) Vane thickness (t)
3) Height of vane (h1)
4) Outer radius (R)

Changing any of the design variables affects the total exposed area and the wall convective heat transfer coefficient. The wall convective heat transfer coefficient from Limpert's model [17] is defined in equation 2.

$$h = 0.023\left[1 + \left(\frac{4*A}{l*p}\right)^{0.67}\right] * \left(v * \left(\frac{4A}{p}\right) * \frac{\rho}{\mu}\right)^{0.8} * Pr^{0.33} * \frac{Ka*p}{4*A} \qquad 2$$

Calculation of the wall convective heat transfer coefficient requires

- Total area exposed to air (A)
- Average flow velocity (v)
- Total perimeter exposed to air (P)
- Length of cooling vane (l)
- Density of air (ρ)
- Dynamic viscosity of air (μ)
- Thermal conductivity of air (Ka)

For substituting the values of area, perimeter, and velocity in Limpert's equation of wall convective heat transfer coefficient, it is necessary to define each of these quantities in term of the design variables. A mathematical expression is derived for each of the following properties in terms of the design variables for both the straight and curved vane rotor cases.

- Total exposed area = f (R, N, t, h1)
- Wetted perimeter = f (R, N, t, h1)
- Velocity = f (R, N, t, h1)
- Total weight of rotor = f (R, N, t, h1)
- Cross-section view for straight vane rotor

a. Mathematical Expressions for Straight Vane Rotor

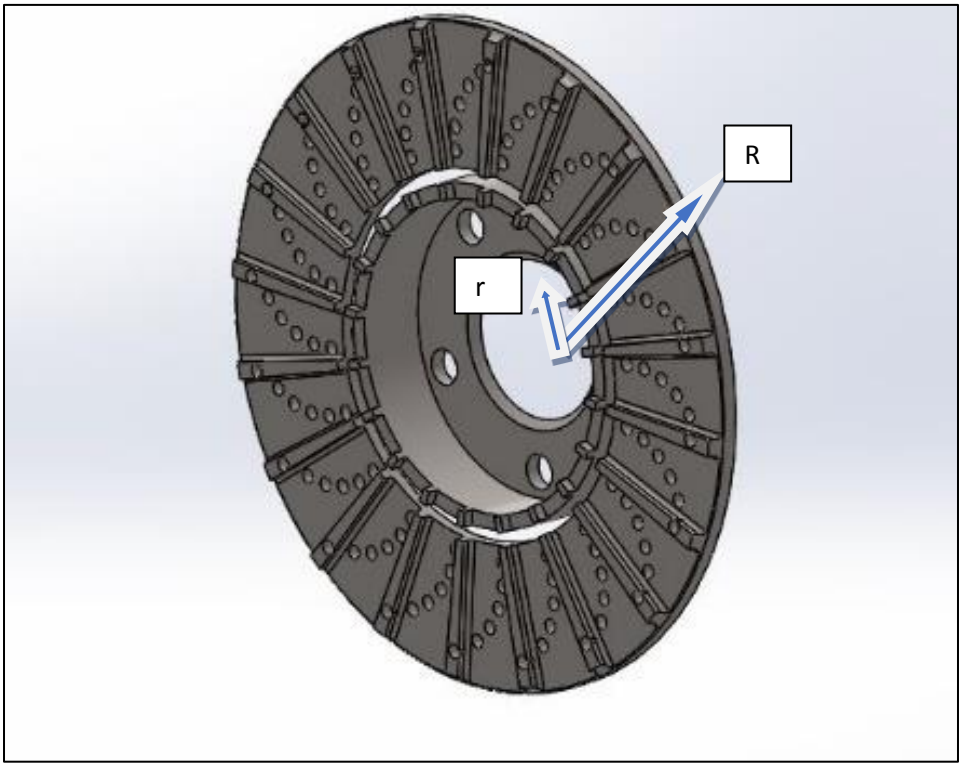

Figure 54: Cross-sectional view of straight vane brake rotor

As shown (Figure 54), cross-sectional view of straight van rotor. Small part of rotor is considered to derive the expression of area exposed to air. Figure 55 represent the small area of straight vane rotor. design parameter's terminology is defined in the figure.

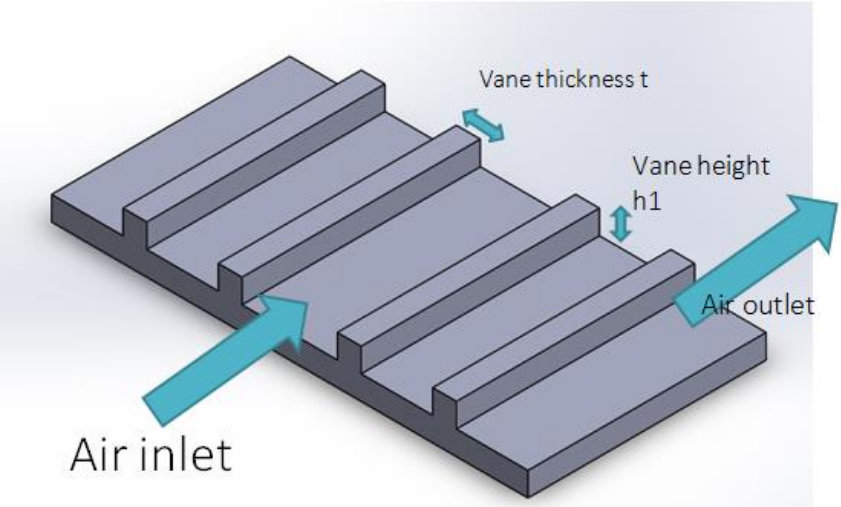

Figure 55: Cross-sectional view of straight vane brake rotor

1. Total exposed area

Equation of total exposed area available is derived as follows

$$\text{area of the circle} = \pi[\,R^2 - r^2]$$

$$\text{area of single vane} = t * [\,R - r]$$

$$\text{total area of the N vanes} = Nt * [\,R - r]$$

$$\text{area exposed to air} = 2 * (\pi[\,R^2 - r^2]) - (Nt * [\,R - r])$$

$$\text{increased area of 1 vanes} = 2 * [\,(R - r) * h1]$$

$$\text{area of the solid disks} = 2 * [\,\pi R^2 - Nt(R - r)]$$

$$\text{Total exposed area} = 2[\pi R^2 - Nt(R - r)] + 2[(R - r)h1 * N]$$

$$A = 2[\pi(R^2 - r^2) - Nt(R - r)] + 2[(R - r)h1 * N] \qquad 34.$$

2. Wetted perimeter of vane rotor

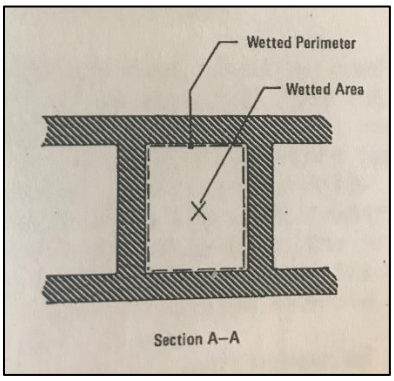

Figure 56: Wetted perimeter for given vane rotor

As given in Limpert's study [6] wetted perimeter and flow velocity should be taken into consideration while calculation of wall convective heat transfers co-efficient. (Figure 56) shows the typical wetted perimeter for any vane brake rotor. Hence the total perimeter and velocity is defined as follows.

$$\text{Total wetted permieter of all vanes} = 2\left[\frac{2\pi R}{N} - (t - h1) * N\right]$$

$$p = 2\left[\frac{2\pi R}{N} - (t - h1)N\right] \qquad 35.$$

3. Average flow velocity

For calculation of the average flow velocity, the velocity at the inlet and the velocity at the outlet should be calculated first.

$$\text{Inlet area} = \left[\left(\frac{N}{360^2} * 2\pi r\right) - t\right] * h1$$

$$\text{Outlet area} = \left[\left(\frac{N}{360^2} * 2\pi R\right) - t\right] * h1$$

$$\text{Avarage flow Velocity } = \omega * \xi * R\left\{1 + \frac{\left[\left(\frac{N}{360^2} * 2\pi r\right) - t\right] * h1}{\left[\left(\frac{N}{360^2} * 2\pi R\right) - t\right] * h1}\right\}$$

$$V = \omega * \xi * R * \left\{1 + \frac{\text{inlet velocity}}{\text{outlet velocity}}\right\} \quad (36.)$$

4. Total weight of rotor

Now the expression is derived to calculate the weight of rotor

$$\text{Volume of vane rotor } = \pi * (R^2 - r^2) * h1$$

Now, knowing the material used, the mass of a solid rotor can be calculated as,

$$\text{Weight of vane rotor } = \pi * (R^2 - r^2) * h1 * \rho_m$$

Now this expression will give weight of a solid rotor without vanes. To calculate the weight of a vane brake rotor, the air passage area must be subtracted from the total mass of the rotor. It can be expressed as

$$\text{Weight reduced due to no of vanes} = N * (w * t * (R - r) * \rho_m)$$

Hence, the final weight of vane rotor is expressed as

$$\text{Total weight of vane rotor} = (\pi * (R^2 - r^2) * h1 * \text{density}) - ((N * (w * t * (R - r) * \rho_m))$$

$$W = (\pi * (R^2 - r^2) * h1 * \text{density}) - ((N * (w * t * (R - r) * \rho_m)) \quad (37.)$$

b. Mathematical Expressions for Curved Vane Rotor

Figure 57 shows the geometric construction of a curved vane. R is the outer radius of the brake rotor and r is the inner radius. If a circle is drawn in such a way that it will touch R and r with radius of (R-r)/2, that will be maximum possible vane curvature.

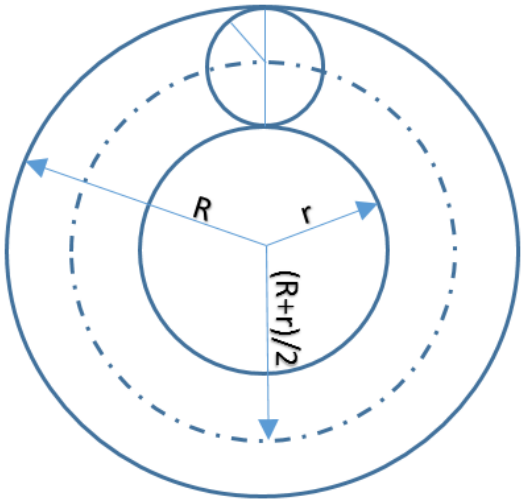

Figure 57: Maximum possible curve vane constriction for any given rotor OD (R-r)

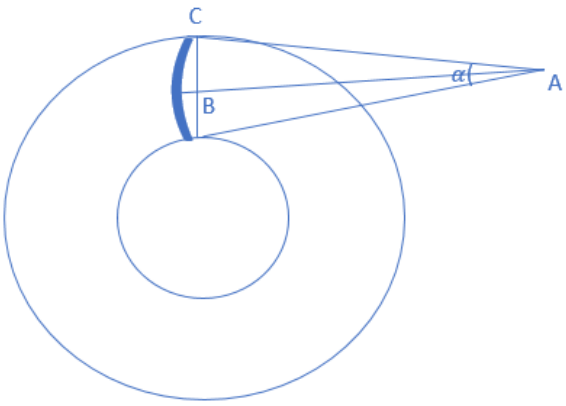

Figure 58: Geometric construction for curved vane rotor

Now consider that for any curvature between R and r, shown in (Figure 58), the radius of curvature can be determined by geometric construction. The intersection point to the curve can give a mathematical equation for radius of curvature.

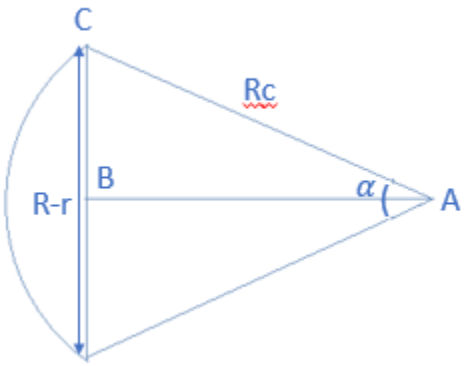

Figure 59: Geometric construction to derive radius of curvature for curved vane

Considering (Figure 59), in triangle ABC, $\sin\frac{\alpha}{2} = \left(\frac{BC}{Rc}\right) = \left[\frac{(R-r)}{2*Rc}\right]$

$$\frac{\alpha}{2} = \sin^{-1}\left[\frac{(R-r)}{2*Rc}\right]$$

where Rc = radius of curvature of the curved vane

The maximum curvature occurs when $\sin^{-1}(1) = 90$ and $\alpha = 180°$. Referring to Figure 58,

$$\text{Sin } \alpha/2 = 1\left[\frac{(R-r)}{2*Rc}\right]$$

Hence the radius of curvature can be defined as

$$Rc = 1\left[\frac{(R-r)}{2*\sin(\frac{\alpha}{2})}\right]$$

For a curved vane rotor, the length of the cooling vane depends on the curvature of the vane and it is expressed as

$$(\mathrm{R}-\mathrm{r}) = 1 * \left[\frac{(\mathrm{R}-\mathrm{r})*\alpha}{2*\sin(\frac{\alpha}{2})}\right] \quad 38.$$

$$\alpha = 0 \text{ to } \pi$$

If α = 0, $\sin\left(\frac{\alpha}{2}\right) = \frac{\alpha}{2}$ and the expression becomes (R-r), which is case of straight vane.

If $\alpha = \pi$, $\sin\left(\frac{\alpha}{2}\right) = \pi/2$, and (R-r) is replaced with (R-r) *π/2.

If the radius of the curved vane is (R-r)/2, the surface area is increased by $\frac{\pi}{2}$.

Now to compare the surface area of straight vane vs. curved vane, the surface area of the curved vane can be calculated as,

$$\text{surface area of a straight vane (along the vane)} = (\mathrm{R}-\mathrm{r}) * \mathrm{h1}$$

For curved vane with maximum curvature, we know that radius is (R-r)/2 hence,

$$\text{circumference of circle} = 2 * \pi * \frac{\mathrm{R}-\mathrm{r}}{2}$$

As we are considering a semicircle for a curved vane,

$$\text{surface area of a curve vane} = \pi/2 * (\mathrm{R}-\mathrm{r}) * \mathrm{h1}$$

Therefore,

$$\text{Surface area of the curved vane} = \frac{\pi}{2} * \text{Surface area of straight vane}$$

1. Total exposed area

Equation of total exposed area available is derived as follows

$$\text{area of the solid disks with curve vane} = 2 * \left[\pi R^2 - Nt((R - r)/(2 * \sin\left(\frac{\alpha}{2}\right)) \right]$$

$$\text{area along N vanes} = 2 * (R - r)h1 * N$$

$$\text{Total exposed area for curved vanes } = 2\left[\pi R^2 - \alpha * \frac{Nt(R-r)}{2*\sin\left(\frac{\alpha}{2}\right)} *\right] + 2\left[h1 * N * \frac{R-r}{2*\sin\left(\frac{\alpha}{2}\right)} * \alpha\right] \quad (39.)$$

2. The perimeter of the vane rotor will remain the same as that of the straight vane rotor, Equation 35.
3. Average flow velocity

For calculation of average flow velocity, velocity at inlet and velocity at out should calculate

$$\text{Inlet area} = \left[\left(\frac{N}{360^2} * 2\pi r\right) - t\right] * h1$$

$$\text{Outlet area} = \left[\left(\frac{N}{360^2} * 2\pi R\right) - t\right] * h1$$

$$\text{Avarage flow Velocity } = \omega * \xi * R\left\{1 + \frac{\left[\left(\frac{N}{360^2} * 2\pi r\right) - t\right] * h1}{\left[\left(\frac{N}{360^2} * 2\pi R\right) - t\right] * h1}\right\} \quad (40.)$$

4. Total weight of rotor

$$\text{Total weight of vane rotor } = (\pi * (R^2 - r^2) * h1 * \text{density}) - [\, N * \left(w * t * \frac{(R-r)}{\left(2*\sin\left(\frac{\alpha}{2}\right)\right)} * \alpha * \rho_m\right)] \quad (41.)$$

c. Rotor Configuration

Figure 60: Vane brake rotor

Brake rotor shown in (Figure 60) is used aa baseline rotor and upper and lower bounds of design variable were decided based on this rotor. The baseline rotor dimensions are

Table 8: Baseline rotor dimensions

Variable	**Actual dimensions**
Inner radius (m)	0.116
Outer radius (m)	0.1715
Number of vanes	44
Vane thickness (m)	0.005
Vane height (m)	0.01

Depending on the wheel hub diameter, the maximum rotor diameter can be fixed. Manufacturing capabilities can be used to decide upper and lower bounds of the rest of the design variables, such as available die size and cast size. For a given case, the upper and lower bounds are defined as,

Table 9: Lower and upper bound specification for vane brake rotor

Variable	Lower bound	Upper bound
Outer radius (m)	0.150	0.1715
Number of vanes	20	100
Vane thickness (m)	0.005	0.01
Vane height (m)	0.01	0.02

d. Vane Brake Rotor Optimization Problem Formulation

For thermal optimization of a vane brake rotor, two optimization problem are formulated.

- Calculate rotor dimensions for maximum heat transfer
- Calculate rotor dimensions for given heat transfer with minimizing mass

Two algorithms are presented with different objective functions and different constraints. The maximum heat transfer algorithm will give the theoretical maximum possible heat transfer rate using the maximum/minimum value of the design variables. It can also be stated as the maximum heat dissipation capacity of the rotor. For a given rotor configuration, the output of the maximum heat transfer rate algorithm shows geometric parameters that are keys to it. But at the same time, it does not consider the material content or material used. Hence, another algorithm is designed which will minimize the total weight of the rotor by satisfying a user-specified heat dissipation criteria.

The second optimization algorithm is more representative of a realistic design process in industry, where the required brake rotor should meet heat transfer constraints with minimum mass. User needs to provide upper and lower bounds of each design variable with the required heat transfer rate, and the algorithm will give the respective values of geometric parameters needed to achieve the desired heat transfer rate with minimum possible mass. The objective functions and constraints for the two algorithms are defined below.

I. Calculate rotor dimensions for maximum heat transfer

Maximize heat transfer, (Q)

42.

$$Q = h * A * \Delta T$$

To maximize Q, the product of h and A should be maximized. ΔT is not a design variable, as it is the temperature difference of the rotor wall and the ambient air. Changing the design variables affects the total exposed area and the wall convective heat transfer coefficient. Substituting the value of the wall convective heat transfer coefficient and the area in Equation (42), this can be written as,

43.

$$\text{Max } f(x) = 0.023\left[1 + \left(\frac{4*A}{l*p}\right)^{0.67}\right] * ((v * d * \frac{\rho}{\mu})^{0.8} * Pr^{0.33} * \frac{Ka*p}{4*A} * 2[\pi R^2 - N * t * (R - r)] + 2[(R - r) * h1 * N]$$

subject to a linear equality constraint of

44.

$$N = \frac{\pi*2R}{(w+t)}$$

and subject to upper and lower bounds, given in (Table 9: Lower and upper bound specification for vane brake rotor).

Algorithm input and output argument

Input to the algorithm is only the upper and lower bounds of each design variables and density of the material. The outputs from the algorithm are the rotor dimensions, the rotor weight, and the heat transfer rate.

II. Calculate rotor dimensions for minimum rotor weight and for required heat transfer

Minimize rotor weight,

45.

$$f(x) = (\pi * (R^2 - r^2) * 3t * \text{density}) - ((\ N * \ (w * t * (R - r) * d * \rho_m))$$

subject to an equality constraint, (refer equation 44)

inequality constraint $g(x)$, can be defined as,

46.

$$0.023\left[1 + \left(\frac{4*A}{l*p}\right)^{0.67}\right] * ((v * d * \frac{\rho}{\mu})^{0.8} * Pr^{0.33} * \frac{Ka*p}{4*A} * 2[\pi R^2 - N * t(R - r)] + 2[(R - r) * h1 * N] * \Delta T \ \geq \text{Required value}$$

subject to upper and lower bounds given in (Table 9: Lower and upper bound specification for vane brake rotor)

Algorithm input and output argument

Input to the algorithm is the upper and lower bounds for each design variables, density of material and required heat transfer rate. The outputs from the algorithm are the rotor dimensions, the rotor weight, and the heat transfer rate.

7. OPTIMIZATION ALGORITHM

Fmincon description

Fmincon is a gradient-based method that is designed to work on problems where the objective and constraint functions are both continuous. Fmincon is a function in MATLAB which can be used to calculate the minimum/maximum value of the objective function within the given constraint limit. Fmincon finds a constrained minimum/maximum of a scalar function of several variables starting at an initial estimate.

Optimization of a vane brake rotor with algorithms 1 and 2 includes:

- A nonlinear objective function
- One equality constraint
- One nonlinear inequality constraint
- Upper and lower bounds for each design variable

Different algorithms can be used by fmincon to calculate the minimum of the objective function

a. interior-point
b. Trust region reflection
c. Active set
d. Sequential Quadratic Programming (SQP)

a. Interior Point

The interior-point approach is constrained minimization approach which solve a sequence of approximate minimization problems. The basic idea is to include an inequality constraint in the objective function. A logarithmic term is added to the objective function with the inequality constraint in the interior point algorithm.

Standard form of the log barrier is,

47.

$$\text{Min } f(X) = f(x) \pm (1/t) \sum_{i=1}^{m} \log(-g(x))$$

Subject to,

$$h(x) = 0 \qquad \text{(Equality constraint)}$$

$$g(x) \leq 0 \qquad \text{(Inequality constraint)}$$

A large barrier is constructed around the feasible region. In fact, the function becomes infinite if any of the inequality is active. Thus, when the iterative process is started from a feasible point, it is not possible for it to go into the infeasible region because it cannot cross the huge barrier on the boundary of the feasible set. For barrier function methods, as t approaches INF, the objective function dominates and we are getting point inside of feasible region. If t approaches 0, the objective function becomes +INF, and hence the log barrier pushes the next step inside the feasible region. To solve the approximate problem, the algorithm uses two main types of steps at each iteration as follows

- A direct step - This step attempts to solve the Karush–Kuhn–Tucker (KKT) equations and Lagrangian multiplication vector for the approximate problem via a linear approximation. This is also called a Newton step as it uses Newton's method of optimization.
- Conjugate gradient step, using a trust region- By default, the algorithm first attempts to take a direct step. If it cannot, it attempts a CG step. One case where it does not take a

direct step is when the approximate problem is not locally convex near the current iteration.

Drawbacks of the barrier function methods are as follows:

- The starting point must be feasible
- The barrier functions tend to be ill-behaved near the boundary of the feasible set, where the optimum points usually lie. Iterate solution inside feasible region and hence active constraints sometimes miss.
- Interior point algorithm can give inaccurate solutions because the barrier function keeps iterates away from inequality constraint boundaries.

For the given problem, gradient and hessian information is not available. Considering the drawbacks of the Interior point algorithm, this algorithm is not good choice for optimization of brake rotor problem.

b. Trust-Region Methods

The trust region approach is strongly associated with approximation. Initializing the current guess of the solution of the optimization problem; an approximate model can be constructed near the current point. A solution of the approximate model can be taken as the next iterate point. In fact, most line search algorithms also solve approximate models to obtain search directions. However, in a trust region algorithm, the approximate model is only trusted in a region near the current iterate. The region that the approximate model is trusted is called the trust region. A trust region is normally a neighborhood centered at the current iterate. The trust region is adjusted from iteration to iteration. If the approximate model works not good enough, then the trust region should be reduced. In the standard trust-region method the first two terms of the Taylor series approximation defined as the quadratic approximation.

Standard format is,

48.

$$\min = \frac{1}{2} s^T H s + s^T g$$

Subject to ||Ds|| ≤ ɗ

Where ɗ is trust region of model.

Where g is the gradient of function at the current point x, H is the Hessian matrix of second derivatives, D is a diagonal scaling matrix, s is trial step, ɗ is a positive scalar. Decision regarding enlarging or compressing the trust region is depends on reduction ration. Reduction ratio is defined as, ratio of actual reduction to predicated reduction.

49.

$$R_k = \frac{f(x^k) - f(x^{k+1})}{f_q^k(x^k) - f_q^k(x^{k+1})}$$

Where $f_q^k(x^k)$ is quadratic approximation of the problem at point k. for good quadratic approximation ration is neat to 1. And hence following approached is generally used.

- If the ratio r is between $0 < \eta_1 < r$ and $r < \eta_2 < 1$ we have that the model is quite appropriate; we accept the step and do not modify the trust region.
- If the ratio r is small $r \leq \eta_1$ we have that the model is not appropriate; we do not accept the step and we must reduce the trust region by a factor $\Upsilon_1 < 1$
- If the ratio r is large $r \geq \eta_2$ we have that the model is very appropriate; we do accept the step and we enlarge the trust region factor $\Upsilon_2 > 1$
- The algorithm is quite insensitive to the constant η_1 and η_2. Typical values are $\eta_1 = 0.25$, $\eta_2 = 0.75$, $\Upsilon_1 = 0.5$ and $\Upsilon_2 = 3$.

The current point is updated if

$$f(x + s) < f(x);$$

Otherwise, the current point remains unchanged. The neighborhood N is usually spherical or ellipsoidal in shape. Iterations involve the approximate solution of a large linear system using the method of preconditioned conjugate gradients (PCG). Line search strategies choose the direction first, followed by the distance, where Trust-region strategies choose the maximum distance first, followed by the direction.

Limitations of trust region reflective algorithm

- Trust region reflective algorithm is recommended if and only if bound constraints, (upper and lower) or linear equality constraints is available.
- Gradient information is required to use large-scale algorithm and is most effective when the matrix of second derivatives, i.e., the Hessian Matrix H(x), is used.

c. Active Set

Active set method solves constrained optimization problems by searching solutions in the feasible sets. If constraints are linear and one can guess the active constrains for the optimal solution, then one can use the active constraints to reduce the number of unknowns, and then perform algorithms for unconstrained optimization problems. One major problem is how to guess the set of active constraints. Linear programming is an active set method. The solution procedure involves two phases. The first phase involves the calculation of a feasible point (if one exists). The second phase involves the generation of an iterative sequence of feasible points that converge to the solution. Active set algorithm used quadratic form of objective function stated as,

50.

$$\min q(d) = c^T d$$

Subjected to,

$$A_i^T d = b, \quad i \in \varepsilon$$

$$A_i^T d \leq b, \quad i \in I$$

To incorporate inequality constraints, lagrangian form of equation can be written as

51.

$$L(d, \lambda) = \frac{1}{2} d^T G x + d^T c - \lambda^T (Ad - b)$$

A general strategy for linear equality constraints is variable elimination. For nonlinear equality constraints, variable elimination may not feasible, which make problem unbounded and hence for inequality active method is used. The solution procedure involves two phases. The first phase involves the calculation of a feasible point (if one exists). The second phase involves the
generation of an iterative sequence of feasible points that converge to the solution.

d. Sequential Quadratic Programming (SQP)

SQP method mimic's the Newton's method for constrained optimization just as is done for unconstrained optimization. At each major iteration, an approximation is made of the Hessian of the Lagrangian function using a quasi-Newton updating method. This is then used to generate a Quadratic programming (QP) sub problem whose solution is used to form a search direction for a line search procedure. The principal idea is the formulation of a QP sub problem based on a quadratic approximation of the Lagrangian function. SQP converts objective function, equality constraint and inequality constraint is QP sub problem, Lagragian approach is used in incorporate inequality constraint in objective function. Standard format is,

$$\underset{d}{\text{Min}} \ \frac{1}{2} d^T H_k d + \nabla f(x_k)^T d \qquad 52.$$

Subjected to,

$$\nabla h_i(x_k)^T d + g_i(x_k) = 0$$

$$\nabla g_i(x_k)^T d + g_i(x_k) \leq 0$$

This sub problem can be solved using any QP algorithm. Step length parameter α_k is determined by an appropriate line search procedure so that a sufficient decrease in a merit function is obtained SQP works in following 3 steps.

- Updating the Hessian Matrix
- Quadratic Programming Solution
- Line Search and Merit Function

Once the problem is converted into QP problem, Lagrangian function is introduced.

KKT conditions for SQP,

53.

$$\nabla L(x, u, v) = \nabla f(x) + \nabla A(x)u + \nabla h(x)v = 0$$

$$h(x) = 0$$

$$gA(x) = 0$$

$$u \geq 0$$

SQP Algorithm

- Guess initial value x^0 and calculate $f(x^0)$, $g(x^0)$, $h(x^0)$
- At x^k, calculate the $\nabla f(x^k)$, $\nabla g(x^k)$, $\nabla h(x^k)$
- Update the hessian matrix (gradient of lag. Function)
- Solve the quadratic problem (equation 52)
- Check the solution with KKT conditions to conclude the result
- Find the new search direction using Newton's method and again calculate divergent and gradient and hessian of objective function, inequality constraint, equality constraint.

Advantages

- It does not require hessian or gradient to calculate the minima of function
- It considers equality and inequality constraints as well as bound constraints.
- It does not use barrier function and hence potential inaccuracy can be avoided.

After discussing the limitations of internal point algorithm, it is not suitable for this problem. SQP, trust region reflective and Active set algorithm are well suitable for the given problem because those are QP. The SQP algorithm combines the objective and constraint functions into a merit function. The algorithm attempts to minimize the merit function subject to relaxed constraints. This modified problem can lead to a feasible solution. If the nonlinear constraints are not satisfied, the SQP algorithm attempts to obtain feasibility using a second-order approximation to the constraints. The second-order technique can lead to a feasible solution.

e. Calculate Rotor Dimensions for Maximum Heat Transfer Rate

As discussed in chapter 6 section d, objective function and constraints are defined for calculation of maximum heat transfer rate. (Optimization Problem 1) To calculate the maximum heat transfer rate, different set of initial guesses were run. Ideally speaking, a robust algorithm should always converge to the same value irrespective of initial conditions. Changing the initial condition is a good measure of checking whether the algorithm has converged to local or global minima/maxima for the objective function. Convergence to same value indicates that algorithm is robust and the solution is optimal within feasible region.

Design of Experiment (DOE) is widely used for examining the effect of various design parameters on the value of an objective function. The DOE approach is based on number of combinations of design parameters and their level. For example, if an objective function consists of two design variables and three levels of each design parameter, then the DOE approach will run 2^3 combinations to analyze the effect of individual design parameters on the objective function. Now considering the vane brake rotor optimization problem, four design variables are available. But, discrete levels for the respective parameters are not available and hence a standard DOE approach cannot be used. To check the effect of a single design variable on the heat transfer rate, the following approached is used.

- All the parameters are set on lower bounds.
- Individual parameter is varied from its lower bound to upper bound with approximate step size.
- 28 different tests were analyzed by varying the initial guess of a single design parameter starting from its lower bound to upper bounds while holding rest of design parameter's constant. Results are tabulated as follows.

Table 10: Rotor geometric specifications for maximum heat transfer

Geometric parameters	**Optimal value**
Outer Radius (m)	0.1715
No of vanes	72
Vane thickness (m)	0.005
Vane height (m)	0.020

From the above table following points can be concluded about local/global maxima

- For varied initial guess and tolerance criteria, the maximum heat transfer never exceeds 22.92 kW and hence it can be concluded that for the given rotor configuration, the maximum heat transfer rate is 22.92kW
- Rotor dimensions for the maximum heat transfer rate are tabulated in (Table 10)

Now comparing the results with the upper and lower bounds on the variables, the active constraints can be found. The outer radius, vane height and number of vanes are all at their upper bounds, while the vane thickness is at its lower bound. All the given constraints are active for the given objective function.

f. Calculate Rotor Dimensions for Required Heat Transfer Rate

Fmincon is used to solve the Optimization Problem 2 (Equation 45-46) subjected to constraints in (Table 9). As this problem is designed in such a way that user can provide the required amount of heat transfer rate, fmincon solves Optimization Problem with given heat transfer rate as a constraint and will give geometric parameters as output to achieve desired heat transfer rate. (Table 11) shows the design variable solutions and weight of the rotor for each given heat transfer rate.

Table 11: Effect of heat transfer rate on rotor's specifications

Heat transfer const.(kW)	Outer radius	Vane thickness	Vane height	Number of vanes	Weight of rotor
10	0.1715	0.005	0.010	65	8.52
13	0.1715	0.005	0.0115	72	10.76
16	0.1715	0.005	0.0140	72	13.02
19	0.1715	0.005	0.0162	72	15.09
22	0.1715	0.005	0.0182	72	17.03

From above table, all design variables are active at their upper or lower bounds except the vane thickness. Vane thickness is just a parameter which keeps changing from 10kW to 22kW. For achieving heat dissipation less than 13kW, total number of vanes can be varied but outer radius and vane thickness are still active constraints. Comparing weight of rotor with heat dissipation capacity, it can be concluded that weight of rotor increases with increasing heat dissipation capacity.

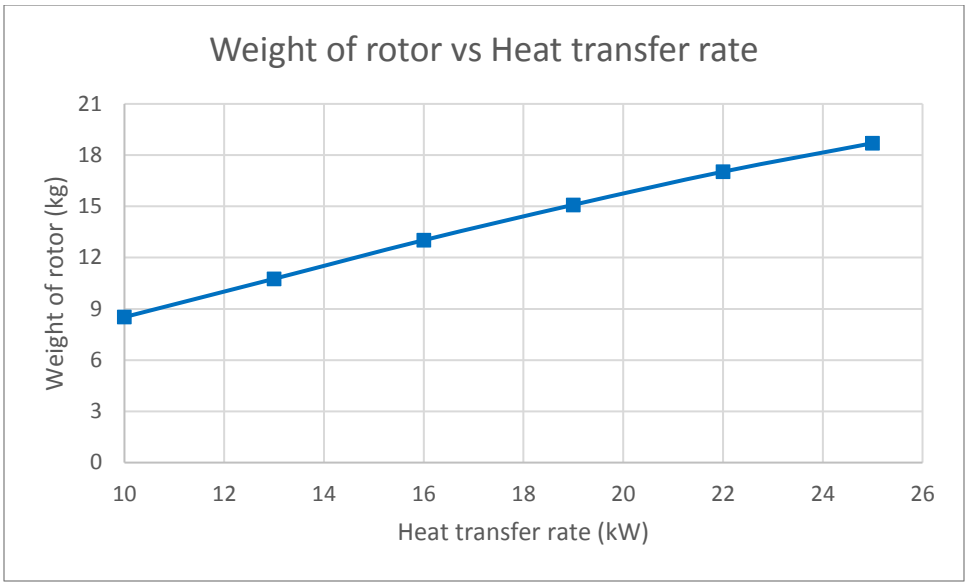

Figure 61: Effect of rotor's weight on heat transfer rate

As shown in (Figure 61), it can be concluded that weight of rotor is proportion to heat dissipation capacity. When rotor's weight is maximum (18kg), heat dissipation capacity is largest (25kW) all the geometric constraints become active at their boundaries. Geometric parameter approaches its maximum value, which results in increase in total weight of the rotor.

8. EFFECT OF INDIVIDUAL DESIGN PARAMETERS ON HEAT TRANSFER RATE

Different design parameters such as the number of vanes, vane thickness, total surface area, and vane structure affect the aero-thermal performance of the disc brake rotor. The effects of individual parameters on the heat transfer rate were studied by constraining other properties and varying individual one at a time. Changing any design parameter will change total exposed area, weighted perimeter, velocity of flow, and convective heat transfer rate, which will eventually change heat transfer rate. For the analysis of individual parameters, all other parameters were fixed at their highest limit.

a. Comparison of Curved Vane Rotor Vs Straight Vane Rotor

To compare heat transfer capacities for the curved vane rotor vs. the straight vane rotor, the first optimization algorithm (Chapter 6 section d) is used while holding the lower bound and upper bound constant. The algorithm is designed in such a way that it will give the maximum heat transfer capacity of the rotor with exact values of design parameters. We can compare maximum heat transfer capacity of different rotors. (Table 12) shows the heat transfer capacity of two different rotors.

Table 12: Straight vane vs curved vane results

	Straight vane	Curved vane
Outer radius (R), m	0.1715	0.1715
Number of vanes (N)	72	72
Vane thickness (t), m	0.005	0.005
Vane height (h1), m	0.02	0.02
Weight (W), kg	18.65	21.95
Heat transfer (Q), kW	22.92	25.48

Form the above table, it can be concluded that, Heat transfer capacity of the curved vane rotor is 11% more than the straight vane rotor for the same design variables because, curved vane rotor has more surface area which is exposed to air. But, weight of curved vane is 3.30 kg greater than that of straight vane rotor.

Second optimization Problem defined in (chapter 6 section d, II) is used to analyze the set geometric parameters for given rate of heat dissipation. As an example, for 10 kW of heat transfer, (Table 13) shows the geometric parameters for respective rotors with their weight.

Table 13: Design specification of straight and curved vane for given rate of heat transfer

Heat transfer rate (kW)	**Parameters**	**Straight vane rotor**	**Curved vane rotor**
10	Outer radius (m)	**0.1715**	**0.1715**
	Number of vanes	**60**	**56**
	Vane thickness (m)	**0.005**	**0.005**
	Vane height (m)	**0.01**	**0.01**
	Weight of rotor (kg)	**10.22**	**10.76**
	Radius of curved vane(m)		**0.0275, (R-r)/2**

From the above table, it can be concluded that all the design parameters are active either at their upper bound or at lower bounds expect total number of vanes. For a curved vane rotor, the total number of vanes required to extract the same amount of heat is less compared to the straight vane rotor.

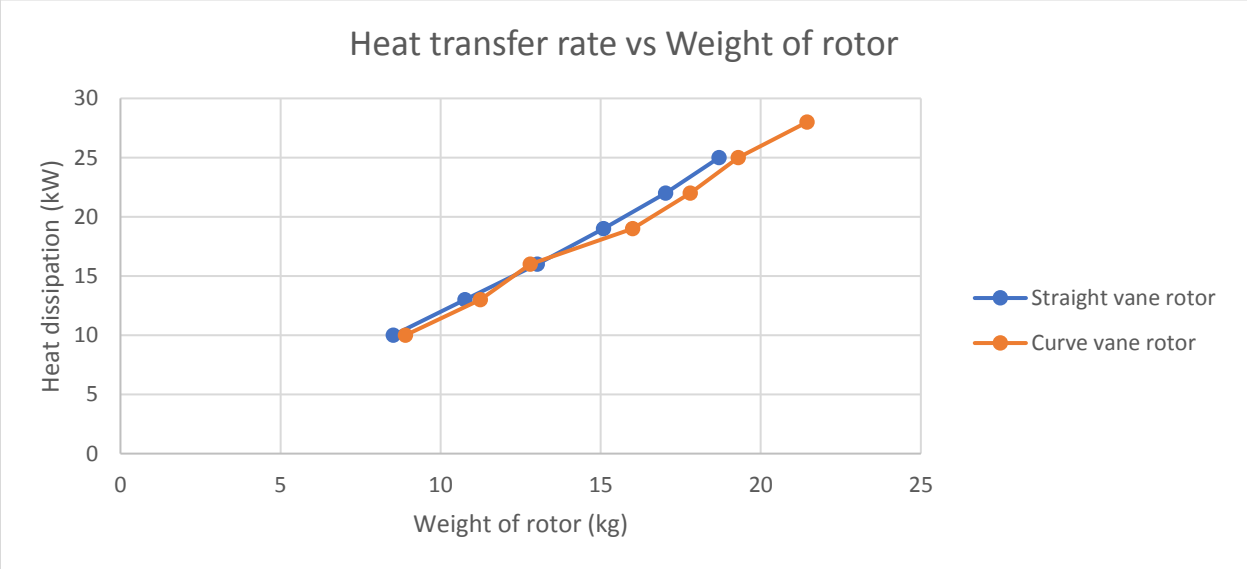

*Figure 62:*Trade-off between weight & heat dissipation capacity for different design rotors

As shown in (Figure 62), for same amount of heat dissipation, weight of curved vane rotor is more than straight vane rotor for low heat dissipation. As heat dissipation requirement increases, curved vane rotor can able to dissipate the same amount of heat with less number of vanes and hence total weight of rotor is decreased a bit compared to straight vane rotor. Further increasing heat dissipation requirement, curve vane rotor can give more heat dissipation compare to straight vane rotor.

b. Effect of Number of Vanes

(Figure 63) shows the effect of the number of vanes on heat transfer. Increasing the number of vanes results in increased surface exposed area on two sides. The maximum number of vanes that can be accommodated in any rotor is dependent on vane thickness (Equation 5). For given configuration of rotor, the maximum heat transfer rate of 22.92kW can be achieved if the total number of vanes is 72.

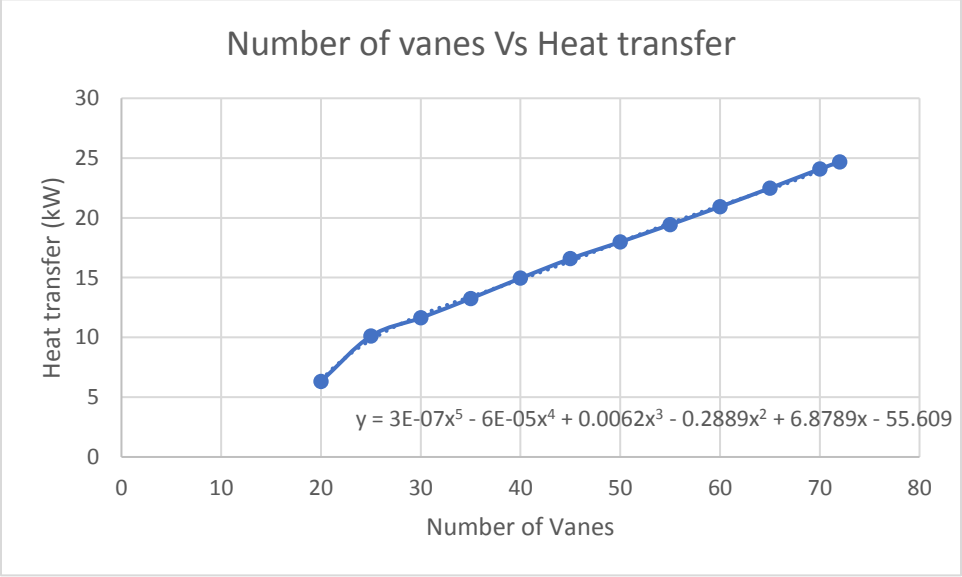

Figure 63: Effect of total number of vanes on heat transfer rate

From the above analysis, it can be concluded that as number of vanes increases, heat transfer rate increases. For designing vane type disc brake rotor, minimum no of vanes is function of structural stability. Upper and lower surface of brake rotor is connected through vanes. Ex. Suppose, four vanes in rotor where portion between two successive vanes are hollow can reduce the structural stability of rotor. There are two types to manufacture vane brake rotor

- Drilled the solid vane rotor from its OD to ID. This is time consuming and not reliable process to manufacture vane brake rotor. Because of excessive material use, weight of rotor and after machining time.

- Casting which can be define as designing mold/die for given vane rotor configuration and filling the molten metal can be filled in die to get final product of vane rotor. This is reliable and easy process to manufacture brake rotor.

Most of brake manufacture uses second method for manufacturing vane brake rotor given its advantages over the first one. For a given vane rotor, minimum no of vanes are 20. And maximum no of vane that can be fit is function of vane thickness defined in (Equation 5) which is 72. So, Number of vanes can be varied from 20 to 72. At minimum number of van while holding rest of design variables constant, heat transfer rate is 6.23kW. as number of vane increased from minimum to maximum, heat transfer rate is increased to 25kW. Increasing the number of vane from its minimum to maximum affect the total amount of heat dissipation by 300%

c. Effect of Outer Radius

(Figure 64) shows heat transfer rate vs. outer radius. Varying the outer radius of the disc will increase the heat transfer rate. This is because the outer radius is directly proportional to the exposed area and wetted perimeter. For the given rotor, at maximum outer radius (0.1715m) the heat transfer rate is maximum (22.92kW).

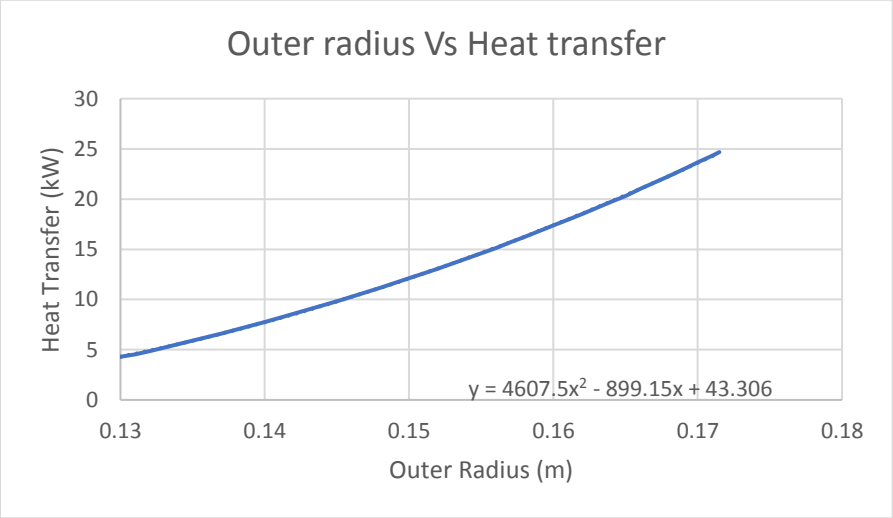

Figure 64: Effect of outer radius on heat transfer rate

Variation of outer radius follows quadratic trend with total heat transfer rate. Increasing outer radius increases length of cooling vane (R-r) for each vane which contributes in heat transfer from rotor's surface. At minimum outer radius (0.13m), length of cooling vane is (0.0135 m) where at maximum outer radius (0.1715) it increased to (0.55m) total increased in length of cooling vane from minimum to maximum is 400%. Effect of increased cooling vane can be calculated as, for minimum length of cooling vane holding rest of design variables constant, heat transfer rate is 5kW approx. as length of cooling vane is increased to maximum possible value, heat transfer rate is recorded as 25kW. Total change in heat transfer rate from minimum length of vane to maximum length of vane is 400%. From this study, it can be concluded that, length of cooling vane is directly proportional to heat transfer rate and length of cooling vane is directly proportional to rotor's outer radius.

d. Effect of Vane Thickness

(Figure 65) shows the effect of vane thickness on heat transfer rate. Vane thickness is directly proportional to the number of vanes and inversely proportional to exposed area. Hence, increasing the vane thickness will reduce the effective exposed surface area, which eventually reduces the total heat transfer rate. For the given rotor configuration, the maximum heat transfer can be achieved if vane thickness is smallest (0.005m).

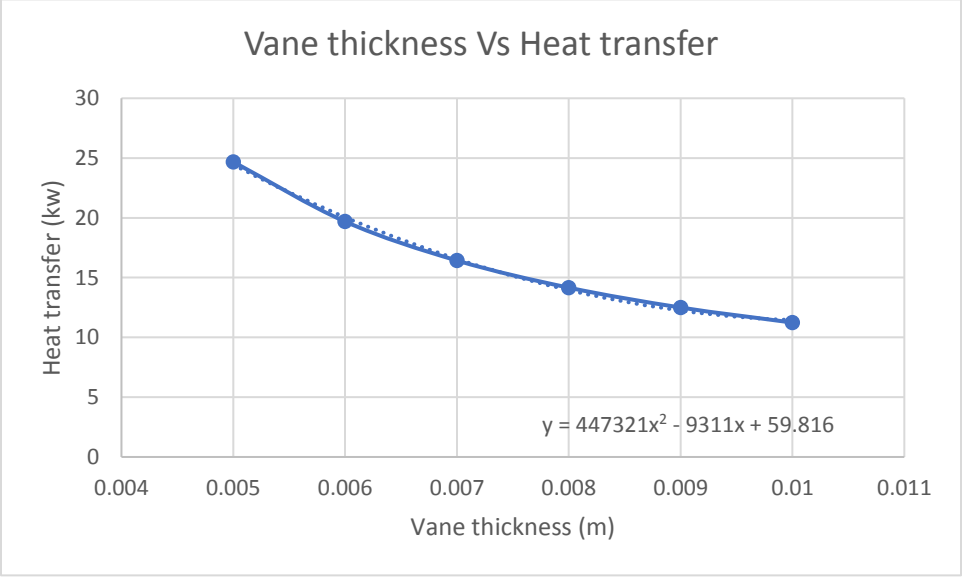

Figure 65: Effect of vane thickness of heat transfer rate

The graph of vane thickness and heat transfer rate is nonlinear and quadratic in nature. Maximum heat transfer can be observed at minimum vane thickness. By varying the vane thickness from its maximum to minimum value holding rest of design variable constant, heat transfer rate increased by 140%. Comparing all the design variables with vane thickness, it is the only constraint which is active on its lower bound because at lower bound more surface area is available to expose the air. On the other hand, one drawback is structural stability is directly proportional to vane thickness vane thickness should be good enough to handle mechanical and thermal stresses developed during braking. Hence, from thermal point of view, decision of vane thickness is considered as last option.

e. Effect of Vane Height

(Figure 66) shows the effect of vane height on heat transfer rate. Generally, vane thickness is determined by manufacturing abilities and available cast and die size. For most of the rotors, vane height varies from 0.01m – 0.02m. Vane height is directly proportional to weighted perimeter and exposed area. Maximum vane height will give maximum heat transfer rate, but at the same time it will increase the total material use and total weight of the rotor. For the given rotor configuration, the maximum vane height (0.02m) will result in the maximum heat transfer rate of 22.92kW.

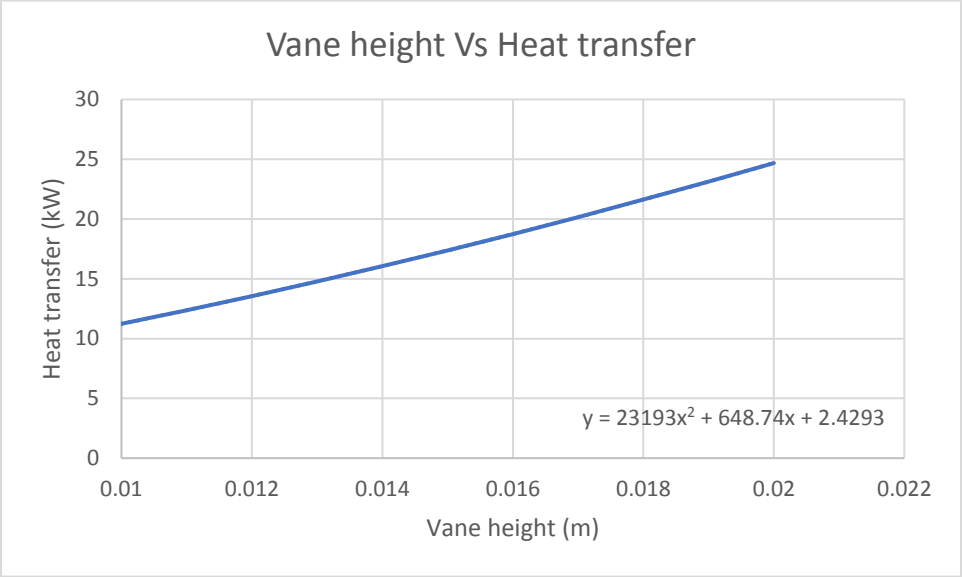

Figure 66: Effect of vane height of heat transfer rate

Graph indicated the second order quadratic relationship between vane height with heat transfer rate. As vane height is varied from its minimum to maximum holding rest of design variables constant, the heat transfer rate is increased by 150% which is huge contribution. On the other hand, vane height will increase the rotor's thickness which might create a problem during assembly of rotor on wheel hub. Vane height is least significant parameters among all design parameters. For a, given heat transfer rate, algorithm try to fit rest of design parameters on their lower or upper bounds and then jumps to vane height.

9. CONCLUSION

With combined approach of CFD and design optimization, it is possible to study, understand and optimize the vane brake rotors geometry for given amount of heat dissipation and for maximum heat dissipation. Limpert's empirical formulae for convective heat transfer coefficient is successfully validated using CFD approach with error and stability analysis (Error Analysis, Grid Sensitivity Analysis). Vane brake rotor's geometric parameters and convective heat transfer coefficient is successfully integrated in terms of design variables to form optimization problem. With the help of design problem, it is possible to distinguish the effect of individual design parameters on rotor's heat dissipation capacity. Further, based upon individual parameters effect, engineering recommendations are presented for break rotor model.

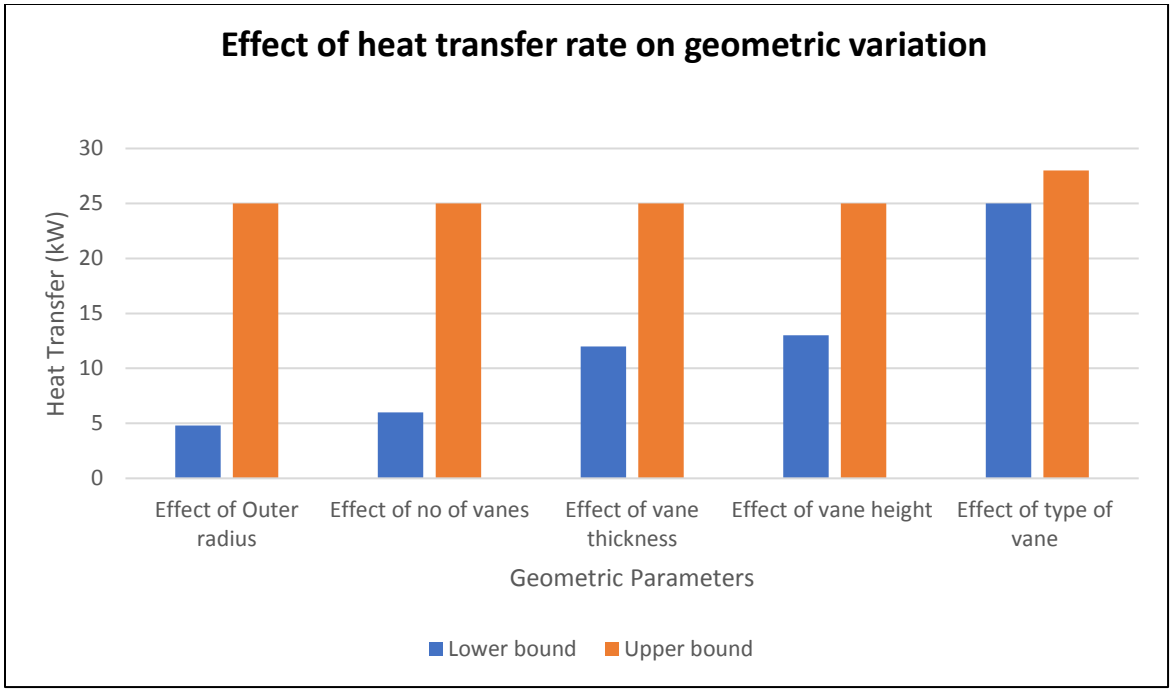

Figure 67: Effect of variation of different geometric parameters on heat dissipation

As shown in (Figure 67) , five different design parameters and their effect (varied from lower boundto upper bound) on heat transfer rate are plotted. Factors are ranked

according to their effect on heat dissipation capacity. Outer radius is most significant factor as increasing OD increases the length of cooling vane along its peripheri. Number of vanes is second significant factor as increasing vanes increases the surface area which contributes in heat dissipation. Vane thickness is only factor which is active at its lower bound varying vane thickness from lower bound to upper bound increases heat dissipation by 100%.

10. ENGINEERING RECCOMMENDATIONS

- As more total surface area is exposed to air, more heat transfer will occur. It is always recommended to use a rotor with maximum OD. Though increasing the OD can increase the material content and total weight of rotor, at the same time the increased OD increases surface area and hence heat transfer by convection will increase.
- Vane thickness should be the minimum possible, as increasing the vane thickness increases the material on the rotor and reduces the air flow passage. The increased material is not exposed to air and hence heat transfer by convection decreases. Increasing the material also increases the total weight and density of brake rotor, which is not recommended.
- Vane height, i.e. distance between two rotors, is considered as significant factor in heat transfer rate. Increasing the vane height increases the surface area of vanes and hence the weight of the rotor further increases. Considering the vane constraints, it is always recommended to set vane height as small as possible.
- Curved vane rotors are generally used where the OD is small and the heat dissipation requirement is greater. This is generally the case for sports cars. Curved vane rotors are highly complex in design and require more production time and cost compared to straight vane rotors. Though curved vane rotors have greater heat dissipation capacity over straight vane rotors, it is always recommended to use straight vane rotor if possible because of complexity, cost of production and weight of rotor. For high-performance cars, it is always recommended to use a curved vane rotor as heat dissipation requirements are greater.

11. BIBLOGRAPHY

[1] S. C. Singh, "Reasons for Crashes Investigated in the National Motor Vehicle Cras Causation Survey".

[2] A. J. a. T. P. N. Day, "The dissipation of frictional energy from the interface of an annular disc brake.," *Proceedings of the Institution of Mechanical Engineers, Part*

[3] [Online]. Available: http://ae-plus.com/milestones/frederick-lanchester-inventor of-the-disc-brake.

[4] [Online]. Available: http://auto.howstuffworks.com/auto-parts/brakes/brake-types/disc-brake4.htm.

[5] [Online]. Available: http://www.cquence.net/blog/types_of_rotor_vanes/.

[6] R. Limpert, "Cooling analysis of disc brake rotors (No. 751014)," in *SAE Technical Paper*.

[7] [Online]. Available: http://www.modot.org/team/2014/documents/GeneralMotorsMilfordProvingGundRoadSystemsandAdvancedSafetyFeaturesinVehiclesTaverna.pdf.

[8] [Online]. Available: BremboInnovation." | Brembo. N.p., n.d. Web. 08 Nov. 2015.

[9] [Online]. Available: "Wilwood High-Performance Disc Brakes - Drag Race Rotors.' Wilwood High-Performance Disc Brakes - Drag Race Rotors. N.p., n.d. Web. 08 N 2015.

[10] [Online]. Available: TRW – World Leader in Braking Technology." D-Tec Brake Pa N.p., n.d. Web. 08 Nov. 2015.

[11] [Online]. Available: http://www.wilwood.com/PDF/DataSheets/ds254.pdf.

[12] T. K. J. W. R. a. A. D. Kao, "Brake disc hot spotting and thermal judder".

[13] V. P. a. S. N. B. Sergienko, "Noise and Vibration in Nonstationary Friction Processes." In Noise and Vibration in Friction Systems, pp. 133-195," *Springer International Publishing.*

[14] A. THURESSON, "CFD and Design Analysis of Brake Disc".

[15] R. (. Limpert, "The thermal performance of automotive disc brakes (No. 750873), *SAE Technical .*

[16] T. P. &. M. N. (. Newcomb, "Cooling rates of brake drums and discs.Proceedings o the Institution of Mechanical Engineers," *Automobile Division,180(1), 191-205.*

[17] R. (. Limpert, "Cooling analysis of disc brake rotors (No. 751014)," *SAE Technical.*

[18] D. &. D. G. (. Parish, "Aerodynamic investigations of ventilated brake discs," *Proceedings of the Institution of Mechanical Engineers, Part D: Journal of Automobile Engineering, 219(4).*

[19] A. D. &. J. D. A. (. McPhee, "Experimental heat transfer and flow analysis of a vented brake rotor," *International journal of thermal sciences, 47(4), 458-467.*

[20] A. E. (. Sisson, "Thermal analysis of vented brake rotors (No. 780352)," *SAE Technical .*

[21] M. D. &. R. R. L. (. Hudson, "Ventilated brake rotor air flow investigation (No. 971033)," *SAE Technical.*

[22] A. R. (. Daudi, "72 Curved Fins and Air Director Idea Increases Airflow through Bra Rotors (No. 1999-01-0140)," *SAE Technical.*

[23] J. J. (. Zhang, "A high aerodynamic performance brake rotor design method for improved brake cooling," *SAE Technical .*

[24] G. N. N. A. P. A. &. D. M. I. C. H. E. L. E. (. Barigozzi, "Combined experimental and CFD investigation of brake discs aero-thermal performances (No. 2008-01-2550), *SAE Technical .*

[25] G. P. A. P. P. &. G. R. (. Barigozzi, "Aero-thermal characteristics of an automotive CCM vented brake disc (No. 2005-01-3930)," *SAE Technical .*

[26] F. Z. M. D. T. K. &. W. J. (. Shen, "Computational flow analysis of brake cooling (N 971039)," *SAE Technical .*

[27] R. &. S. G. (. Krüsemann, "Analysis and optimization of disk brake cooling via computational fluid dynamics (No. 950791)," *SAE Technical .*

[28] G. Pulugundla, "CFD design analysis of ventilated disc brakes." (2008)".

[29] C. H. Galindo-Lopez, "Optimisation of convective heat dissipation from ventilated brake discs.(2009)".

[30] H. K. a. W. M. Versteeg, An introduction to computational fluid dynamics: the fin volume method. Pearson Education, 2007.

[31] J. H. ". c. M. Ferziger, "Ferziger, Joel H. "Peri c M," *Computational Methods for Fl Dynamics.*

[32] Ansys, Ansys theory guide.

[33] [Online]. Available: http://www.cfdonline.com/Wiki/Introduction_to_turbulence/Nature_of_turbule.

[34] I. C. E. M. ". Ansys, ICEM CFD theory guide, Ansys inc.

[35] M. Cable, "An evaluation of turbulence models for the numerical study of forced and natural convective flow in Atria".

[36] J. E. S. S. C. D. J. T. a. R. C. M. Hunter, "Brake fluid vaporization as a contributing factor in motor vehicle collisions. No. 980371," *SAE Technical.*

12. APPENDIX

TRW brake rotor temperature cooldown procedure

1. Purpose

The purpose of this test is to measure the front and/or rear rotor cooling characteristics by calculating the cooling coefficient based on the cool down rate.

2. Requirements

The test vehicle and corner components should be representative of production intent design. The test vehicle does not have to be built with new linings and rotors. The brake components should be in good working order and must not have experienced any previous severe thermal testing or conditioning.

3. Instrumentation

Rotor thermocouples, at inner and outer brake plate at each corner, ambient thermocouple on top of vehicle, slip ring assemblies to transmit temperature data from wheeled to data acquisition system, Data acquisition system recording at a minimum sample rate of 1 Hz

4. Facilities

Proving ground or suitable test area with dry, level road with smooth concrete or asphalt surfaces that allow smooth, continuous driving (i.e. oval). Wind speed during testing cannot exceed 15mph.

5. Vehicle preparation

Install brake test hardware and check all brake adjustments. Install rotor thermocouples. Reference SAE procedure number J79 for thermocouple installation procedures. Install all instrumentation and calibrate as required.

6. Procedure

Record the weather conditions at the test site. This includes ambient temperature, relative humidity, wind speed, wind direction, and wind direction relative to the vehicle. Heat the rotors to a certain temperature above ambient by performing snubs from 60 mph to 20 mph at the highest possible deceleration without locking the wheels or activating ABS. Perform as many snubs as necessary. Upon completion of the final snub, accelerate the vehicle to 80 mph and trigger the instrumentation to start recording. Maintain a steady 80 mph until the rotor temperatures reach a point such that the average rotor temperature drops less than 5^0F within a minute. Stop recording. If 80 mph is unattainable or unsafe, run at 70 mph. Repeat at a vehicle speed of 60 mph, 40 mph.

During the braking, all the kinetic (motion) energy of the vehicle is converted into thermal energy. Energy (Heat) Factors,

$$E = 1/2\ MV^2$$

Therefore, the brake power required to stop the vehicle is directly proportional to the vehicle weight and square of velocity. Thus, if the weight of the vehicle is doubled, the energy of motion (converting to heat) is doubled. The effect of vehicle speed is even more serious. If the speed of the vehicle is doubled, the brake system would require four times the power to stop the vehicle, which means the brake mechanism must absorb and dissipate four times as much as heat. The total energy resulting from the increase of vehicle weight and speed is multiplied, i.e. if both the weight and speed of a vehicle is doubled then your brake system would require generating eight times more power or eight times more of heat to absorb and dissipate.

Since all the converted heat needs to be absorbed and dissipated, the rotor comes into play as the “heat sink,” As the rotor heats up, it absorbs heat, if the temperature of the rotor increases at a rate faster than the rotor can cool down; consequent damages are likely to occur.

Per thermodynamics, amount of heat generation is defined in term of mass, specific heat, and temperature difference

$$Q=m^* cp^* DeltatT$$

When the vehicle comes into rest from longitudinal motion, according to physics all the Kinetic energy get converted into Heat energy.

Hence, we can say that,

$$Q = KE$$

$$m^* cp^* DeltatT = 1/2\ MV^2$$

$$Delta\ T = [(1/2\ MV^2) / m * cp)]$$

Now brake force is distributed unevenly on front and rear axle, hence to incorporate percentage of work done on respective axel with respective to temperature rise

$$Delta\ T = [(1/2\ MV^2) * ((\%work\ axle)/2) / m * cp)]$$

This equation gives estimation for one stop temperature rise.

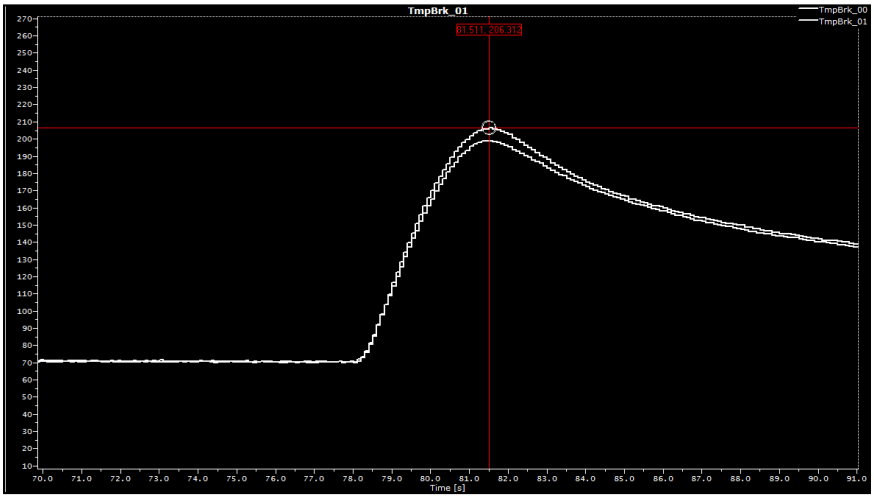

Figure 68: Temperature rise for single stop

As shown in (Figure 68), Temperature rise vs. time for the single braking event. Data is collected at Milford Proving Ground (GM facility) using “Data minor” internal tool designed by TRW automotive. The maximum temperature rise for single stop is 205^0C which is equivalent to 478^0 K.